Sonar properties of the lower jaw of the Atlantic bottlenose dolphin (tursiops truncatus)

Sonar Properties of the Lower Jaw of the Atlantic Bottlenose Dolphin (*Tursiops truncatus*)

by

Simon Dible, M Eng(Hons) DIS.

A Doctoral Thesis submitted in partial fulfilment of the requirements for the award of Doctor of Philosophy of Loughborough University

February 2008

ABSTRACT

THE primary function of this research project has been to investigate the physical properties of the lower jaw of the Atlantic Bottlenose Dolphin (*Tursiops truncatus*). This has been achieved through numerical modelling techniques, established physical measurements and modern Laser Doppler Velocity Measurements.

During the course of this work some interesting characteristics of the dolphin jaw structure have been discovered. Sound speeds and attenuation levels of the jawbone have been determined and the implications assessed. The geometric array formed by the dolphin teeth of the lower jaw can be used to form an end-fire array which produces a beam pattern similar to those of the dolphin. The geometric array has also been analysed for its passive acoustical properties, in particular its ability to form acoustic stop bands within the audible range of the dolphin.

The results of this research show that the directivity of the dolphin can be reproduced using the morphological features of the lower jaw.

ACKNOWLEDGEMENTS

First and foremost I would like to thank my primary supervisor Dr. James Flint for all the help, guidance and patience he has shown me throughout my postgraduate time at Loughborough University.

I would also like to thank Dr. Paul Lepper who has also worked closely with me and has taught me a great deal about underwater acoustics and how to conduct practical measurements.

I would like to thank Dr. John Tyrer of the Mechanical Engineering Group for enabling me to use his research group's Laser Doppler Velocimeter that made a great deal of this work possible.

There have been many other academic members of staff in the department of Electrical and Electronic Engineering who have given me encouragement and passed on their knowledge to me. In particular I would like to show my gratitude to David Goodson with whom I had the pleasure of working with and was my first supervisor, he is greatly missed.

Finally I would like to thank my girlfriend and my parents for all the support and encouragement they have given throughout this work.

CONTENTS

LIST OF ABBREVIATIONS AND SYMBOLS

ACOUSTICS, THE PHYSICAL PROPERTIES OF MATERIALS, AND WAVES

Symbol	Denotes
c	Speed of sound in water $\approx$ 1500 (ms^{-1})
d	Distance (m)
dB	Decibel
f	Frequency (Hz)
f_{max}	Cutoff frequency (Hz)
k	Wavenumber (m^{-1})
λ	Wavelength (m)
P	Acoustic pressure (Pa)
P_{max}	Maximum pressure of a source (Pa)
ρ	Density kgm^{-3}
Z_A	Acoustic impedance.
ω	Angular frequency =2π f (rads s^{-1})

MATHEMATICS

Symbol	Denotes
A	Amplitude of Gaussian signal
σ	Standard deviation

ABBREVIATIONS

Abbreviation	Expansion
ABC	Absorbing boundary condition
ABR	Auditory Brainstem Response
BMT	Biosonar Measurement Tool
CF	Constant frequency
CT	Computer tomography
CW	Continious Wave
DI	Directivity index
DFT	Discrete Fourier transform
DT	Detection Threshold
EFA	End-Fire Array
FFT	Fast Fourier transform
LOM	Laminated object manufacturing
MLDB	Monkey Lip Dorsal Bursae
MRA	Maximum Response Axis
MRI	Magnetic Resonance Imaging
NL	Noise Level
PET	Positron Emission Tomography
PML	Perfectly match layers
PPM	Portable pixel map
PSV	Polytec Scanning Vibrometer
PZT	lead zircon titanate compound
RL	Reverberation level
SL	Source level
SONAR	Sound navigation and ranging
SPECT	Single Photon Emission Computed Tomography
TLM	Transmission Line Matrix Modelling
TS	Target strength
TL	Transmission loss
TTL	Transistor Transistor Logic

LIST OF FIGURES

LIST OF TABLES

CHAPTER 1:
INTRODUCTION

ACOUSTICS is the study of sound production, propagation and interaction with its medium and any perturbing objects. There are many applications of acoustic theory ranging from simple transducer design for audible sound generation (e.g. clock alarm) to signicantly more complex systems capable of imaging (e.g. medical ultrasonic imaging). This thesis focuses on a particular application which has been exploited in the animal kingdom - echolocation. In particular this thesis will examine the implementation of sound reception in the Bottlenose Dolphin (*Tursiops truncatus*) using a variety of techniques.

1.1 Background

SOund Navigation and Ranging or as it is more commonly know SONAR has been in existence in an elementary form since 1490, when Leonardo Da Vinci was quoted as saying, 'If you bring your ship to a stop and place the head of a long tube into the water and place the outer extremity to your ear, you will hear ships at great distances from you' [1.1]. This basic principle was not applied until the turn of the 20th century, when the submarine bell was invented. This was a device that was used by ships to navigate around coastal areas. The device exploited the difference between the speed of sound in air to that of water. A simultaneous noise was produced in both the water and the air by using an under water bell and a loud horn. The distance from the shore could then be calculated by knowing the speed at which the sound travelled in both mediums and the different times of arrival.

The next major progression in sonar came in 1914, when R. A. Fessenden built a moving coil transducer, capable of detecting an iceberg at a range of 2 miles, this is one of the earliest examples of a man made active sonar system. Following this in 1914 was the start of World War 1. As a result a significant effort was invested into the development of SONAR. By 1918, both Britain and the United States of America had built active SONAR systems, and had them put them into operation on a small number of marine vessels. The development of these systems had been made possible by the discovery and exploitation of the piezoelectric effect and by advances in vacuum-tube technology.

As electronic technology progressed, German scientists concentrated on the development of the physics of underwater acoustic propagation, and Lichte et al. [1.2] published the first paper on underwater acoustics. This paper demonstrated the complex paths that sound follows under the sea, with respect to changing temperature boundaries. It was not until the onset of the second world war that the American Navy stared to use the term SONAR. Since these first steps, SONAR systems have undergone many evolutions and have now become a mature and well understood discipline. In a mature discipline however there is still grounds for improvement!

1.2 Sonar

It was not until World War 2 that the main mathematical formulas regarding sound propagation were formed and published [1.3]. The first calculations were used to predict the basic range characteristics of a sonar system. These equations are useful for describing the performance of existing designs and are useful for providing guidelines on designing and manufacturing new systems. The sonar equations relate the various properties of sound production, transmission and reception, and these can be grouped into both the desired and undesired properties. The desired property is the signal, which you are trying to measure while the undesired part is the signal loss. Signal loss is a product of noise from a variety of sources, although these can generally be classified

into three groups; Reverberation, self induced noise and Ambient Noise. Signal loss also stems from absorption in the transmission medium and spreading.

As with any system, the goal is to increase the ratio between the desired signal and the undesired noise and loss component. Self noise can be controlled by good system design, whereas the other components are more difficult to control and, in the case of spreading, is unavoidable. Reverberation can be minimised by the use of short pulsed signals and by using a narrow beam angle on the transmitter and receiver, however this is still a major issue for shallow water system and is one of the main reasons for the study in this PhD thesis.

Sonar systems are generally grouped into two types, Passive or Active sonar. Passive sonar is when only a receiving array is operated and the system listens for sounds produced externally to the system, these could range from marine mammal noises such as dolphin click and whistles to engine noise for a submerged submarine. In this case, the receiving array is typically large with many elements so that the maximum amount of information can be obtained and processed from the received signals. In contrast active sonar systems contain elements that can transmit signals of various frequencies and time durations and then a receiving system that is made up similar to the passive system.

1.2.1 Basic Sonar Equations

Although Sonar covers a very diverse field of applications in a large variety of mediums which each have their own individual properties, the principles of sound transmission and reception within a homogeneous medium can be modelled by the general sonar equations. These equations are built from several simple values that explain what happens to a pressure signal as it is produced, and propagates around its environment.

All the general sonar equations use the decibel as a scalar unit due to the large scale of the units involved in sound propagation. The decibel is defined in Equation 1.1

$$dB = 10 \log \frac{POWER}{reference} \tag{1.1}$$

Source level (SL) is the theoretical pressure 1 meter away from the source of an object, SL is defined in Equation 1.2. The reference intensity used in underwater acoustic applications is typically 1 μ pascal.

$$SL = 10 \log \frac{Intensity\ at\ 1\ meter}{Reference\ Intensity} \tag{1.2}$$

When a signal is transmitted from a point source the wave front spreads out. The way in which it spreads out is a function of the transmitter directivity and the geometry of the sound channel. In a free field, a point source will spread spherically. When this happens the total energy of the field stays constant (neglecting absorption) but the intensity at a single point is reduced, this is called Transmission Loss (TL) and is proportional to the distance from the source r. The spherical spreading equation is shown in Equation 1.3. Cylindrical spreading is another common type of spreading that often takes place within a waveguide. The cylindrical equation is shown in Equation 1.4. In many cases spherical or cylindrical spreading can be used to estimate the best or worst case for transmission loss. Other techniques provide better approximations such as, ray tracing, normal mode models, fast field models, multipath expansion method and parabolic equation models, each of these methods have their own strengths and drawbacks [1.4].

$$TL = 20 \log r \tag{1.3}$$

$$TL = 10 \log r \tag{1.4}$$

Target Strength (TS) is a property that defines the amount of incoming energy that is re-radiated by an object, this is the ratio of reflected intensity to the incident energy and is calculated 1m from the target.

$$TS = 10 \log \frac{Intensity\ reflected}{Intensity\ incident} \tag{1.5}$$

Noise Level (NL), as stated earlier, is a product of ambient noise in the environment as well as self noise, which could be caused by the electrical components in the system

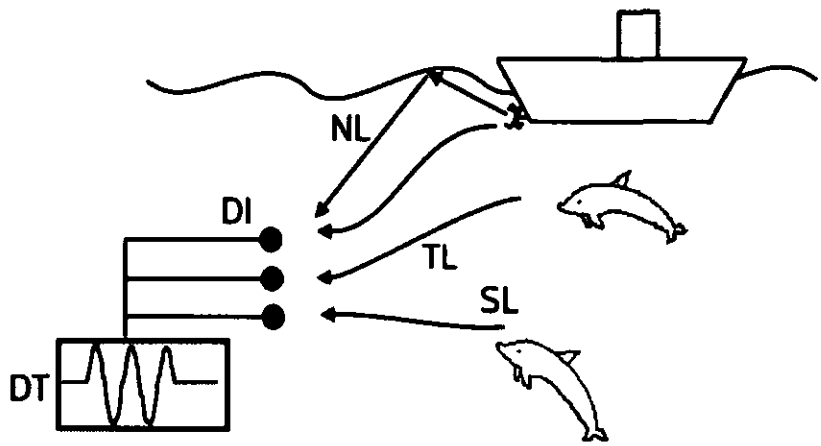

Figure 1.1: Passive Sonar System

as well as the acoustic noise that could be produced by the operating vessel. There are a variety of techniques that can be used to suppress noise in a system, these range for simple solutions such as turning off all engines on a vessel while measuring to complex signal processing, using filtering and correlation techniques. Noise level is typically expressed in dB re 1μPa.

Directivity Index (DI) is the gain that is produce by the transmitter / receiver not having an even power / sensitivity in all directions, this causes an increase in some directions and a decrease in others. For shallow waters where high reverberation between the bottom and the surface is likely to occur a highly directional transmitter and receiver is desirable. DI is defined in Equation 1.6.

$$DI = 10\log\frac{Peak\ Intensity\ of\ Radiated\ Pattern}{Average\ Intensity\ of\ Radiated\ Pattern} \tag{1.6}$$

Using the basic sonar parameters a full system can be constructed. Figure 1.1 shows a simple system for passive sonar operation. This system is trying to detect the signals sent from the dolphins in the figure but is also receiving background noise generated from the ship. From this diagram it can be seen that the detection threshold (DT) of the system is influenced by the directivity of the receiving array, the background Noise Level (NL) and the transmission loss (TL) from the source signal with a Source Level of (SL). The system is shown mathematically in Equation 1.7, this is the fundamental

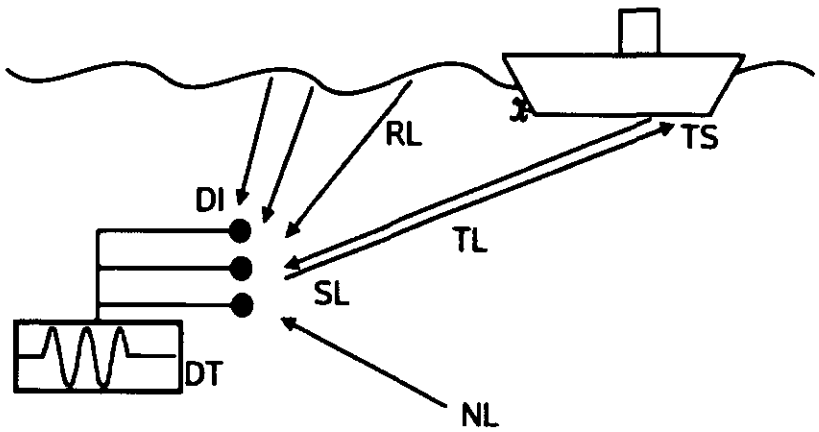

Figure 1.2: Active Sonar System

equation for passive sonar operation.

$$DT = SL - TL - NL + DI \tag{1.7}$$

A similar scenario can now be constructed for an active sonar system. Figure 1.2 shows an active system, in this system a signal is transmitted from a point source and received on the hydrophone array. The sound signal is transmitted from the point source with a source level (SL) the signal then undergoes spreading which causes a transmission loss (TL), the signal then reflects off the bottom of the ship which has an associated target strength (TS), this signal again undergoes spreading which causes more transmission loss (TL) the signal is then received at the hydrophone array along with background noise (NL) and additional multipath transmission signals which is commonly known as reverberation level (RL). The equation for systems of this type is shown in Equation 1.8. In this case the noise in the system is a product of the reverberation level and the background noise level.

$$DT = SL - 2TL - (NL + RL) + DI \tag{1.8}$$

These basic equations can be used to estimate the maximum performance of a sonar system.

1.2.2 Bioacoustics

Bioacoustics is the study of acoustics that originates from, or is intercepted, by animals including humans. The subject area is constructed from a wide variety of disciplines such as neurophysiology, physiology, biology, engineering, signal processing and acoustics. The primary aim of researchers within this field is to define how sounds are produced, received and the information encoded and decoded from them. In this thesis an engineering view of sonar is presented which examines how the physiology of the dolphin can be used to provide enhanced signal processing information to the processing system and increase the information gained from echolocation signals.

1.3 Document Description

The remainder of this chapter will describe the work that will be presented in the rest of this thesis. In this thesis unless otherwise specified the term 'Dolphin' refers to the Atlantic Bottlenose Dolphin (*Tursiops truncatus*).

Chapter 2 provides a background literature review of the subject of bioacoustics. This literature review provides the motivation for the work that is presented in the remainder of this thesis.

Chapter 3 examines the properties of the lower jaw when the teeth are assumed to act as individual pressure receptor elements. The work in this chapter is based on numerical simulations within Matlab. The construction and testing of a real end-fire array system is also discussed and comparisons between real and simulation results are also presented.

Chapter 4 presents measurement work carried out on a real jawbone, using a variety of techniques. The aim of this work is to define more accurately what happens as sound travels through the lower jaw and teeth of the jaw. This work provides data that can be used in future experiments and modelling work.

Chapter 5 describes the verification of custom TLM modelling software for use in simulating acoustic wave propagation. This software is then benchmarked and used to examine jaw properties that were identified in the earlier chapters of this work. In particular acoustic band gap structures are examined.

Chapter 6 draws conclusions from the work that has been presented and suggests further work that could be performed to further expand on the work within this thesis.

References

[1.1] R. Urick, *Principles of underwater sound for engineers.* McGraw-Hill, 1967.

[1.2] H. Lichte, "On the influence of horizontal temperature layers in sea water on the range of underwater sound signals," *Physik*, vol. 385, no. 17, 1919.

[1.3] A. D. Waite, *Sonar for practising engineers.* John Wiley and Sons Ltd, 3rev ed ed., 3 2002.

[1.4] P. C. Etter, *Underwater acoustic modeling and simulation.* Spons Architecture Price Book, 2003.

CHAPTER 2:
BIOACOUSTICS AND DOLPHIN ECHOLOCATION

BIOACOUSTICS is the study of acoustic energy that is emitted or received by a living biological creature. This can be for a range of purposes such as communication, navigation, object classification and ranging. It has been reported by many authors [2.1, 2.2, 2.3, 2.4] that in the 1770's the Italian scientist Lazzaro Spallanzani observed that bats were capable of avoiding objects in a dark room even when owls were incapable of navigating. He continued to observe that bats which had been visually blinded could still fly with the same precision. This observation was followed up by Swiss scientist Charles Jurine who conducted experiments with bats which gave the first evidence of the use of acoustics in navigation by animals. In this experiment he filled the ears of a bat with wax. He found that the bats became unable to navigate when the ear canal was obstructed and collided with obstacles that they had previously avoided. He concluded that the bats hearing was an important part of the orientation and obstacle avoidance capability, however, he was unsure of the reasons for this dependency, as the bats were completely silent to the human ear.

After the sinking of the Titanic in 1912 Hiram Maxim [1] suggested that icebergs could be located in the same way he hypothesised bats echolocated. He thought that by using low frequencies generated by the flapping of bats wings and listening to the returning echos, icebergs could be detected through the water and avoided. Although it is now known that sound generation takes place in the larynx of a bat [2.6], this is the first documented example of biologically inspired design in underwater acoustics.

It wasn't until 1938 that the correct high frequency mechanism of bat echolocation was

[1] who previously invented the machine gun in 1885 [2.5]

experimentally proven by Pierce and Griffin [2.7]. In their work they describe how they were able to use a recently available piezoelectric microphone and a super heterodyne receiver to down shift the ultrasonic vocalisations of the bat to human audible frequencies. They demonstrated that bats transmitted pulse bursts between 1-2 ms in duration between 30 and 70 kHz. In 1942 Robert Galambos was the first person to publish cochlear potentials evoked when ultrasonic frequencies were used to stimulate the ear of a variety of bat species [2.8] demonstrating their ultrasonic hearing capabilities. This is the first example of a physiological study of a biological sonar system and was one of the pivotal works on the subject that laid proof for echolocation in bats.

Following the work on echolocating bats came the discovery of echolocation in Dolphins by McBride in 1947 [2.3]. He observed that at night in turbid conditions during capture exercises, dolphins (The Atlantic Bottlenose Dolphin) were able to evade fine nets that were masked by the darkness. This reminded him of the way in which bats were able to navigate around room void of light. He is also reported to have noted that dolphins were able to identify gaps in the nets and move through them even though this was beyond their visual capabilities. It is this capability that has caused scientists up to the present day to be fascinated by the abilities of the dolphin sonar system.

2.1 Early Biosonar Discoveries

In 1961 Kenneth Norris was the first person to conduct an experiment with a Bottlenose Dolphin to prove without doubt that dolphins did use echolocation to navigate and locate [2.9]. In his experiment he trained a dolphin to navigate across a tank of water and to avoid metal poles and other obstacles that were present. The test was then repeated with suction cups placed over the eyes of the animal to inhibit the use of its visual system. The poles were rearranged to verify that the dolphin was not navigating from memory, the dolphin completed the task successfully, while emitting ultrasonic signals and avoiding the obstacles, proving that dolphins could navigate without the use of eyesight.

In 1962 Evans and Prescott [2.10] were the first people to report that a Atlantic Bottlenose Dolphin was capable of transmitting 'low frequency whistle like cries' at the same time as producing echolocation clicks. From this they concluded that unlike bats, dolphins possess a system that is capable of using two domains of sound simultaneously and that this may work in the same way that humans use taste and smell. This lead to a great deal of research into the dolphin sound production system and the dual sound production theory.

In 1964 and 1968 Norris published the founding papers on the sonar systems of Cetaceans [2.11, 2.12]. His work documents what was known about dolphin echolocation and narrates the dolphin's evolution from being a land based species back in to the sea. This was one of the first pieces of work that studied the dolphin physiology in depth and to highlight the morphological features that form the echolocation reception system. Using experimental recordings it was shown that Dolphins emitted click trains in the region of 0.7-2.4 ms duration, with an extremely broadband frequency content. Further experimental evidence showed that sound was projected forward of the head of the dolphin in a narrow beam. The main projection area was hypothesised as being located behind the forehead and not out of the larynx as in other mammals. This was based upon work carried out by Evans and Prescott [2.10] who had noted that the sound intensity reached a peak level when a receiver was positioned in front of the forehead of the animal and was lower at the larynx.

When observing the skull of a porpoise that had washed up on the shore in Mexico, Norris noted that the lower jawbone was constructed from a pair of hollow channels with a sponge like bone material that was filled with blood and fatty oils. As the bone approached the ear, it formed a pair of very narrow homogeneous bones. When this section of bone was held up to the sunlight he observed the light passing through a specific oval shaped area (labelled k in Figure 2.1). This area he termed the 'Acoustic Window'. He hypothesised that this area was thin enough to allow sound to pass directly through and be coupled by the surrounding fat to the inner ear of the animal. When examining a number of different species of odontocete this jaw structure was

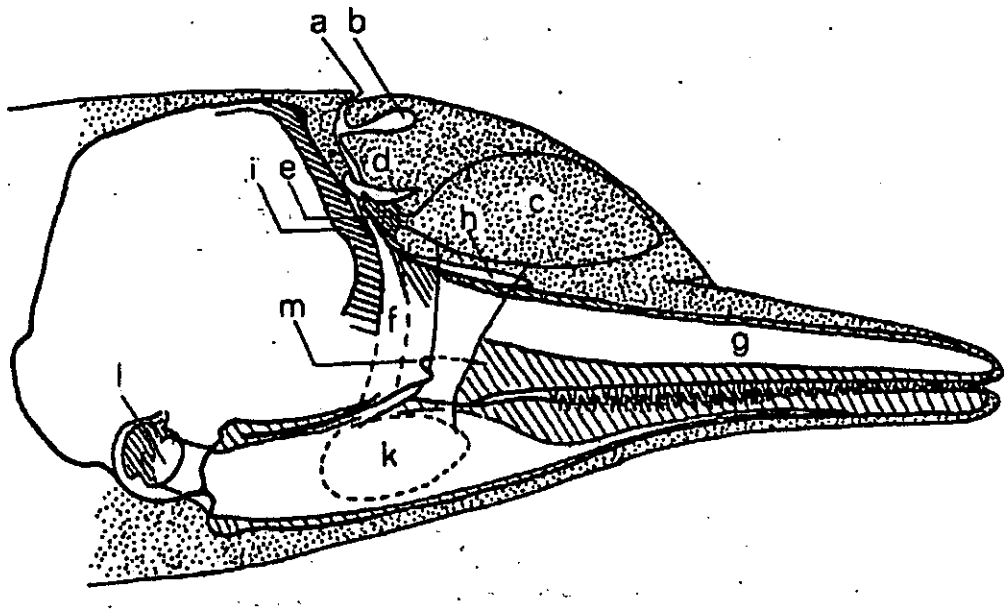

Figure 2.1: Structures in the dolphin head, reproduced from Norris [2.12]. a, blowhole; b,vestibular sac; c, melon; d, tubular sac; e, nasal valve with lip entering tubular sac; f, internal nares; g, mesorostral cartilage; h, premaxillary nasal sac; i, cribriform plate; k, Acoustic window in the mandible, and the site of overlaying fatty window.

also evident. On closer examination the acoustic window was overlapped by soft tissue devoid of muscle fibres with an oval fatty material which matched the area of the thinnest bone. From this he speculated that this could aid the sound transmission by impedance matching the incoming sound to the bone and then back into the inner ear.

2.2 *The Dolphin*

Dolphins come in a variety of species, however they are fundamentally similar, with the notable exception of river dolphins such as the Ganges river dolphin, which are not considered in this thesis. They are all carnivorous animals that travel the seas and oceans as single animals or as packs of up to a few hundred. Although dolphins are an

aquatic mammals that don't often leave the water [2], they still possess an excellent visual ability in air, where they are able to tell the difference between complex shape at ranges above 100 m . The visual sense is the parallel of its echolocation system in water. There has been a great deal of research into target discrimination by the Bottlenose Dolphin including work by Pack and Herman [2.13]. They suggest that the acoustic system allows for an acoustic imaging capability. In their work they show that the dolphin is able to interchangeably identify a target in air with its eye sight and then identify the same target in water using echolocation.

2.3 Sound Transmission System

Although the main objective of this thesis is to examine the reception system of the Bottlenose Dolphin, the characteristics of the transmission system have a direct impact on how the reception systems operates, and thus a basic overview will be presented here.

2.3.1 Transmission Source

There have been many questions raised over the years about the methods of sound production in dolphins. The dual source theory is now well established thanks to the work of Evans *et al.* [2.10] and Norris *et al.* [2.14]. Norris used X-ray motion pictures to observe the movement of the nasal sac and the larynx during high frequency sound production. They found that the movement in the nasal sac correlated with high frequency sound emissions and did not correlate with the larynx theory. They continued this work further and concluded that the larynx is not used in high frequency (>30 kHz) sound production. This work was validated by a number of further studies that used a variety of techniques to measure the change in air build up and pressure before, during and after sound emission in both the larynx and in the nasal sac. The nasal sac can be seen in Figure 2.1.

[2] unlike seals

Dormer [2.15] presented a list of twenty references that suggest possible sites of sound production in various species of dolphins. He surmised from this literature that the most probable two sites for sound production were the larynx and the nasal sac system.

Cranford *et al.* [2.16, 2.17], took advantage of modern advances in medical Computed Tomography (CT) and Magnetic Resonance Imaging (MRI) as well as using more conventional dissection techniques to help locate the actual source of sound production. Using frozen but otherwise unblemished specimens of 19 different species, Cranford identified 'a small pair of fatty bursae embedded in a pair of connective tissue lips, a cartilaginous blade, a stout ligament, and an array of soft tissue air sacs'. They found that this structure was present in all echolocating toothed whales in their sample set. This morphological feature is commonly referred to as the Monkey Lip Dorsal Bursae (MLDB) complex, this area is identified on the CT slice shown in Figure 2.2. When air is massed through this structure the lips vibrate and slap together, he hypothesised that this could create repeatable and controllable clicks.

Goodson *et al.* [2.18] contradicted this theory, favouring the theory that cavitation occurs when bursae in the MLDB are ripped apart under muscle control. This in turn releases a reservoir of high pressure air and an implosion of bubbles create a high energy source to cause a click.

2.3.2 *Transmission Beam Forming*

The CT data obtained by Cranford *et al.* [2.16] allowed other researchers to examine the effect of the melon structure on the sound transmission system. Aroyan [2.19] used the data set from a Common Dolphin *Delphinus delphis* and was able to linearly map the CT Hounsfield units to density, then assuming a linear correlation between density and sound velocity constructed a three dimension numerical model. This geometry was then used in Finite Difference Time Domain (FDTD) modelling in which a continuous sine wave of 75 kHz was injected at a point source near the site of the MLDB. From this the emerging beam pattern was obtained. Flint *et al.* [2.20] used a 2 dimensional slice of the CT data for a Harbour Porpoise (*Phocoena phocoena*) and applied the

Figure 2.2: A CT slice of a Bottlenose Dolphin taken through the Central axis of a dolphin.

Transmission Line Modelling algorithm to examine the propagation. They established that the melon acted as a beam former for the outgoing sound wave in this animal. The authors used a piston excitation in the space behind the melon (shown in the top left of Figure 2.3) which produced an outgoing wave in the near field, which was flattened out as it passes through the melon and obtains far-field conditions at the tip of the rostrum. This effect can be seen in Figure 2.3 in a series of snap shots at different time intervals. A sound speed of 1273 - 1376 m/s have been reported at the Central core of the melon of a Bottlenose Dolphin and 1682 m/s towards the outer shell [2.21]

More recently Houser *et al.* [2.22], using CT and MRI techniques were able to scan a living Dolphin under sedation. The advantage of using a live dolphin is that the air sacs that are distributed around the forehead and the ear structure remain in their original shape. In earlier studies the specimens were post-mortem and these structures were changed by the freezing and thawing process. It was also possible to use Single Photon Emission Computed Tomography (SPECT) and Positron Emission Tomography (PET). The combination of these techniques and increased resolution provided further proof that the MLDB is the pneumatic echolocation click source. The scans showed that air sacs are displaced around the head which would successfully isolate the click source from the receiving ear. Using SPECT the blood flow around the animal was also anal-

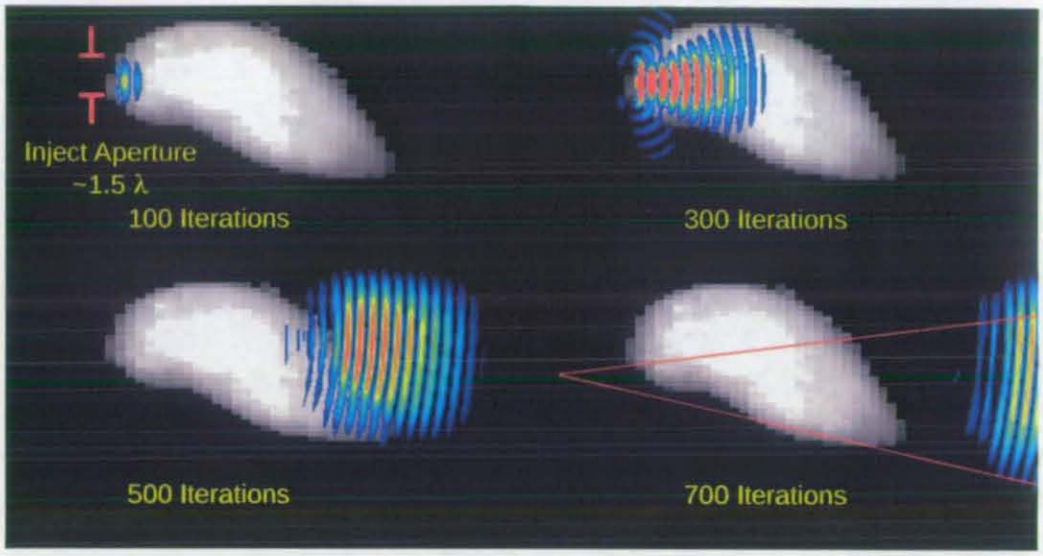

Figure 2.3: A series of snap shots of sound propagating through the melon of a Harbour Porpoise

ysed. This showed high levels of blood flow around the brain, the lower jawbone and the melon. Houser suggests that the reason for high blood flow in the melon and lower jaw is to regulate the temperature of the fatty lipids contained within these structures which are used in echolocation. This is desirable as Fitzgerald [2.23] showed that sound speed in lipids is inversely proportional to temperature. If dolphins could not control the temperature of the focusing lens, then changes in water temperature due to changes in dive depth and seasonal variation would alter the click propagation characteristics, by maintaining the temperature the wave guide properties remain constant.

2.3.3 Transmission Signals

Dolphin signals were recorded and examined by Evans *et al.* [2.24]. In this paper the three operation bands are defined for a number of species and evidence is presented that each of the bands can be used interchangeably. As the main area of interest in this thesis is echolocation, click type signals that emanate from the MLDB will be examined. Table 2.1 defines the acoustic spectrum used by the dolphin and the associated application. Signals below 30 kHz are believed to emanate from the larynx [2.16].

Evans *et al.* [2.24] also presented beam patterns for the acoustic emissions from the Bottlenose Dolphin. They noted that when examining each click on a pulse to pulse basis that the pattern changed and there was an energy difference of 'several dB.' This lead them to conclude that the animal possessed a beam forming capability. The experiments of Evans were performed on a captive animal in a shallow water environment. The source level of the peak to peak click was reported to be an average of 170 dB re 1μPa at 1m with the peak energy being at 52 kHz. Au *et al.* [2.25] measured the echolocation clicks of free range dolphins during target detection tasks. They showed that free ranging dolphins have a higher SL than captive animals in reverberant environments. They measured the average peak–to–peak signal of 220 dB re 1μPa. They concluded that the change in amplitude could be due to the different environmental situation. Evans conducted his test in a reverberant swimming pool whereas Au conducted his trials in open waters situated in a busy harbour. This suggests the ability of the animal to control the amplitude of its output. Au's work again showed a difference in the peak levels that were seen by Evans. The most important observation of Au's was that the frequency content was seen to have the peak energy focused at a frequency between 120 kHz and 130 kHz which was much higher than previously thought. Au [2.26] measured the clicks of a Beluga whale in San Diego bay before relocating the animal to the Kaneohe Bay, which has a higher ambient noise level. The whale was observed to increase its click energy by 17 dB re 1μPa while the peak energy moved from being focused at 40 kHz to 60 kHz up to 100 kHz to 120 kHz. This demonstrates how echolocating animals are capable of adapting to their environment.

The length of each pulse was reported to be 'fairly uniform' with a pulse duration between 35 to 45 μs. Au agreed with Evans that the dolphin was in complete control of the inter-click period, he measured delays between clicks when the dolphins were at a controlled distance from a target, the inter-click time was always longer than the two-way transit time. A typical Bottlenose Dolphin click recreated from Au [2.3] can be seen in Figure 2.4. Ivanov has since conducted a more in-depth study of the inter click period with a increasingly distant target and drawn the same conclusion [2.27].

Frequency Band	Description	Passive / Active	Function
Coarse Long Range Capability			
200-900 Hz	Phase coherent listening	Passive	Source Location
4-30 kHz barks, yelps, rasps	One way signalling	Active	Intra species communications
Fine short Range Capability			
30-150 kHz	Spatially coherent reflections	Active	Location, Ranging and potential acoustic imaging

Table 2.1: Table of acoustic frequencies used by the Bottlenose Dolphin and their possible uses. The larynx is used to produce the low frequency whistles and the pneumatic MLDB system is used to produce the high frequency echolocation signal.

2.3.4 *Transmission Pattern*

The early work conducted by Norris and Evans [2.28] noted that the sound beam that emanated from in front of the dolphin's forehead was highly focused. Evans *et al.* [2.10, 2.29] examined the corpse of a Spinner Dolphin and placed a continuous wave sound source in the nasal sac complex. He was able to measure the transmission pattern of the source through the melon, and determined that the beam was focused on axis in the horizontal and 15° above the rostrum in the vertical. They also noted the beam width was inversely proportional to the source frequency.

Au [2.30] and Au *et al.* [2.31] measured the vertical and horizontal beam patterns of the high frequency clicks of the Bottlenose Dolphin. The pattern was measured using an array of five hydrophones in both the horizontal and vertical plane. The signals were recorded by stationing the dolphin on a bite plate mid-water and then making it perform a target detection task. Alignment was performed by monitoring the orientation of the

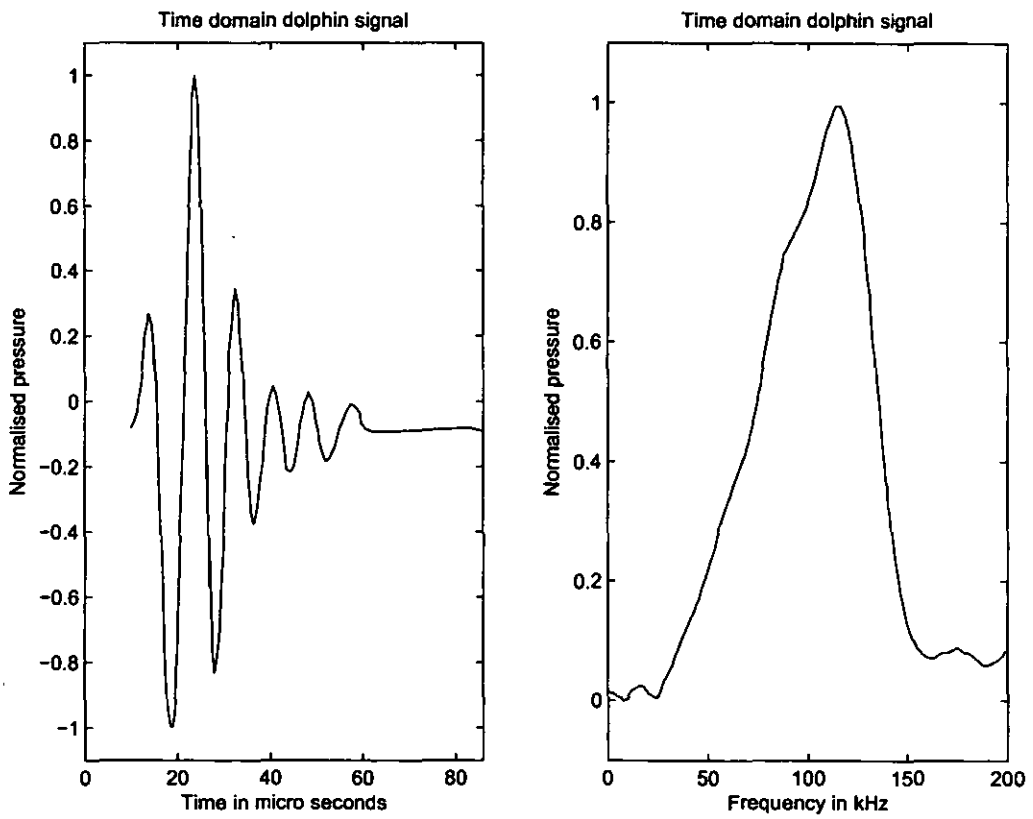

Figure 2.4: A typical Bottlenose Dolphin echolocation signal in a noisy environment and its frequency content. [2.3]

dolphin with an underwater video camera. Beam patterns from Au, Au, Pawloski and Moore, and Au, Moore and Haun are reproduced from [2.3] in Figure 2.5. The 3 dB beam width can be seen as being approximately 10^o in both the horizontal and vertical planes

Work conducted by Moore *et al.* in recent years has demonstrated adaptive control over the focus of the echolocation beam [2.32]. Using a 24 element circular hydrophone array spaced approximately 12^o apart in the horizontal plane and 8^o apart in the vertical planes, echolocation clicks were recorded from a dolphin performing a target detection task. The dolphin was located at a bite plate and presented with a target to echolocate upon. The target was positioned at increasingly greater distances to the left or right of the presumed Maximum Response Axis (MRA) of the echolocation beam. The results

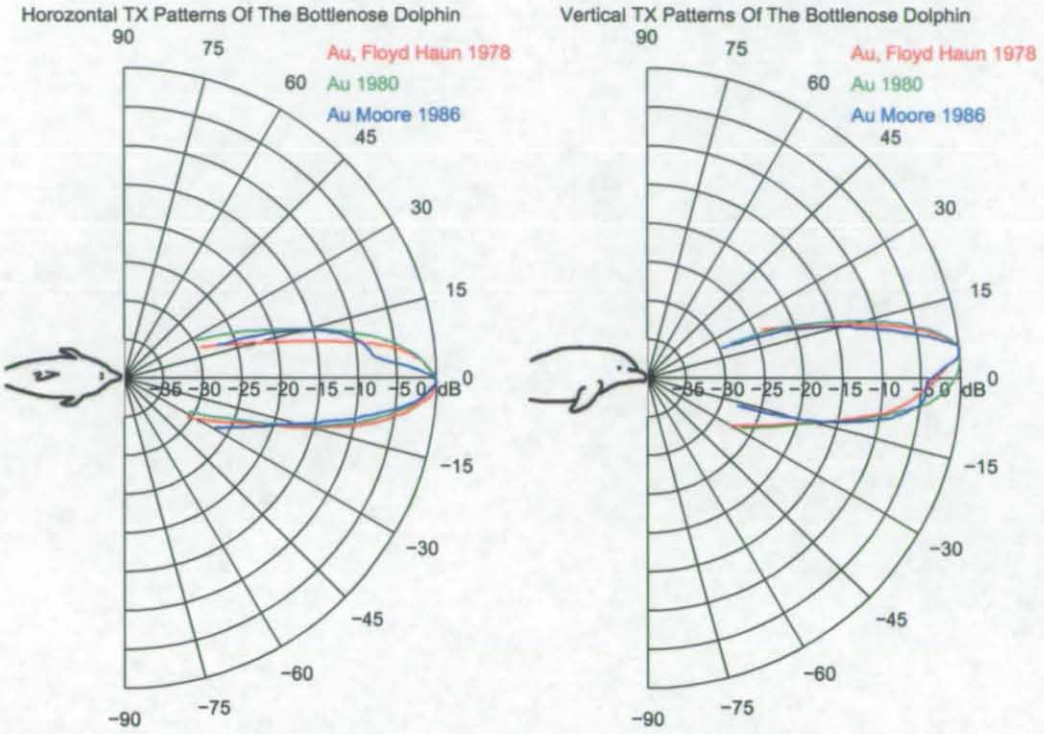

Figure 2.5: Click transmission patters of the Bottlenose Dolphin.

of the study demonstrated not only that dolphins were capable of detecting metal sphere and cylinder targets well off of the MRA of the echolocation beam, 21-26^0 and 13-19^o respectively, but that the dolphin was capable of shifting the focus of the echolocation beam in both the horizontal and vertical planes. There is currently an ongoing study by Houser [2.33] into the suggestion that the dolphin can change the shape of the melon under muscle control. This would have the effect of changing the focus of the melon and alter the beam width.

2.3.5 *Sonar Operation Strategy*

In recent years the advances in electronics and data acquisition systems have allowed more complex measurements of the echolocation click to take place. Martin *et al.* [2.34] constructed an acoustic acquisition system which they named the 'Bio-sonar Measurement Tool (BMT).' This tool measures depth, velocity and the incoming and

outgoing echolocation clicks from free swimming animals during target detection tasks. The equipment is mounted upon a bite plate that the dolphins are trained to carry in it's mouth. A single hydrophone is mounted approximately 1 m from the phonic lips and in line with the presumed MRA. Two receivers are mounted at a separation of 12.5 cm, similar to the separation of the ears, to listen to returning signals and ambient noise. This equipment has allowed researchers to analyse how dolphins change their search strategy for a particular task. Results of search and detect trials using the BMT on two Bottlenose Dolphins demonstrated that considerable variation in search strategies existed for animals performing the same task [2.35]. One animal was searched its environment slowly (greater than 10 s) whilst emitting typical clicks with a peak frequency of 30-60 kHz and always approached the target closely prior to verifying target presence to the human observer. The second animal searched the environment with greater speed (less than 10 s) and produce fewer clicks with a greater variability in its frequency content with the output being anywhere between 20-120 kHz. Both animals increased the power of the echo returning from the target by either increasing the source level of the click or moving closer to the target during final target inspection. Houser suggested that the 'Temporospatial relationships between the animals and the targets during the echolocation task suggested that dolphins often initially detected the target well off the MRA of the echolocation beam and then oriented toward the target for identification.' This behaviour indicates that dolphins have a variability in search strategies from animal to animal as well as the adaptive control of echolocation.

2.4 Reception System

2.4.1 Reception Site

As has already been discussed, Norris [2.28] confirmed that the Bottlenose Dolphin did use echolocation to navigate. In one experiment suction cups were placed over the external ear openings to disturb the sound reception path. Even with the obstruction of the external openings the dolphin continued to echolocate. In 1968 Norris published

Figure 2.6: The Lower Jaw and Acoustic Window (shown dotted) as suggested by Norris [2.11].

data showing the lower jawbone structure of 11 different species of echolocation animal. In all the species examined the lower jaw was a hollow channel containing a fatty tissue which connected to the tympanic bulla of the middle ear. Norris proposed that sound could pass through the thin 'pan bone' region and couple to the ear. The pan bone region is also known as the 'acoustic window', which is shown as a dashed line in Figure 2.6.

Later work which involved electro-physiological studies conducted by Bullock *et al.* [2.36] gave further support to this hypothesis. The acoustically evoked potential was measured when a vibrating source was placed at various locations around the head of the animal. It was found that the maximum response was obtained when the source was placed on the front half of the lower jaw.

McCormick *et al.* [2.37] performed invasive surgery to investigate the physiology of the ear. In these tests they removed the connection from the outer ear to the middle ear (tympanic conus and tympanic membrane) and measured the cochlear potential when a sound vibrator was placed near the animal. The results showed that there was no difference to the cochlear response of the animal. They concluded that the tympanic conus and tympanic membrane played no role in sound reception to the inner ear. They next measured the effect of cutting the tympanic ligament, which connects the ear drum to the malleus of the middle ear. The results showed no effect when this was removed and thus the sound conduction via this path was excluded. In further tests the cochlear response was measured from a vibrational source at various frequencies up to 100 kHz, pressed up against the animal and the maximum response area was plotted. It was found that the maximum response area was below the ear and along the lower jaw

in the vicinity of the acoustic window. They also noted a strong response when the vibrator contacted the teeth of the lower mandible and that the cochlear response varied depending on the driving direction on the tooth. The maximum response was obtained when the tooth was driven in a direction parallel with the jaw and a response of -25 dB at a right angle to the jaw axis. Overall it was demonstrated that the external auditory meatus (ear) played no part in sound reception and added support for the reception of sound via the lower jaw.

Brill [2.38, 2.39] investigated the sound reception area by acoustically shielding the lower jaw of a dolphin and carrying out behavioural studies and acoustic measurements. In these trials the lower jaw of the dolphin was covered with two different types of neoprene. The first type was dense neoprene that is believed to induce approximately 1 dB of attenuation to incoming sound while the second material was air filled neoprene which was believed to attenuate sound in the order of 30 dB. The dolphin had suction cups placed over its eyes so that sight could not influence the navigation and behaviour of the animal. Obstacle avoidance tests were performed with the lower jaw being covered in either one of the two neoprene materials, however the ear openings remained unobstructed. It was found that the animals acoustic transmission waveform was not affected by the acoustic shielding however the animal failed to echolocate when the high attenuation material was worn. This experiment further demonstrates that the larynx was not the main click generation source as the outgoing clicks would have been altered by the presence of the neoprene. More importantly, in the context of this thesis this establishes that sound is indeed received via the lower jaw area. What was not established was the precise position of the reception zone on the jawbone. In the trial, the neoprene covered the entire jawbone including the acoustic window, the teeth and tip of the jaw. As a result it is not possible to be more specific about the main reception site.

The work of Bullcok *et al.* [2.36] lead to the observations by Goodson *et al.* [2.40] that the teeth were periodically spaced and could act as individual pressure transducers. This hypothesis will be followed up in Chapter 3.

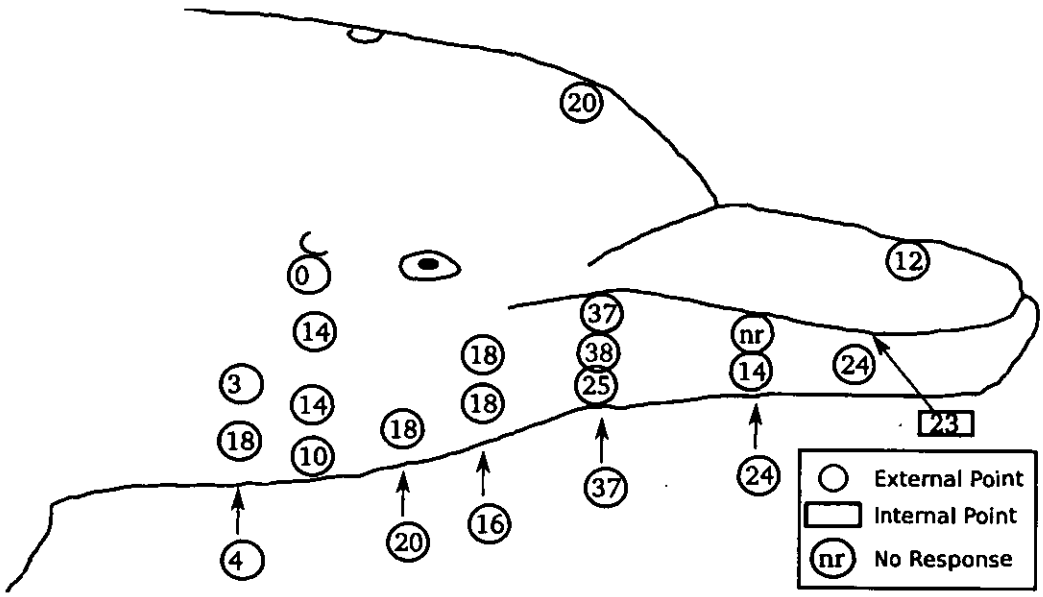

Figure 2.7: ABR results of the sensitivity of a female Bottlenose Dolphin. The values in the circles indicate the attenuation in dB applied to the transmitter to evoke a potential of 1μVpp. Therefore a higher value indicates a greater sensitivity. Reproduced from [2.41]

The sensitivity mapping of the sound reception system was repeated using more modern techniques by Møhl [2.41]. This time a non-invasive technique was employed which utilised the measurement of the Audio Brainstem Response (ABR) [2.33]. A PZT transducer was placed in various locations around the head transmitting a broadband synthetic click with a repetition rate of 10 Hz. The results of this work are recreated in Figure 2.7 They suggest that the region just in front of the acoustic window of the dolphin is the most sensitive. The results also show a significant sensitivity from the front half on the jaw near the rostrum which could indicate multiple sound paths. It was also noted that the propagation delay down this path was longer than expected for the construction tissues and the path length. This will be examined in more detail in Chapter 5

Section 2.3.2 discussed the structure of the melon and the ability of the graded density lipids to impedance match and shape the beam of the outgoing signal. Koopman *et el.* [2.42] have shown that a similar structure exists towards the rear of the pan bone. They

have shown that a similar structure of fatty lipids exists around the acoustic window, which could serve to increase directivity and to reduce or nullify the impedance mismatch between water and the pan bone. However at the current stage the exact function of these materials is uncertain.

2.4.2 Reception Sensitivity

The first studies to identify the audiogram of the Bottlenose Dolphin were conducted by Johnson [2.43] as reported by Au [2.3]. Figure 2.8 shows the audiogram of a Bottlenose Dolphin plotted from Johnson's data. Johnson used the same approach that is used to measure the heating ability of humans. A 2 second tone was played and the dolphin responds with a 'yes' or 'no' response[3] if a tone is heard. The level of the tone is decreased and increased until the minimum threshold level is found and repeated 10 times. Johnsons results show that the Dolphin is capable of hearing continuous tones from 75 Hz up to 150 kHz. Since this first experiment, others have repeated the tests with different methodologies including the modern technique of the ABR [2.44], all of which broadly agree with Johnsons' original observations.

2.4.3 Reception Pattern

There have been various studies to investigate the reception beam pattern of the dolphin in order to understand how the dolphin achieves its exceptional shallow water echolocation skills. The results from trials conducted by Au, Au and Moore [2.45, 2.46, 2.3] on a captive Atlantic Bottlenose Dolphin can be seen in Figure 2.9. The tests were conducted by training a Bottlenose Dolphin to station itself on a bite plate, and then transmitting a tonal signal and a masking noise. The difference in intensity between the tonal and the masking noise as a function of angle was measured, until the maximum difference was obtained and repeatable. This avoids the need for invasive physical measurements. The masked hearing threshold is directly related to the hearing sensi-

[3] This is indicated by the animal touching different paddles.

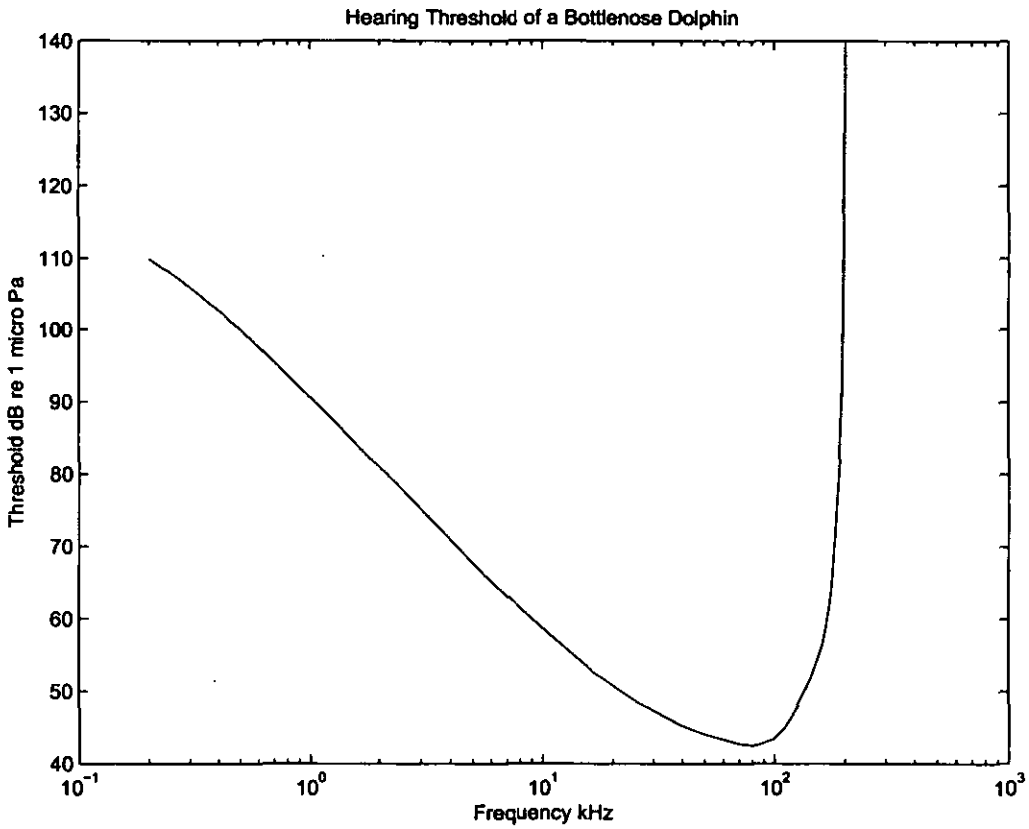

Figure 2.8: Audiogram of an adult Bottlenose Dolphin from the work by Johnson [2.43].

Frequency kHz	Horizontal -3 dB width	Vertical -3 dB width
30	59.1^{o}	30.4^{o}
60	32.0^{o}	22.7^{o}
120	13.7^{o}	17.0^{o}

Table 2.2: The 3 dB beam widths of the Bottlenose Dolphin, reproduced from [2.46].

tivity. A summary of reception beam patterns is shown in Table 2.2, reproduced from experimental results of Au and Moore [2.46].

The vertical receiver pattern shows a sharper decline above the head then below, which seems to be in good agreement with the hypothesis of hearing via the lower jaw. The

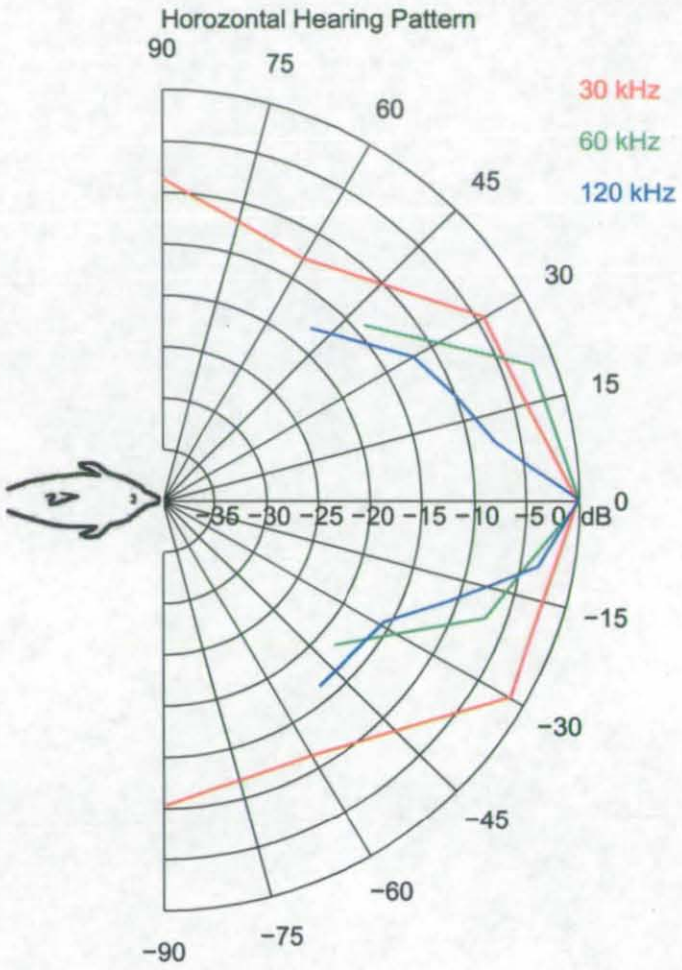

Figure 2.9: The horizontal hearing pattern of the Atlantic Bottlenose Dolphin, performed by Au and Moore [2.3]

pattern also shows the the main response angle is 15^o-25^o above the central axis of the head, when the zero point is taken at the centre of the pan bone. The horizontal pattern also shows asymmetry around the central axis. In both planes the pattern narrows as the frequency increases. This allows the animal to use different frequency bands for different activities. The narrow beam patten is highly desirable when trying to locate a target in a noisy reverberant environment. The use of a narrow beam would also be desirable when combined with a physical sweeping technique that is often used by dolphins during target detection tasks.

2.4.4 Conclusion

The dolphin exploits its broadband acoustic system to perform a range of tasks, and social interactions. They are capable of detecting a 76.2 mm stainless steel sphere at a distance of 119 m [2.47], discriminate between aluminium, copper, and brass circular targets; between circles, squares, and triangular targets; and can recognise aspect-dependent objects at a variety orientations [2.47, 2.48, 2.49]. The Bottlenose Dolphin and cetaceans in general have a well matched transmitter and receive pattern and sensitivity which use their energy resources efficiently. The signal transmitted towards a target by the dolphin appears to be very versatile allowing the gathering of direction, speed and acceleration and represents the result of millions of years of evolution.

Dolphins have been credited with having a high performance sonar detection and classification system for many years and are now regularly deployed in hostile situations for the detection of mines, buried objects and other objects [2.34, 2.50]. Gaining an understanding as to how these systems operate could potentially enhance human ability to operate in difficult shallow water reverberant environments. Some work on recreating this sonar system is underway [4]

Whilst the current trend in cetacean research is to examine what signal processing might be taking place in the dolphin brain, the aim of this thesis is to examine the signal processing within the physical structure of the dolphin skull. The viability of some current ideas will be examined and then some novel measurement techniques used to look for previously uncharacterised properties. Finally numerical computer simulations using CT data will be shown which shed new light on the role of the lower jaw in echolocation.

[4] A Dolphin Based Sonar has been implemented by the U.S. Navy constructed from a single piston transducer with a 12° beamwidth at 110 kHz and side lobes below 17 dB along with twin receivers with 20° 3 dB beamwidths at 110 kHz and a separation of 12.5 cm [2.50].

References

[2.1] R. Galambos, "The avoidance of obstacles by flying bats: Spallanzani's ideas (1794) and later theories," *Isis*, vol. 34, no. 2, pp. 132–140, 1942.

[2.2] D. R. Griffin, *Listening in the dark: The acoustic orientation of bats and men.* Yale University Press. New Haveu (Reprinted in New York), 1958.

[2.3] W. W. L. Au, *The sonar of dolphins.* New York: Springer-Verlag, 1 ed., 1993.

[2.4] G. Jones, "Echolocation," *Current Biology*, vol. 15, no. 13, pp. 484–488, 2005.

[2.5] K. Graff, "Historical highlights in ultrasonics - 2," *Frequency Control Symposium and Exposition, 2004. Proceedings of the 2004 IEEE International*, pp. 5–10, 23-27 Aug. 2004.

[2.6] G. Jones and E. C. Teeling, "The evolution of echolocation in bats," *Trends in Ecology & Evolution*, vol. 21, no. 3, pp. 149–156, 2006.

[2.7] G. W. Pierce and D. R. Griffin, "Experimental determination of supersonic notes emitted by bats," *Journal of Mammalogy*, vol. 19, no. 4, pp. 454–455, 1938.

[2.8] R. Galambos, "Cochlear potentials elicited from bats by supersonic sounds," *The Journal of the Acoustical Society of America*, vol. 14, no. 1, pp. 41–49, 1942.

[2.9] K. S. Norris, J. H. Prescott, P. V. Asa-Dorian, and P. Perkins, "An experimental demonstration of echolocation behavior in the porpoise, tursiops truncatus (montagu)," *Biological Bulletin*, vol. 120, pp. 163–176, 1961.

[2.10] W. E. Evans and J. H. Prescott, "Observations of the sound production capabilities of the bottlenose porpoise: A study of whistles and clicks," *Zoologica*, vol. 47, no. 12, pp. 1–128, 1962.

[2.11] K. S. Norris, "Some problems of echolocation in cetaceans," *Marine Bioacoustics*, vol. 2, pp. 317–336, 1964.

[2.12] K. S. Norris, "The evolution of acoustic mechanisms in odontocete cetaceans," *Evolution and Environment*, pp. 298–323, 1968.

[2.13] A. A. Pack and L. M. Herman, "Sensory integration in the bottlenose dolphin: Immediate recognition of complex shapes across the senses of echolocation," *The Journal of the Acoustical Society of America*, vol. 98, no. 2, pp. 722–733, 1995.

[2.14] K. S. Norris, K. J. Dormer, J. Pegg, and G. T. Liese, "the mechanism of sound production and air recycling in the porpoise.," in *Conference on Biological Sonar Diving Mammals*, vol. 8, pp. 659–664, 1971.

[2.15] K. J. Dormer, "Mechanism of sound production and air recycling in delphinids: Cineradiographic evidence," *The Journal of the Acoustical Society of America*, vol. 65, no. 1, pp. 229–239, 1979.

[2.16] T. W. Cranford, M. Amundin, and K. S. Norris, "Functional morphology and homology in the odontocete nasal complex: Implications for sound generation," *Journal of Morphology*, vol. 228, no. 3, pp. 223–285, 1996.

[2.17] T. W. Cranford, "In search of impulse sound sources in odontocetes," *Hearing by Whales and Dolphins, edited by W. Au, A. Popper, and R. Fay (Springer-Verlag, New York)*, pp. 109–156, 2000.

[2.18] A. D. Goodson, J. A. Flint, O. Farooq, and S. Datta, "An ultrasonic marine animal - the harbour porpoise (phocoena phocoena)," *Journal of the Acoustical Society of India*, vol. 30, no. 3-4, pp. 284–289, 2002.

[2.19] J. L. Aroyan, *Three–dimentional numerical simulation of biosonar signal emission and reception in the Common Dolphin*. PhD thesis, University of California at Santa Cruz, 1996.

[2.20] J. A. Flint, A. D. Goodson, G. Leonard, and S. C. Pomeroy, "Transmission line modelling of the harbour porpoise (phocoena phocoena) melon," *Journal of the Acoustical Society of India*, vol. 30, no. 3–4, pp. 294–297, 2002.

[2.21] K. S. Norris and G. W. Harvey, "Sound transmission in the porpoise head," *The Journal of the Acoustical Society of America*, vol. 56, no. 2, pp. 659–664, 1974.

[2.22] D. S. Houser, J. Finneran, D. Carder, W. Van Bonn, C. Smith, C. Hoh, R. Mattrey, and S. Ridgway, "Structural and functional imaging of Bottlenose Dolphin (Tursiops truncatus) cranial anatomy," *Journal of Experimental Biology*, vol. 207, no. 21, pp. 3657–3665, 2004.

[2.23] J. W. Fitzgerald, "The LarynxMelonVestibular Lips (LMVL) model of the dolphin sonar. II. The melon beam former," *The Journal of the Acoustical Society of America*, vol. 105, no. 2, pp. 1262–1263, 1999.

[2.24] W. E. Evans, "Echolocation by marine delphinids and one species of freshwater dolphin," *The Journal of the Acoustical Society of America*, vol. 54, no. 1, pp. 191–199, 1973.

[2.25] W. W. L. Au, R. W. Floyd, R. H. Penner, and A. E. Murchison, "Measurement of echolocation signals of the Atlantic Bottlenose Dolphin, Tursiops truncatus Montagu, in open waters," *The Journal of the Acoustical Society of America*, vol. 56, pp. 1280–1290, 1974.

[2.26] W. W. L. Au, D. A. Carder, R. H. Penner, and B. L. Scronce, "Demonstration of adaptation in beluga whale echolocation signals," *The Journal of the Acoustical Society of America*, vol. 77, no. 2, pp. 726–730, 1985.

[2.27] M. P. Ivanov, "Dolphin echolocation signals in a complicated acoustic environment," *Acoustical Physics*, vol. 50, no. 4, pp. 469–479, 2004.

[2.28] K. S. Norris, J. H. Prescott, P. V. Asa-Dorian, and P. Perkins, "An experimental demonstration of echo-location behavior in the porpoise, tursiops truncatus (montagu)," *Biological Bulletin*, vol. 120, no. 2, pp. 163–176, 1961.

[2.29] W. E. Evans, W. W. Sutherland, and R. G. Beil, "The directional characteristics of delphinid sounds," *Marine Bioacoustics*, 1964.

[2.30] W. W. L. Au, R. W. Floyd, and J. E. Haun, "Propagation of atlantic Bottlenose Dolphin echolocation signals," *The Journal of the Acoustical Society of America*, vol. 64, no. 2, pp. 411–422, 1978.

[2.31] W. W. L. Au, P. W. B. Moore, and D. Pawloski, "Echolocation transmitting beam of the Atlantic Bottlenose Dolphin," *The Journal of the Acoustical Society of America*, vol. 80, no. 2, pp. 688–691, 1986.

[2.32] P. W. Moore, D. S. Houser, and L. A. Dankiewicz, "Off-axis target detection by an echolocating bottlenose dolphin," *Symposium on Bio-sonar Systems and Bio-acoustics*, vol. 26, April 2004.

[2.33] D. S. Houser, "Current research trends in cetaceans bioacoustics," *Symposium on Bio-sonar Systems and Bio-acoustics*, vol. 29, no. 3, 2007.

[2.34] S. W. Martin, M. Phillips, E. J. Bauer, P. W. Moore, and D. S. Houser, "Instrumenting free-swimming dolphins echolocating in open water," *The Journal of the Acoustical Society of America*, vol. 117, no. 4, pp. 2301–2307, 2005.

[2.35] D. S. Houser, S. W. Martin, E. J. Bauer, M. Phillips, T. Herrin, M. Cross, A. Vidal, and P. W. Moore, "Echolocation characteristics of free-swimming Bottlenose Dolphins during object detection and identification," *The Journal of the Acoustical Society of America*, vol. 117, no. 4, pp. 2308–2317, 2005.

[2.36] T. H. Bullock, A. D. Grinnell, E. Ikezono, K. Kameda, Y. Katsuki, M. Nomoto, O. Sato, N. Suga, and K. Yanigasawa, "Electrophysical studies of the central auditory mechanisms in the cetaceans," in *Vergleich. Physiol*, vol. 79, pp. 117–156, 1968.

[2.37] J. G. McCormick, E. G. Wever, and J. Palin, "Sound conduction in the dolphin ear.," *The Journal of the Acoustical Society of America*, vol. 48, pp. 1418–1428, Dec. 1970.

[2.38] R. L. Brill, *The jaw hearing dolphin: preliminary behavioural and acoustical evidence*, pp. 281–287. Animal Sonar: Processes and performance, NY: Plenum, 1988.

[2.39] R. L. Brill and P. J. Harder, "The effects of attenuating returning echolocation signals at the lower jaw of a dolphin (Tursiops truncatus)," *The Journal of the Acoustical Society of America*, vol. 89, no. 6, pp. 2851–2857, 1991.

[2.40] A. D. Goodson and M. Klinowska, *A proposed receptor for he bottlenose dolphin (Tursiops truncatus) modelling the receive directivity from tooth and lower jaw geometry*, pp. 255–267. NATO ASI Series A Sensory Abilities of Cetaceans, Plenum, 1990.

[2.41] B. Møhl, W. W. L. Au, J. Pawloski, and P. E. Nachtigall, "Dolphin hearing: Relative sensitivity as a function of point of application of a contact sound source in the jaw and head region," *The Journal of the Acoustical Society of America*, vol. 105, no. 6, pp. 3421–3424, 1999.

[2.42] H. N. Koopman, S. M. Budge, D. R. Ketten, and S. J. Iverson, "Topographical distribution of lipids inside the mandibular fat bodies of odontocetes: remarkable complexity and consistency," *Oceanic Engineering, IEEE Journal of*, vol. 31, no. 1, pp. 95–106, 2006.

[2.43] S. C. Johnson, "Sound detection threshold in marine mammals," *Marine Bioacoustics*, pp. 247–260, 1967.

[2.44] R. L. Brill, P. W. B. Moore, and L. A. Dankiewicz, "Assessment of dolphin (Tursiops truncatus) auditory sensitivity and hearing loss using jawphones," *The Journal of the Acoustical Society of America*, vol. 109, no. 4, pp. 1717–1722, 2001.

[2.45] W. W. L. Au, "Echolocation signals of the atlantic Bottlenose Dolphin (Tursiops truncatus) in open waters," *Animal Sonar Systems, edited by RG Busnel and JF Fish (Plenum, New York)*, pp. 251–282, 1980.

[2.46] W. W. L. Au and P. W. B. Moore, "Receiving beam patterns and directivity indices of the Atlantic Bottlenose Dolphin Tursiops truncatus," *The Journal of the Acoustical Society of America*, vol. 75, no. 1, pp. 255–262, 1984.

[2.47] W. W. L. Au and K. J. Snyder, "Long-range target detection in open waters by an echolocating Atlantic Bottlenose Dolphin (Tursiops truncatus)," *The Journal of the Acoustical Society of America*, vol. 68, no. 4, pp. 1077–1084, 1980.

[2.48] C. E. Hammer Jr and W. W. L. Au, "Porpoise echo-recognition: An analysis of controlling target characteristics," *The Journal of the Acoustical Society of America*, vol. 68, no. 5, pp. 1285–1293, 1980.

[2.49] W. W. L. Au and D. A. Pawloski, "Cylinder wall thickness difference discrimination by an echolocating Atlantic Bottlenose Dolphin," *Journal of Comparative Physiology A: Sensory, Neural, and Behavioral Physiology*, vol. 170, no. 1, pp. 41–47, 1992.

[2.50] D. S. Houser, S. Martin, M. Phillips, E. Bauer, T. Herrin, and P. Moore, "Signal processing applied to the dolphin-based sonar system," in *OCEANS*, vol. 1, pp. 297–303, 2003.

CHAPTER 3:

CONSIDERATION OF THE DOLPHIN LOWER JAW AND TEETH AS A PASSIVE ACOUSTIC ARRAY

TO begin the work for this PhD the examination of some current theories of sound reception in the Bottlenose Dolphin will be conducted. This work uses well defined and tested analytical techniques to study the conventional hearing models in addition to some more unconventional hearing hypotheses such as sound reception via the teeth. This is done so that the current research can be evaluated and refinements can be suggested for further work. The work in this chapter is split into two sections. The first section examines some of the common acoustic arrays that can be compared to the dolphin's sound reception system and examines the properties of these arrays using known analytical solutions. The second section then demonstrates via experimentation, the tooth array that has been hypothesised by Goodson *et al.* [3.1] and validates these results against analytical predictions. Beam patterns of the receiver system are presented and discussed in Section 2.4.3.

3.1 Background

There is evidence that man-made sonar systems are outperformed by echolocating marine species in certain situations. This has been demonstrated by the breadth of research carried out in both academic and military establishments over the last 50 years, [3.2, 3.3, 3.4]. Since 1959 the United States military has operated a Mammal Maritime

unit based in San Diego California which uses trained Marine Mammals including Bottlenose Dolphins and Sea Lions to hunt out objects such as mines and hostile divers in shallow waters, rivers and oceans [3.5]. These animals are trained to carry out difficult, dangerous or covet tasks such as locating suspicious devices and marking them with buoy's or restraining hostile divers for inspection or capture by their human handlers. Developing a better understanding of the capabilities that dolphins possess has the potential to influence the future of man made sonar for the better. If it were possible to replicate the performance of these systems then it would reduces our dependency upon these animals.

Goodson *et al.* [3.1] first hypothesised that dolphins could use their teeth as individual pressure transducers. This was based upon the observation that the teeth in the Atlantic Bottlenose Dolphin as well as the Harbour Porpoise are regularly spaced. For most of the jaw they are positioned in a straight line, potentially forming a linear array, however there is a certain amount of curvature towards the tip of the rostrum to account for the shape of the jaw. Figure 3.1 shows a jaw cast taken from an adult Atlantic Bottlenose Dolphin with a metric ruler placed alongside. Potter and Taylor however modelled the teeth as points on a parabolic curve [3.6]. Measurements of tooth casts from adult dolphins indicate that the spacing between the teeth of the Bottlenose Dolphin are approximately 11.4 mm. Assuming a sound speed in sea water of approximately 1475 ms^{-1} and that the inter-dental spacing is equivalent to one wavelength this would suggest an operating frequency of 130 kHz which is close to the maximum observed sonar emission frequency of the Bottlenose Dolphin (see Figure 2.4). The idea that the teeth could operate as passive elements was based on the structural similarity between the jaw and a travelling wave antenna. The Yagi antenna for example has passive rods that are periodically spaced to introduce gain. Yagi antennas typically operate over a relatively small bandwidth while having a high directivity. Therefore the idea of a passive array of this type appears controversial for a relatively broadband animal like the dolphin. However in reality the animal has two such receptors and it will be shown later that the passive array theory is credible when the patten changes are considered. For the current chapter it is worth considering further the possibility that the teeth are acting as

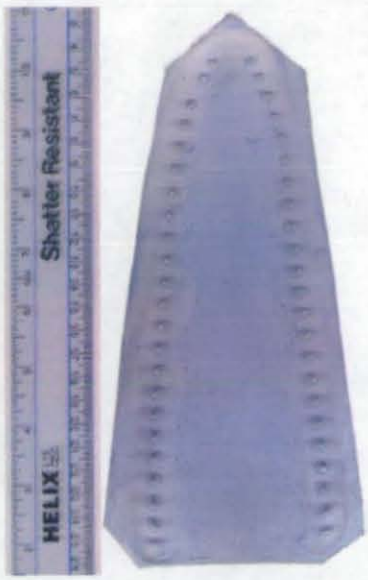

Figure 3.1: Dental Jaw Cast from an Atlantic Bottlenose Dolphin

individual receivers. This is very reasonable and logical approach from a sonar viewpoint as arrays of this type have been used extensively in man made sonar for many years.

3.2 Theory Of The Lower Jaw As An Acoustic Transducer

In this section some basic acoustic theories based on the dolphin morphology will be considered.

3.2.1 Two Element Array Models

The initial suggestion by Norris [3.7, 3.8] is that the dolphins receives sound via the lower jaw through the acoustic pan bone region at the rear of the lower jawbone, as has been illustrated previously in Figure 2.6. This pan bone region can be crudely approximated as a line array of 2 omni-directional elements that are individually separated by approximately 10 cm. This dimension has been confirmed from CT scan data provided by Houser and published in [3.9]. Using the analytical solution for a two omni-direction

hydrophones [3.10] shown in Equation 3.1 it is possible to plot the array pattern. This produces a beam pattern which can be seen in Figure 3.3. In the equation d is the element separation, θ is the beam angle and λ is the wavelength. This pattern demonstrates that there is no usable single beam available from processing the arriving signal as a summed line array with two omni-directional elements due to the high number of side lobes with equal sensitivity.

$$Gain\ dB(\theta) = 20 \log \left(\cos(\frac{\pi d}{\lambda} sin\theta) \right) \tag{3.1}$$

3.2.2 Piston Model

The acoustic pan bone region on the Atlantic Bottlenose Dolphin as observed by Norris is an oval shaped region approximately 7 cm long and 4 cm high. Assuming this is a cylindrical piston transducer with a radius of 5 cm (approximately equal surface area) and using an element separation of 10 cm, the beam pattern can be calculated from a pair of forward facing coplannar transducers using an analytical solution. A single radial piston transducer can be modelled using a Bessel function, and a pair can be considered in the manner described by Urick [3.11] to produce the analytical solution for the beam pattern shown in Figure 3.4. Note that 0^o is defined as the broadside to the array as shown in Figure 3.2. The pattern produced could be very useful as narrow beam patterns can be obtained over a wide frequency range and compares well with the hearing patterns of a dolphin shown in Figure 2.9. Dolphins are known to have a sensitivity to signals 10 dB below their maximum sensitivity [3.2]. In the 2-element piston array there are side lobes present above 10 dB which depending upon the returning signal strength, could still be detected by the dolphin and could be an undesirable characteristic.

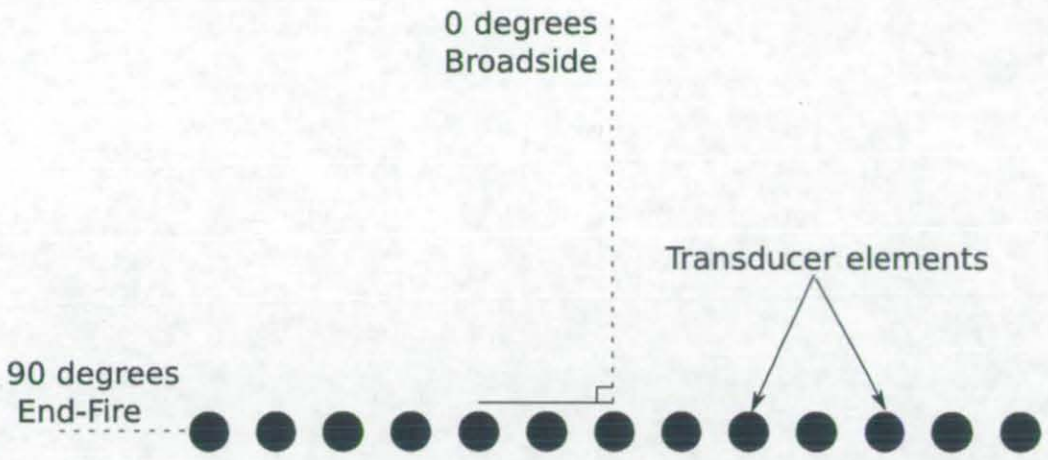

Figure 3.2: A 13 element line array showing the broadside angle at 0^o and end-fire at 90^o

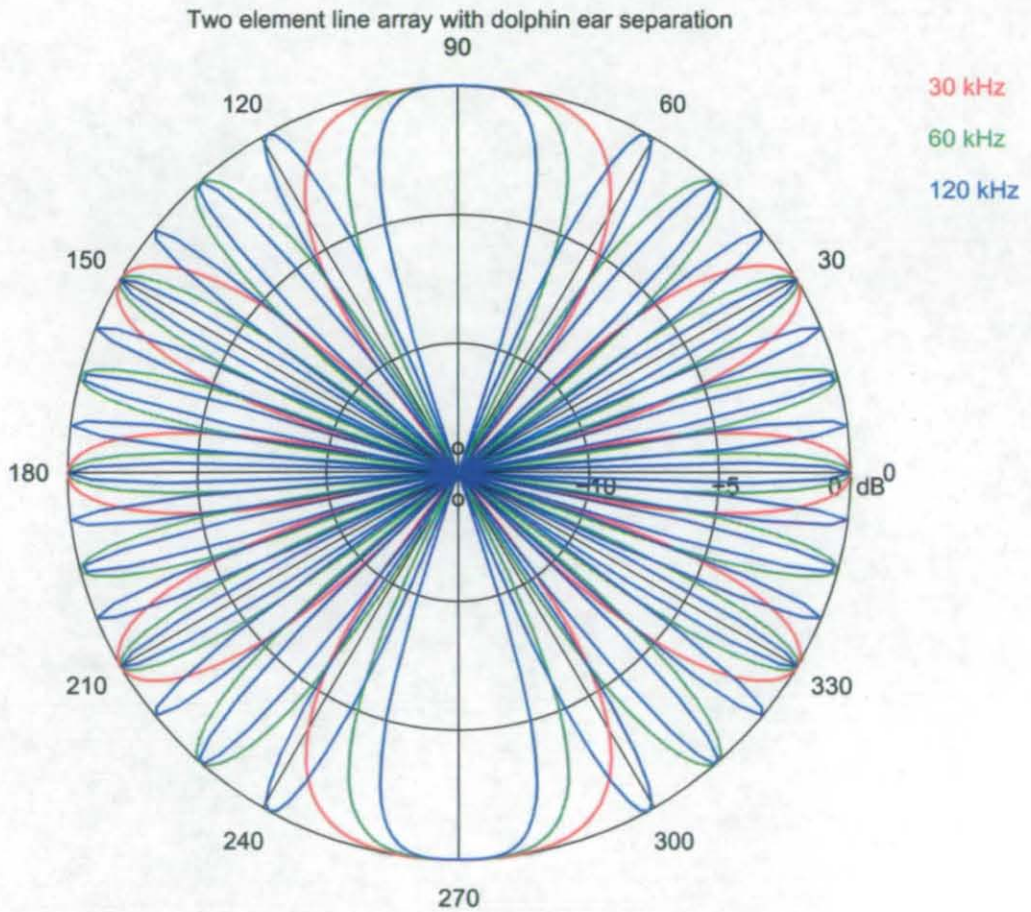

Figure 3.3: Beam pattern at 30 kHz, 60 kHz, and 120 kHz for 2 omnidirectional elements separated by 10 cm.

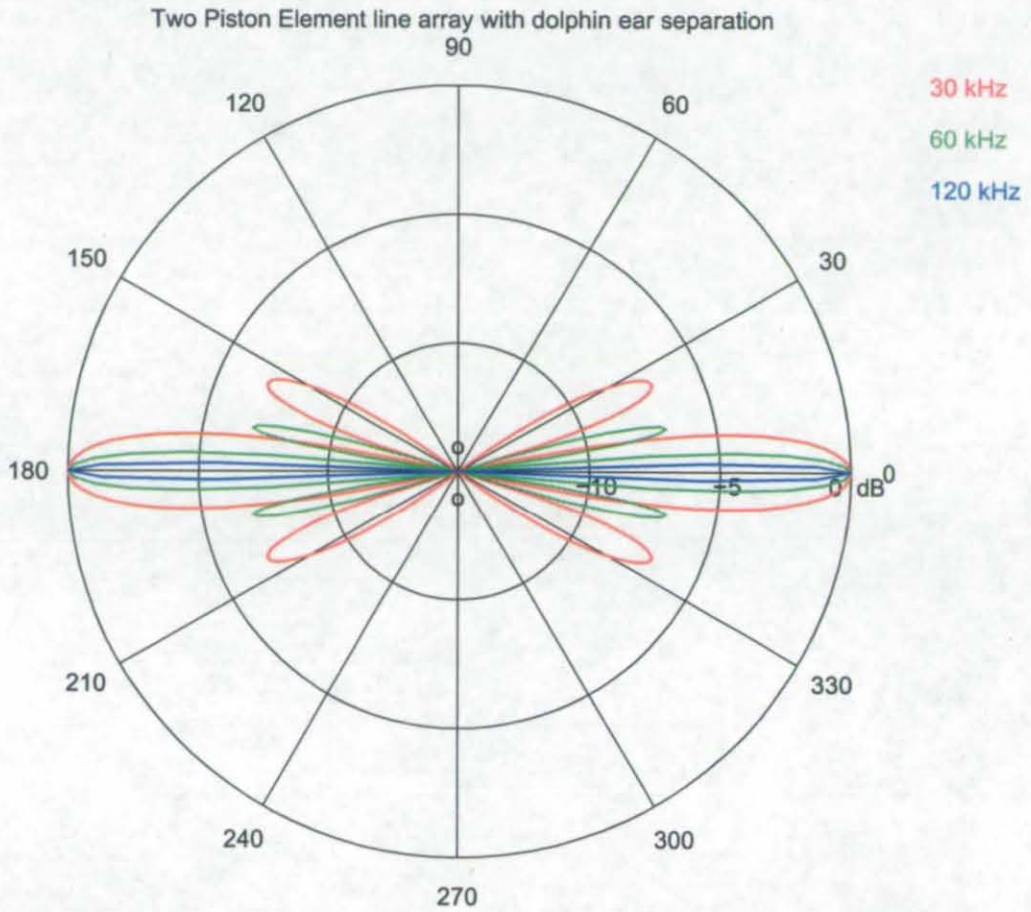

Figure 3.4: Beam pattern at 30 kHz, 60 kHz, and 120 kHz for 2 5 cm radius piston elements separated by 10 cm.

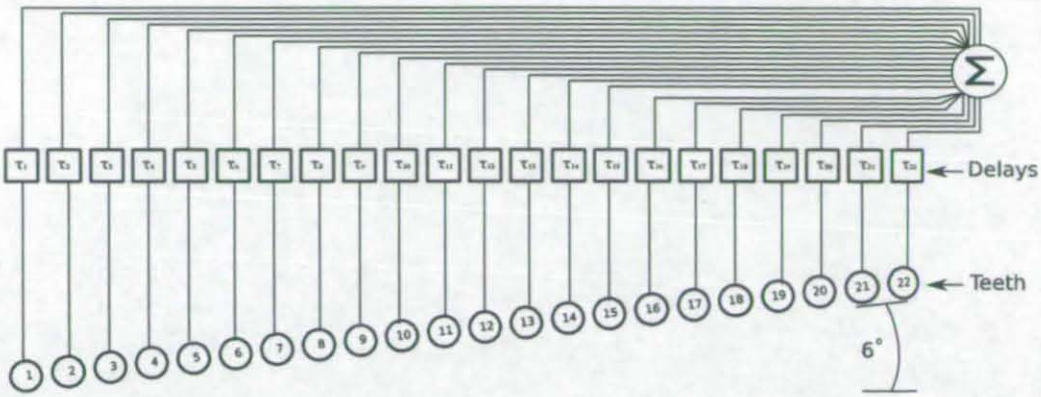

Figure 3.5: The hypothesised model of one side of the tooth array with delay lines.

3.2.3 *Phased Multi-Element Arrays*

Linear phased arrays are commonly used in radio communications, radar applications and in airborne audio systems. They are made from arrays of transducer elements that are equispaced. An individual fixed delay is applied to each channel before being summed together constructively and passed on to some form of processing system. These individual timing delays result in phase differences between adjacent elements which govern the array directivity or beam pattern (Figure 3.5).

The Atlantic Bottlenose Dolphin has 44 teeth in total in the lower jaw which are arranged in two rows along each side. It has been suggested by Dobbins [3.12, 3.13] that each of these two groups of 22 elements act as a line array with the teeth acting individually as independent pressure transducers. The separation between each element, as has been explained, is 11.4 mm and thus at 130 kHz it would represent a λ separated array pair. In this case each half of the array pair represents one side of the lower jawbone.

A line array of n omni-directional sources separated by d has an analytical solution described by Waite [3.10] and shown in Equation 3.2. Using this equation the beam patterns for a line array at λ spacings for frequencies of 30 kHz, 60 kHz, and 120 kHz can be analysed. These frequencies have been modelled as they are the most frequently quoted in the literature. The modelling results are shown in Figure 3.6.

$$Gain\ dB(\theta) = 20 \log \left(\frac{\sin(\frac{n\pi d}{\lambda} \sin\theta)}{n \sin(\frac{\pi d}{\lambda} \sin\theta)} \right) \tag{3.2}$$

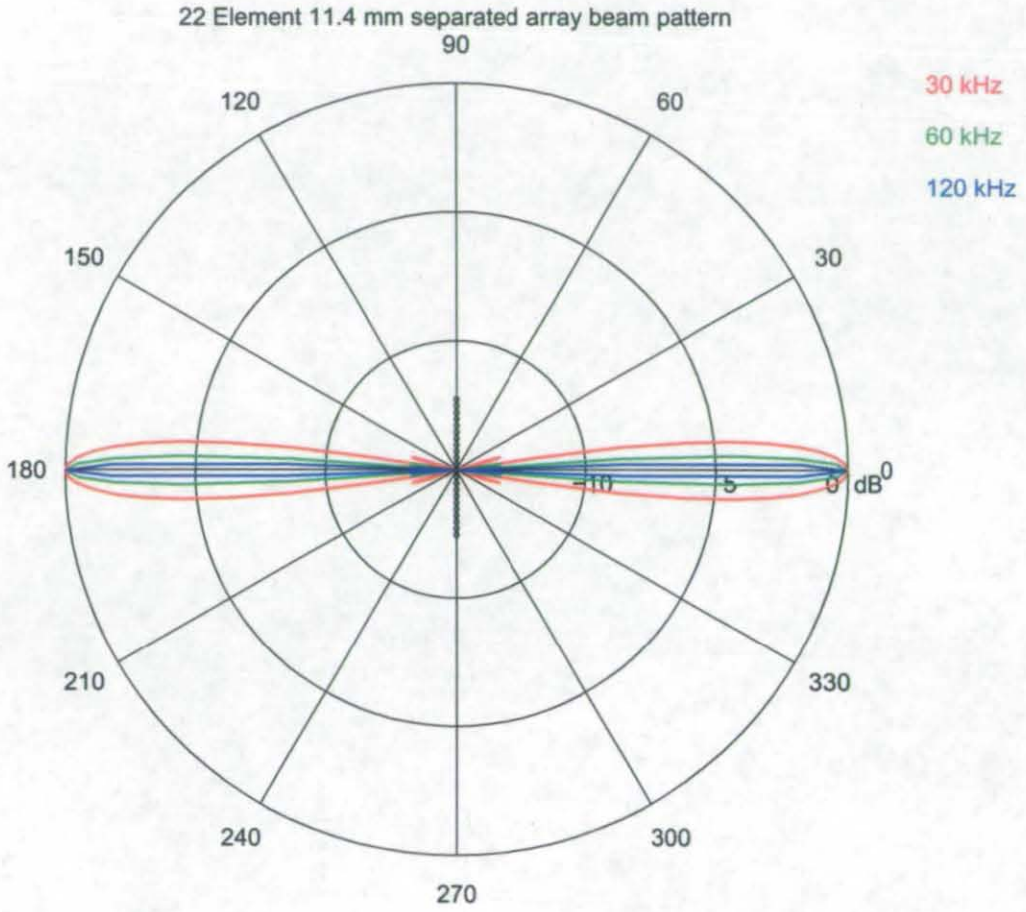

Figure 3.6: The beam pattern of a 22 omni-directional element broadside array with 11.4 mm spacing.

The pattern suggests that an active array is a viable theory. The main lobe is narrow with low side lobes. The directionality in a line array stems from the fact that all the array elements will receive a signal at exactly the same time when the source is in the broadside position. When the signals arrive coherently the signals are summed constructively which causes maximum gain on the receiver. Many conventional array systems introduce delays into the arriving signals of elements. When the array is positioned end on to the transmission source all the signals arrive at the same time in phase at the processing point and produce a high gain due to the constructive interference. When the array is

moved away from this axis, signals will arrive destructively due to the additional delay and reduce the received signal, this technique is know as beam steering. Figure 3.7 shows a pressure signal arriving at a line array of receivers, if a delay is introduced between these elements and the processing system then all the signals can be made to arrive simultaneously.

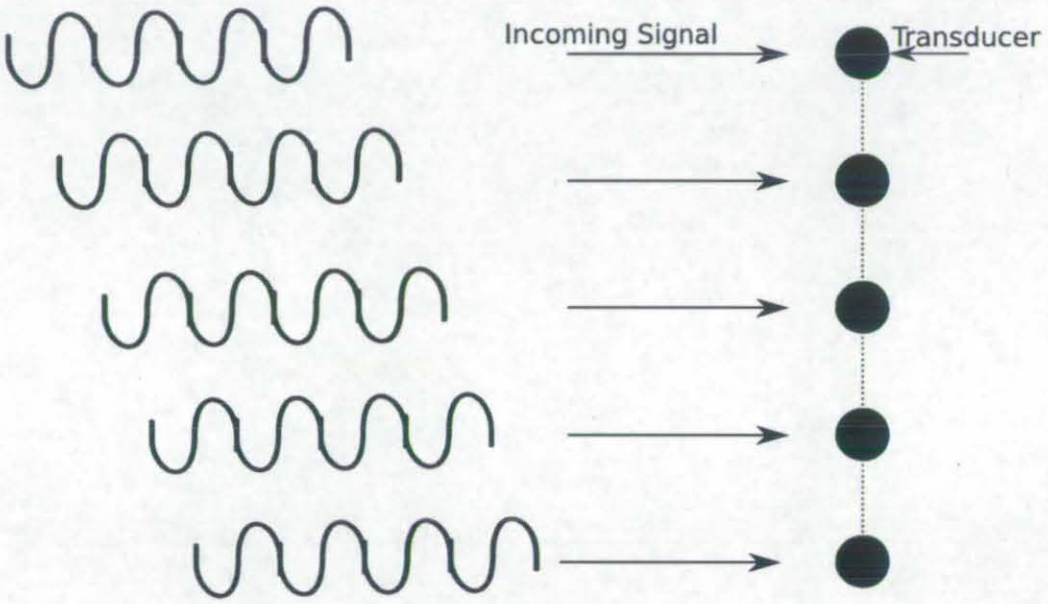

Figure 3.7: Pressure waves arriving out of phase at a line array.

Equation 3.2 can be modified to allow for beam steering, this is shown in Equation 3.3 as described by Waite [3.10] where θ_s is the steer angle.

$$Gain\ dB(\theta) = 20 \log \left(\frac{sin\ n\ \pi(\frac{d\ sin\theta}{\lambda} - \frac{d\ sin\theta_s}{\lambda})}{n\ sin\ \pi(\frac{d\ sin\theta}{\lambda} - \frac{d\ sin\theta_s}{\lambda})} \right) \tag{3.3}$$

Using Equation 3.3 the beam pattens for a 22 element line array separated by 11.4 cm with a beam steer of 90° has been calculated and is shown in Figure 3.8. Other angles have also been plotted in order to demonstrate the steering effect. This pattern shows a very well defined main lobe in the end-fire orientation with side lobes below 12 dB for the forward facing direction. In order to compare this array with the measurements of Au [3.14], the array is modelled at a number of different frequencies that can be seen in Figure 3.9. This pattern shows good correlation with the patterns from animal

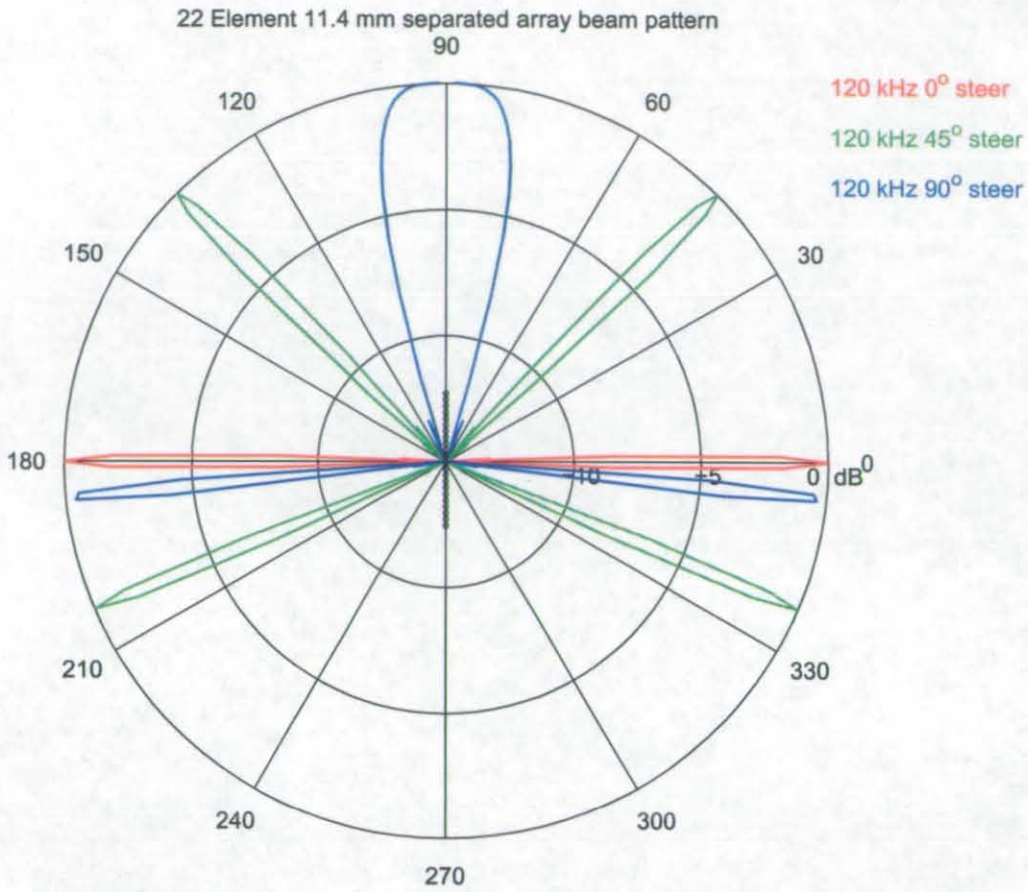

Figure 3.8: The beam pattern produced by 22 elements separated by 11.4 mm with different steer angles.

experiments the 3 dB beam widths are summarised in Table 3.1. These patterns also show that the beam steering has caused a broadening of the main lobe.

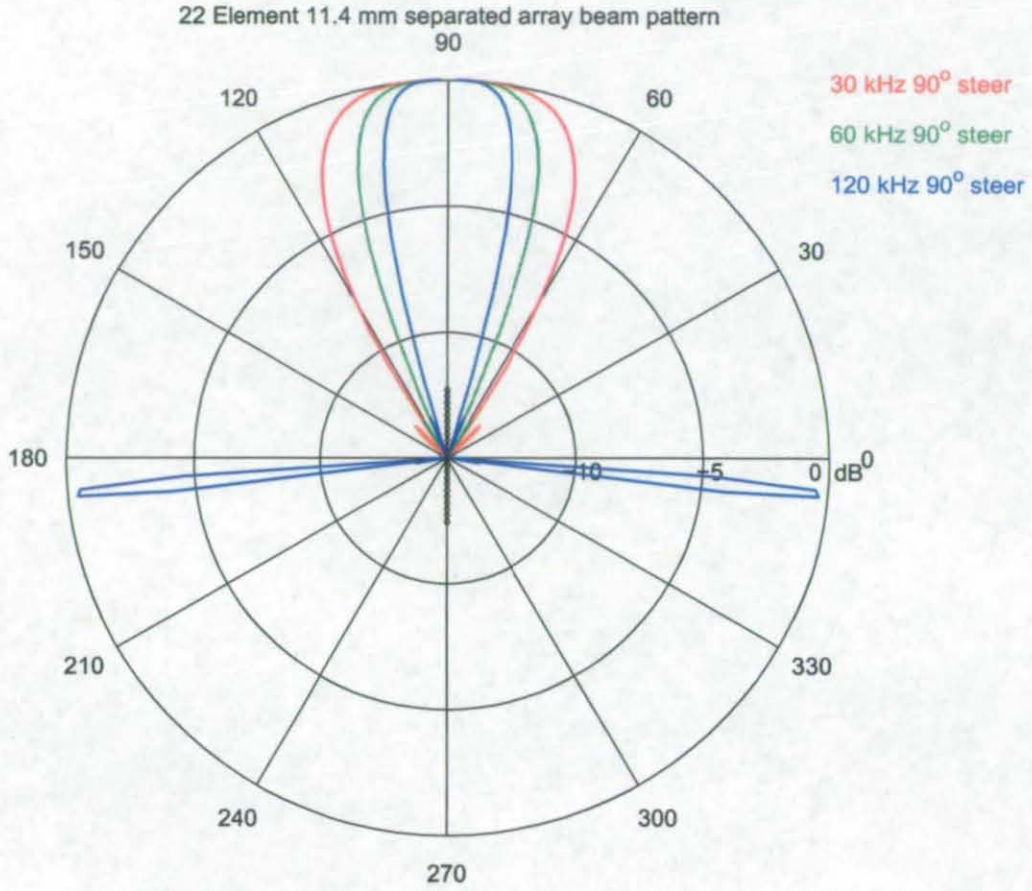

Figure 3.9: The beam pattern produced by 22 elements separated by 11.4 mm with 90° steer angle at different frequencies.

Frequency kHz	Horizontal -3 dB beamwidth Measurements (from Au *et al.*)	Horizontal -3 dB beamwidth Analytical
30.0	59.1°	48°
60.0	32.0°	34°
120.0	13.7°	24°

Table 3.1: The 3 dB beam widths of the a 22 element 90° steered array at different frequencies compared with Dolphin beam width data reported by Au reproduced from [3.14].

3.3 Properties Of An End-Fire Array

The time of arrival delays between elements can be shown to change as a function of incident angle by Equation 3.4, where d is the separation between elements, c is the speed of sound and θ is the beam angle. On examination of this equation in the range of (-90 $\leq \theta \leq$ 90) shown in Figure 3.10 it is clear that δt is nonlinear. A change in angle between 0^o and 10^o produces a larger change in δt than that produced when changing by the same angular amount from 80^o and 90^o'. This effect means that when the array response is measured for beams approaching the end-fire position the signals from each element will start to move into phase faster compared to the broadside position, which produces a wider beam.

$$\delta t = \frac{d\ cos\ \theta}{c} \tag{3.4}$$

So far only the lower jaw structure has been considered, however it is also worth considering what would happen if the teeth of the upper jaw were to be involved. In this case the separation of the teeth would be $\lambda/2$ due to the interleaving of the lower and upper jaws, also in this scenario there would be 44 elements. Figure 3.11 shows the beam pattern from a 90^o steered $\lambda/2$ array. When comparing this to the 22 element array shown in Figure 3.9 we can see there is little change between 44 element $\lambda/2$ array and 22 element λ array. In terms of making a synthetic array, the same performance can be achieved using either of the arrays however the lambda separated array requires less elements.

Up to this point only a single line array has been considered and as a result there exists a left-right ambiguity were the same sensitivity can be created from more than one angle. A more complete geometry of the dolphin's lower jaw is depicted in Figure 3.12, the two arrays are separated by 12^o [3.1]. In order to analyse this more complex situation the co-ordinate system for the singular line arrays must be altered to allow for the combining of the two patterns. In this case the 0^o point has been taken as the point on the centre line at the rear of the two line arrays as indicated in Figure 3.12. Once the

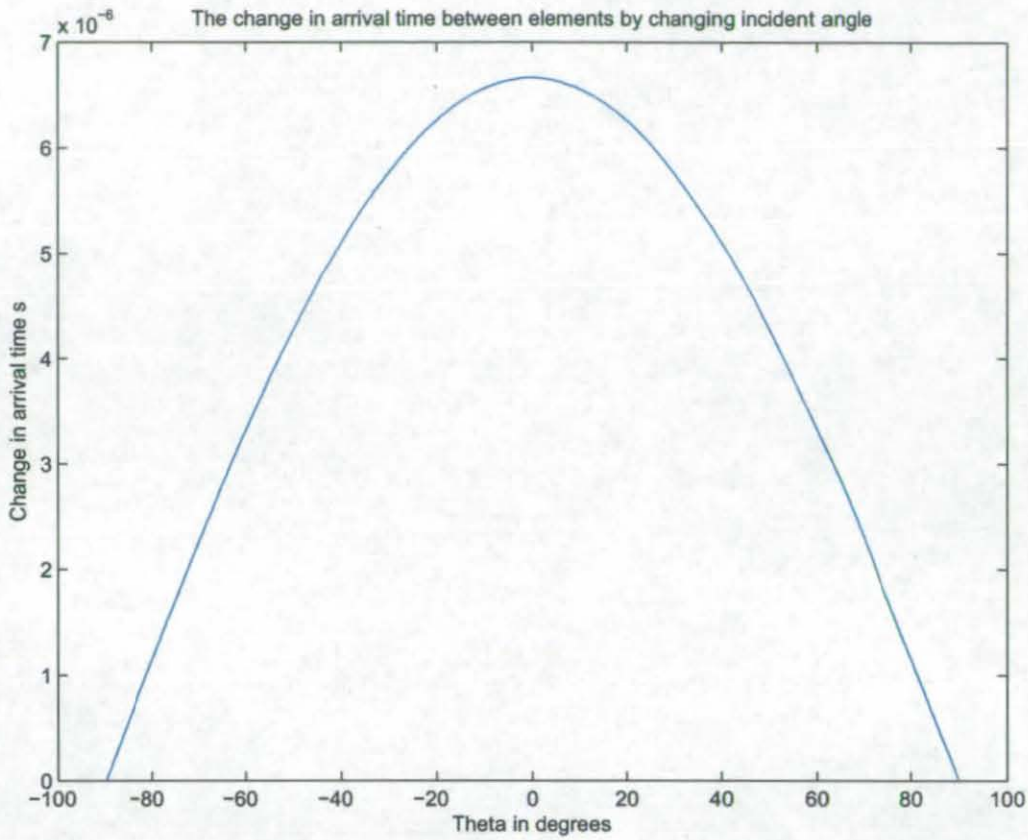

Figure 3.10: The change in time of arrival with angle

two patterns have been mapped to the new co-ordinate system, the gain values can be converted into normalised voltage from their original dB units. In this case the received pressure is proportional to the voltage output of the array. The difference between the patterns of the two arrays can be calculated

One common method of localisation in sonar is to calculate the voltage difference between two spatially separated arrays and examine the effect with change in angle. By applying this technique the theoretical array difference results for this scenario can be calculated and is shown in Figure 3.13. In this graph the linear regions near the end-fire direction of the array shows the useful areas that may be used for target location. In this area there is a direct relationship between signal level and the angle of arrival. This area is approximately 20^o wide on the 120 kHz signal. The graph can be interpreted as three linear regions, which show constant proportionality within its region. The angles

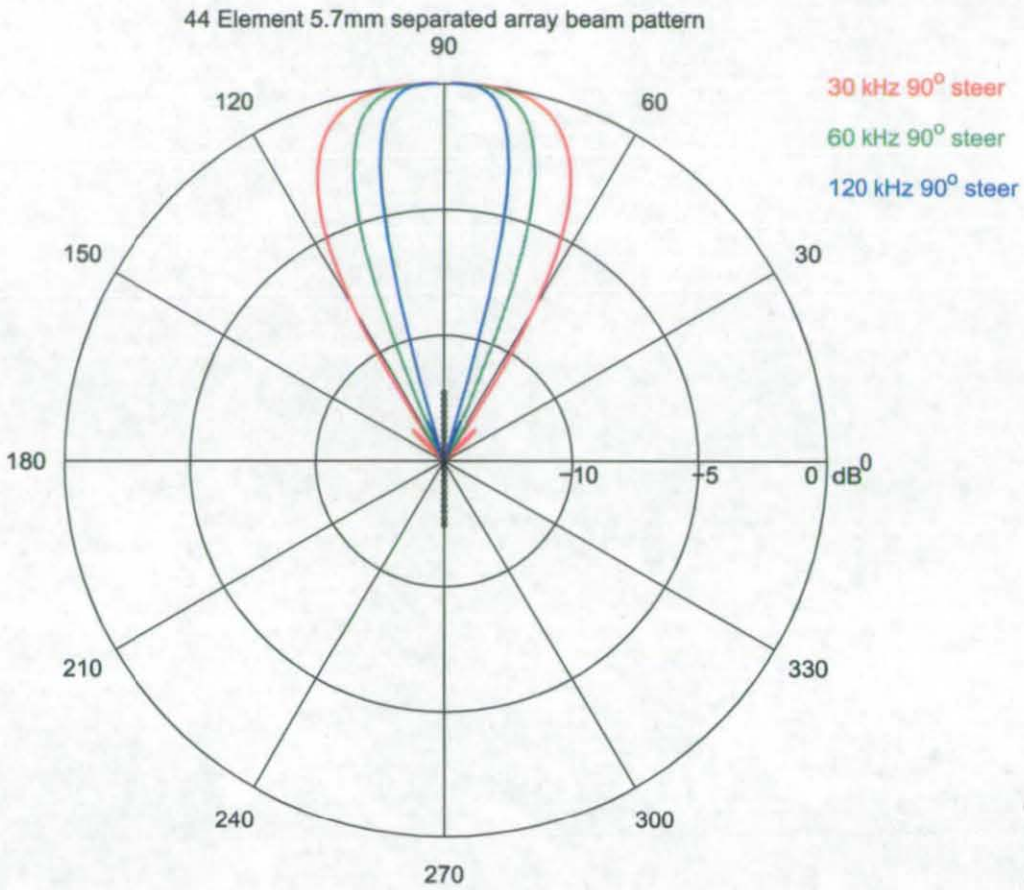

Figure 3.11: 44 element line array separated by 5.7 mm at different frequencies at 90^o steer.

that are trackable by a dolphin are within the linear region of this array and match well with the beam patterns from animal experiments [3.14].

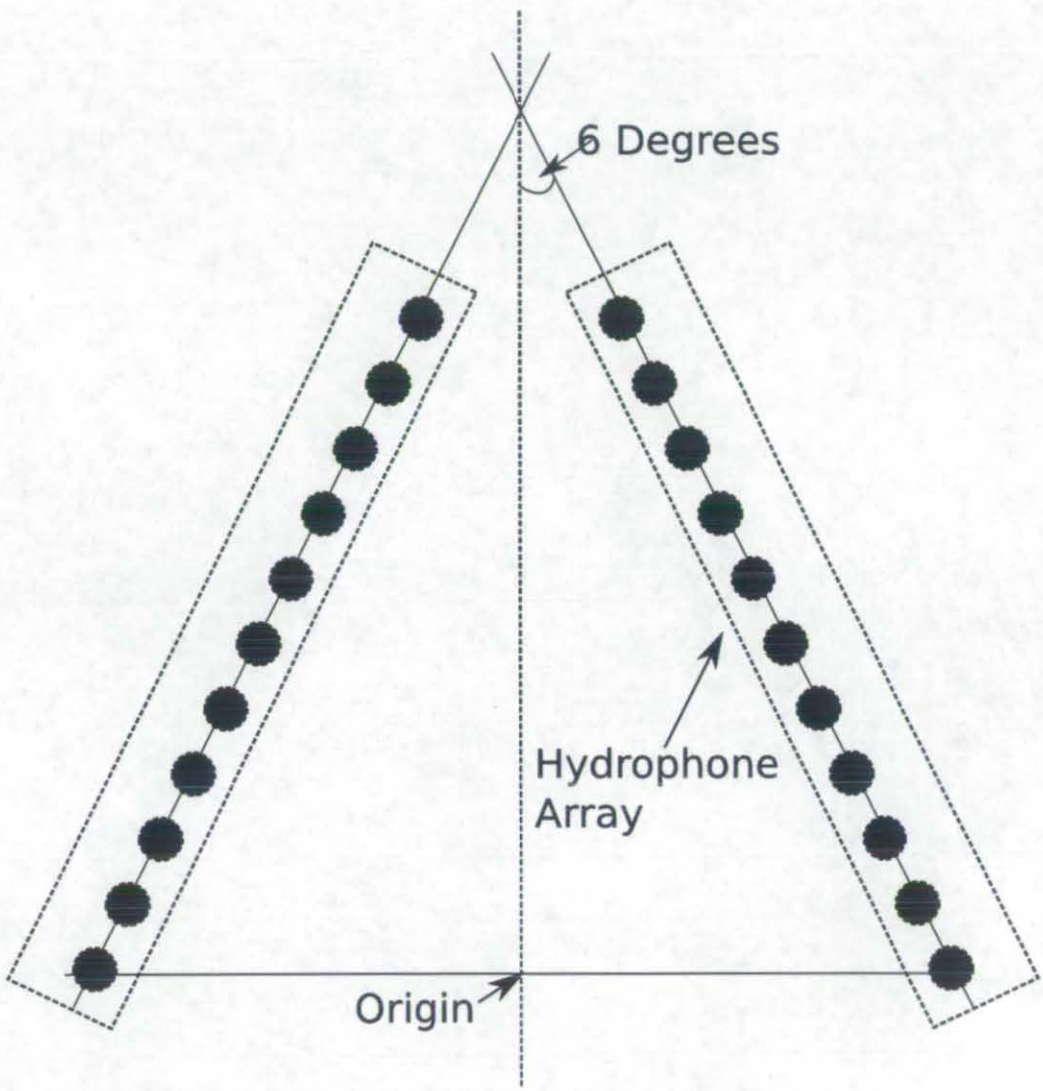

Figure 3.12: Two line array's arranged similar to the dolphin teeth.

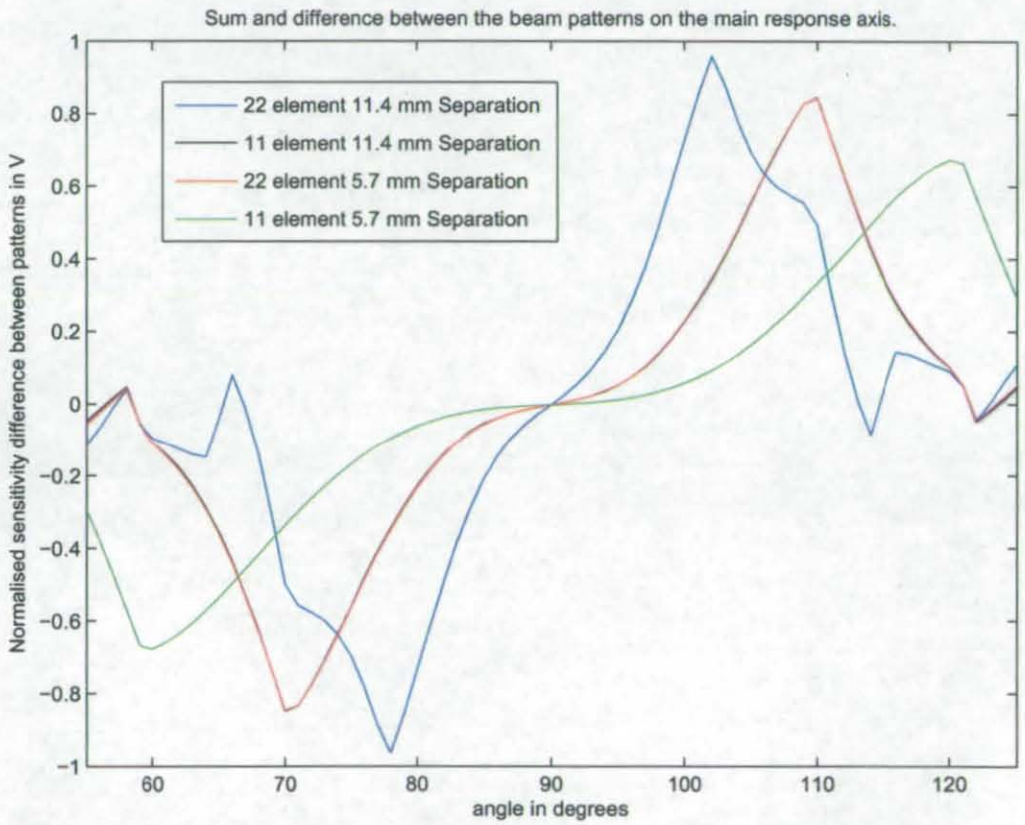

Figure 3.13: The array difference patterns for each type of line array at 90^o Steer.

3.4 End-fire Array Measurements

3.4.1 Methodology

As the theoretical analysis indicated that it is possible to use two end-fire arrays separated at 12 degrees to produce a beam pattern similar to that of the dolphin, this theory was further investigated in the Loughborough University Acoustic tank. The dimensions of the tanks are 5 m by 9 m by 1.8 m in depth. The array used in these tests was provided by Dr. Peter Dobbins of S.E.A. Ltd. and manufactured by BAE Systems. The array was manufactured from 22 active piezo-ceramic elements. The resonance of each element was 380 kHz. The elements themselves were manufactured from a ceramic material and the whole assembly was encapsulated within a perspex block. The individual elements were cylindrical with a diameter of 3.2 mm. The transducers were chosen due to the physical size being similar to those of a typical Bottlenose Dolphin tooth. The centre of each element was separated from its neighbouring element by 9.5 mm, giving a total array length of 218 mm. To achieve a separation of one wavelength with the available array a source frequency of 78.95 kHz must be used assuming that the speed of sound in water in 1500 ms^{-1}. A picture of the array can be seen in Figure 3.14. Unfortunately initial testing revealed that this array would not be suitable for testing this hypothesis due to the high directivity of the array elements. The properties of the array are presented in Appendix A.

In the absence of satisfactory results from the line array, four ceramic ball hydrophones were used to construct a new array. Each element had a diameter of 11.4 mm as measured with digital vernier callipers. The diameter of a tooth is known to be 4 mm as will be discussed in Chapter 5. The tooth diameter and main reception frequency of 120 kHz can be used as a scaling factor to find the frequency that best matches the diameter of the hydrophone. This yielded a frequency of 42 kHz. A mounting jig was constructed with thirteen clamping positions in order to allow moving of the four hydrophones to different positions within the end fire array. The element separation was 35.5 mm or λ separation when assuming a sound speed of 1493 ms^{-1} (the speed of sound at the time

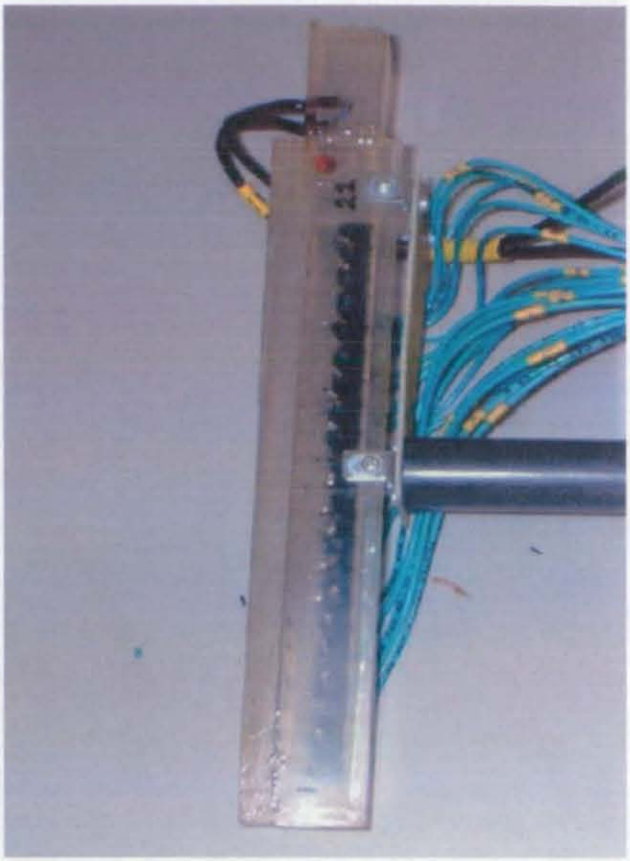

Figure 3.14: The end-fire array that is used in physical testing of the tooth array hypothesis.

of testing).

To determine the beam pattern of the array, the hydrophones were placed in jig positions 1 to 4 and the jig was attached to a pan and tilt system. Careful attention was made to ensure that the centre of the array was aligned to the centre of the pan and tilt system. The source transducer used within the experiment was a piston transducer with a resonant frequency of approximately 60 kHz. The acoustic aperture of the transducer was 5 cm. Equation 3.5 calculates the Rayleigh Distance (D) of an acoustic source with an aperture radius of a is discussed by Kuntz *et al.* [3.15], this was used to calculate the minimum separation of the source and the array (22 cm). The source transducer was placed 50 cm from the centre of the array which ensured that the far field condition was met for every beam angle measured even in the end-fire position.

$$D = \frac{\pi * a^2}{\lambda} \tag{3.5}$$

The time delays that are required in the end-fire design in Figure 3.5 are added after digitisation and will be discussed in a later section.

A Hameg HM8130 function generator was used to produce a pulsed 10 cycle sine wave at a frequency of 42.0 kHz. The output signals from the hydrophones were fed into various pre-amplifiers with gains between 26 dB and 40 dB between 10 Hz and 100 kHz. As different pre-amplifiers were used on the four channels an additional calibration steps was conducted in the post-processing.

The beam patterns were measured using custom PC software. The software controlled the position of the pan and tilt system and captured waveforms from a Tektronix Digital oscilloscope to the controlling PC's hard drive at a sample rate of 1 MHz. Measurements were taken in 1^o steps between $\pm$ 180^o. In order to maintain a fixed time frame for each signal captured, the oscilloscope was triggered from the TTL gating output of the outgoing pulse. Once measurements had been taken for all four hydrophones they were moved to the next set of jig positions and the experiment was repeated until all positions had been measured.

3.4.2 Post-Processing Calibration

All the signals that were captured in the experiment were analysed and post processed using Matlab. When the array is in the broadside position the signals should arrive at each element at the same time and with the same signal strength. On examination of the broadside signals the gain was uneven (see Figure 3.15). To correct the variance in sensitivity a gain factor shown in Table 3.2 were applied to each channel in order to make the broadside response of each channel equal. The gain factors where then applied to all the recordings at each position. A typical return signal is also presented along with its frequency spectrum in Figure 3.16.

Channel Number	Additional Gain in dB
1	10.6160
2	9.1066
3	12.8117
4	0.0606
5	11.3009
6	21.4322
7	9.2859
8	7.8980
9	10.2848
10	20.0434
11	9.5729
12	0
13	11.9319

Table 3.2: Voltage gains applied to each channel to normalise the broadside signal.

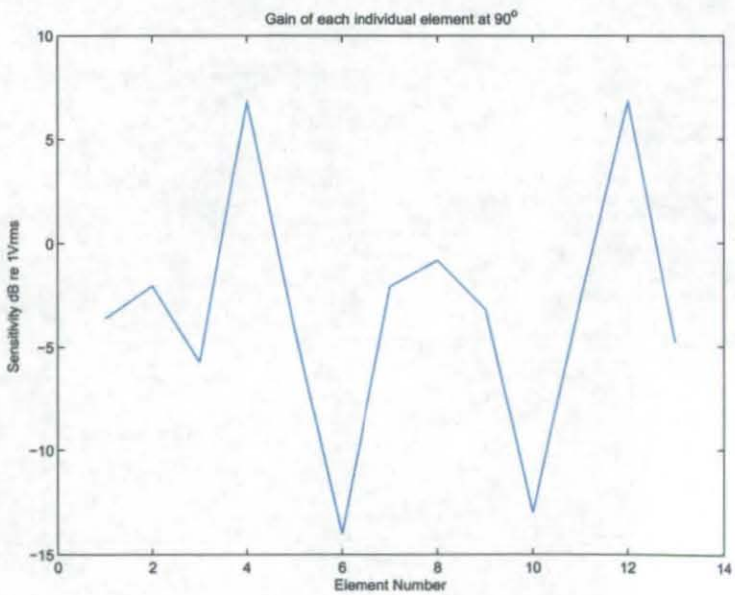

Figure 3.15: Element sensitivity at 90° before gain compensation.

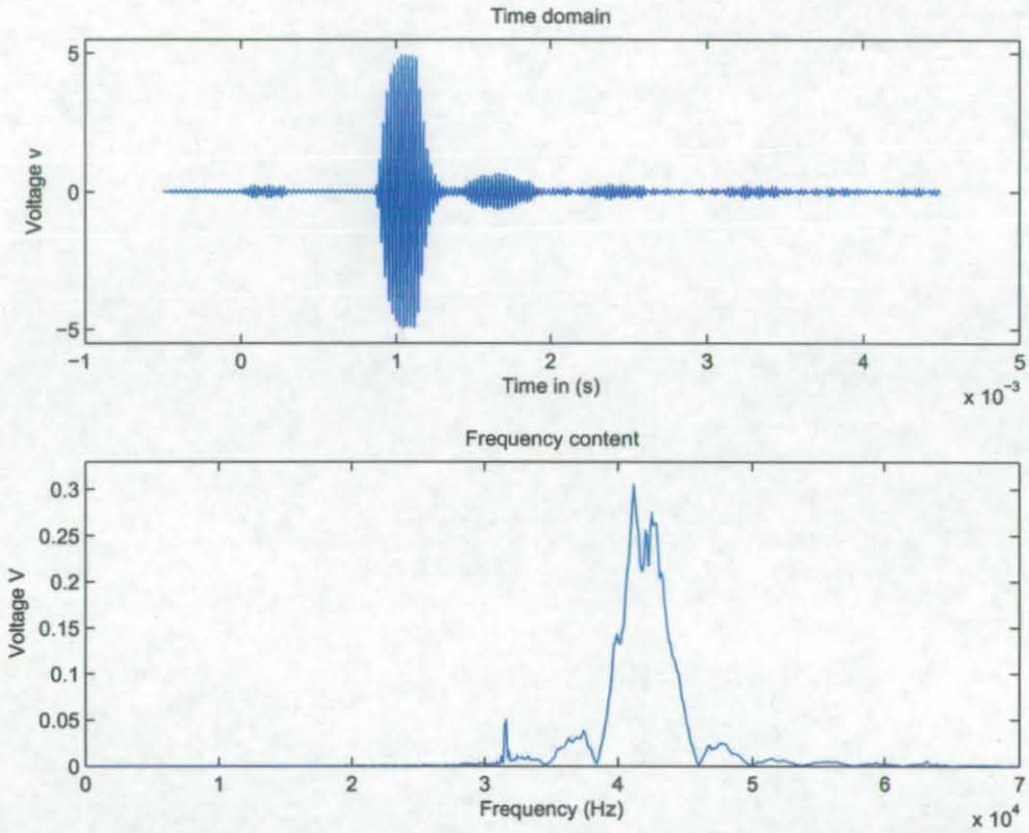

Figure 3.16: A typical signal as received by the end-fire array, along with its frequency spectrum.

Assuming that in the farfield of the transducer there is zero wavefront curvature, when the array is in the broad side position, the time of arrival of the signals should all be equal. Using the cross correlation technique the time of arrival of the signal for each of the channels were determined. The different arrival times can be seen in Figure 3.17, this difference is most likely due to different phase responses of the pre-amplifiers. To correct for the time delay all signals were individually delayed to allow them arrive simultaneously. This was accomplished by padding the start of the fastest digitised signal with zeros.

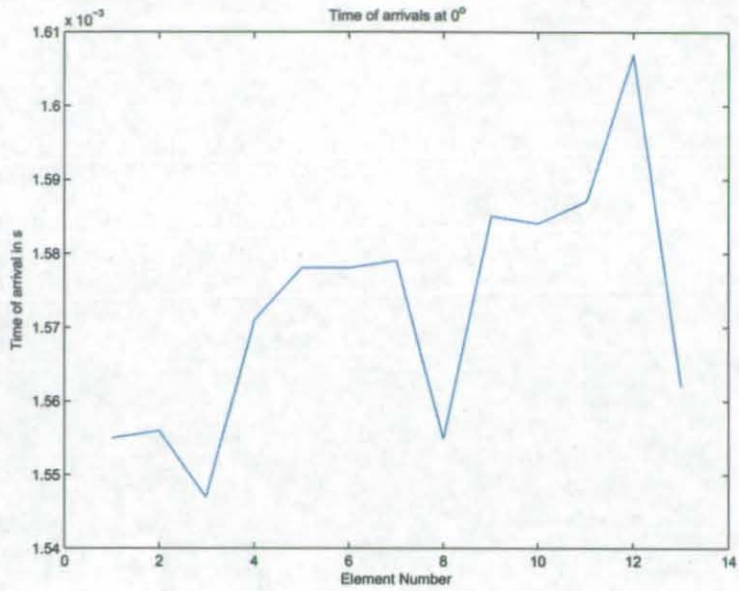

Figure 3.17: The phase / time before correction across the array.

3.4.3 *Results*

Once the electrical artifacts have been removed via signal processing, the beam pattern can be plotted by numerically summing the signals from all the elements up at each angle and determining the rms value. All 13 elements were summed together to make a λ separated array. The beam pattern produced by this array can be seen in Figure 3.18.

Using the theoretical line array that was shown in Figure 3.6 which was for 22 elements (not the 13 element used in the real array) with λ separation, it can be seen that the patterns agree well. The main difference is in the difference in the side lobes to -3 dB. From the experimental results it is also clear that the beam pattern of the 13-element broadside array at λ frequency is narrower than the 120 kHz pattern of the dolphin.

As the main aim of the experiment is to validate the use of an end-fire array in acoustics, the signal captured when the array was orientated 90^o to the source were passed though a correlator to determine the time of arrivals. The aim of an end-fire array is to make all signals arrive simultaneously when the receiver is in the end-fire orientation to the acoustic source[3.10]. Therefore the digital delays shown in Table 3.3 were added to

Channel Number	Signal Delay in microseconds
1	282
2	264
3	228
4	202
5	185
6	160
7	139
8	128
9	87
10	64
11	44
12	2
13	0

Table 3.3: Time delays applied to each channel to allow the array to operate in end-fire mode.

the captured signals.

The beam pattern for the end-fire configuration is shown in Figure 3.19. This pattern shows a narrow beam along the axis of the array, with side lobes below 5 dB. The 3 dB beamwidth of the array is approximately 30^o which when compared to the patterns of Au and Moore (Figure 2.9) is larger, however the analytical analysis shows that as the number of elements increases then the beam width is decreased.

As for the analytical simulations, the single array results can be used to simulate the left and right side of the jawbone, by taking the array pattern, making a copy and then translating the pattern $\pm$ 6^o. The result can be seen in Figure 3.20. The sum and difference pattern for the array is shown in Figure 3.21. This shows an almost linear region near the end-fire orientation and matches the simulation data (see Figure 3.13) well.

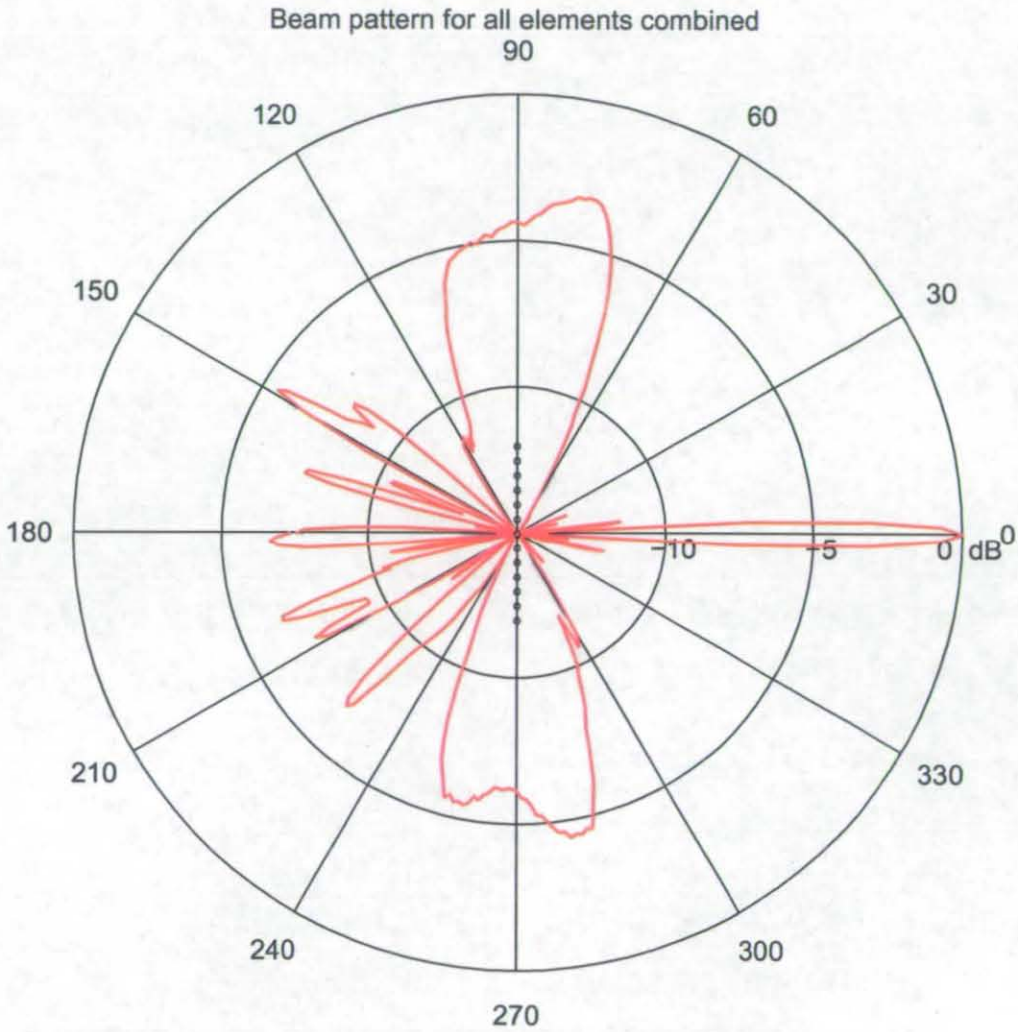

Figure 3.18: The beam pattern of an 13 element λ separated broadside array.

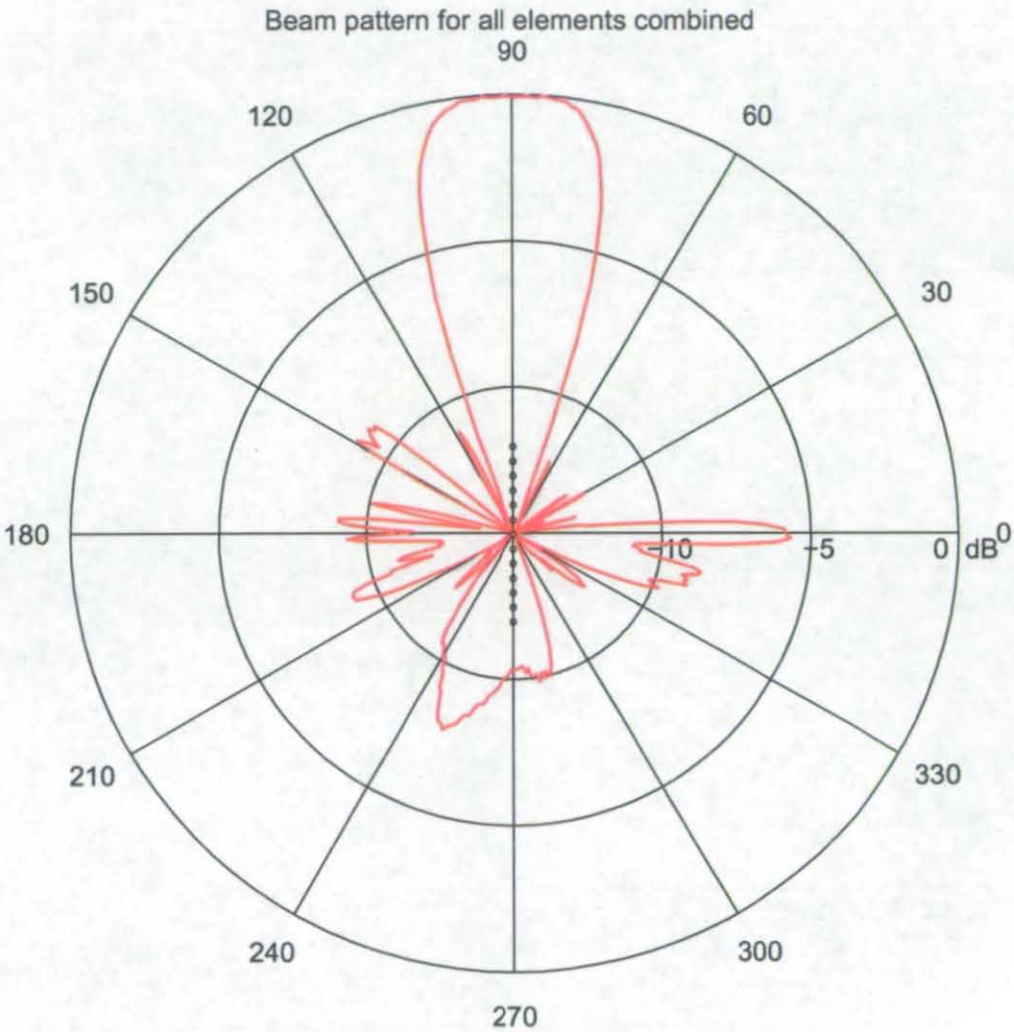

Figure 3.19: The beam pattern of a 13 element λ separated end-fire array.

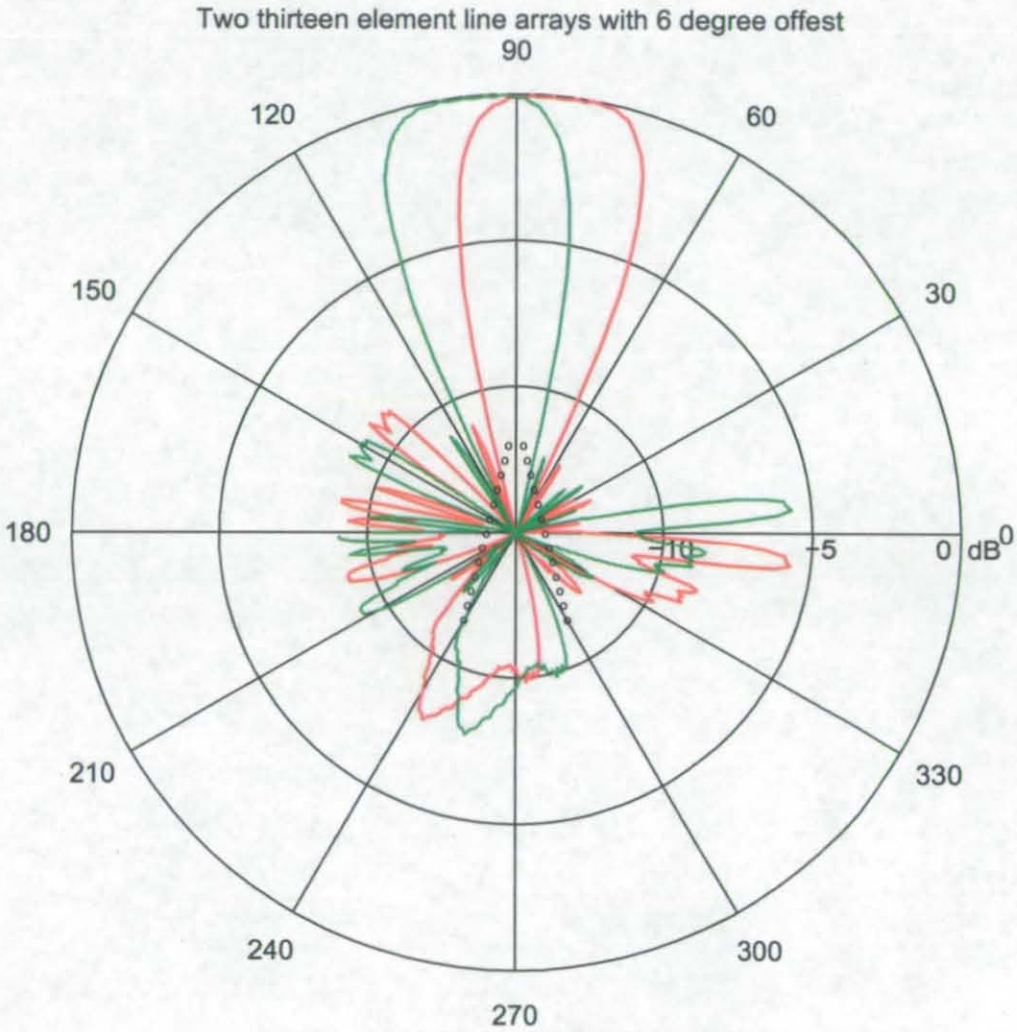

Figure 3.20: Replica dolphin array pattern

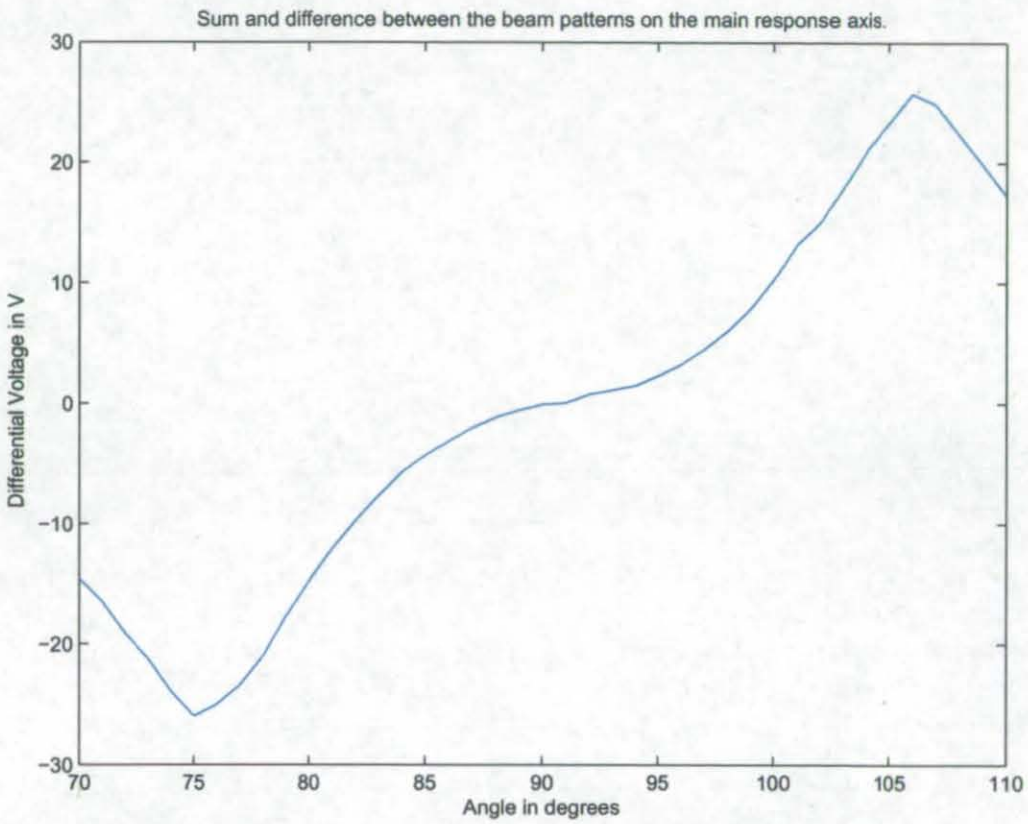

Figure 3.21: The Array Difference Patterns for the replica end-fire array.

3.5 Conclusions

The analytical and experimental studies carried out in this chapter highlight a number of possible array configurations that are capable of providing the beam pattens exhibited by the Atlantic Bottlenose Dolphin. The experimental work shows that an end-fire array is potentially a very useful design for producing a narrow beam with minimal side lobes. This is a feature that would be highly desirable in a shallow water sonar system. The work also proves that the replication of the teeth within the lower jaw does represent a viable sonar array at the frequencies known to be used by dolphins. The analytical expressions agree with the experimental work and can be used to demonstrate the usability of the end-fire array at frequencies of interest. Furthermore the use of two cylindrical pistol elements with 10 cm separation also produces a useful beam pattern although it does process larger side lobes than the end-fire arrangement. From these results no conclusions can be drawn as to the exact mechanism used by the dolphin. Further consideration is given to the Dolphin physiology in the next chapter and other mechanisms will be proposed.

References

[3.1] A. D. Goodson and M. Klinowska, *A proposed receptor for the Bottlenose Dolphin (Tursiops truncatus) modelling the receive directivity from tooth and lower jaw geometry*, pp. 255–267. NATO ASI Series A Sensory Abilities of Cetaceans, Plenum, 1990.

[3.2] W. W. L. Au, *The sonar of dolphins*. New York: Springer-Verlag, 1 ed., 1993.

[3.3] J. E. Sigurdson, "Analyzing the dynamics of dolphin biosonar behaviour during search and detection tasks," in *Proceedings of the Institute Of Acoustics*, vol. 19, pp. 123–132, Institute Of Acoustics, 1997.

[3.4] W. S. Martin, M. Phillips, E. J. Bauer, P. W. Moore, and D. S. Houser, "Instrumenting free-swimming dolphins echolocating in open water," *The Journal of the Acoustical Society of America*, vol. 117, no. 4, pp. 2301–2307, 2005.

[3.5] "Space and naval warfare systems." `http://www.spawar.navy.mil` last accessed January 2008.

[3.6] J. R. Potter and E. A. Taylor, "On novel reception models for bottlenose dolphin," in *Proceedings of the Institute of Acoustics* (A. D. Goodson and P. F. Dobbins, eds.), vol. 23, pp. 103–110, July 2001.

[3.7] K. S. Norris, "Some problems of echolocation in cetaceans," *Marine Bioacoustics*, vol. 2, pp. 317–336, 1964.

[3.8] K. S. Norris, "The evolution of acoustic mechanisms in odontocete cetaceans," *Evolution and Environment, Yale University, Connecticut*, pp. 298–323, 1968.

[3.9] D. S. Houser, J. Finneran, D. Carder, W. V. Bonn, C. Smith, C. Hoh, R. Mattrey, and S. Ridgway, "Structural and functional imaging of bottlenose dolphin (tursiops truncatus) cranial anatomy," *J Exp Biol*, vol. 207, no. 21, pp. 3657–3665, 2004.

[3.10] A. D. Waite, *Sonar for practising engineers*. Wiley Chichester, 2002.

[3.11] R. J. Urick, *Principles of underwater sound for engineers*. McGraw-Hill, 1967.

[3.12] P. Dobbins, "Modelling dolphin echolocation reception," *Proceddings of the Institute Of Acoustics*, vol. 23, no. 4, pp. 123–132, 2001.

[3.13] P. Dobbins, "Dolphin sonar—modelling a new receiver concept," *Bioinspiration and Biomimetics,*, vol. 2, no. 1, pp. 19–29, 2007.

[3.14] W. W. L. Au and P. W. B. Moore, "Receiving beam patterns and directivity indices of the atlantic bottlenose dolphin (tursiops truncatus)," *The Journal of the Acoustical Society of America*, vol. 75, no. 1, pp. 255–262, 1984.

[3.15] H. L. Kuntz, E. L. Hixson, and W. W. Ryan, "The rayleigh distance and geometric nearfield size of nonplane sound radiators," *The Journal of the Acoustical Society of America*, vol. 74, no. S1, pp. 82–83, 1983.

CHAPTER 4:

ACOUSTIC PROPERTIES OF THE LOWER JAW AND TEETH OF THE ATLANTIC BOTTLENOSE DOLPHIN

THE purpose of this chapter of this thesis is to describe and further investigate the sound coupling mechanisms and acoustic properties of the jawbone and teeth. The experiments detailed in the chapter will demonstrate the fundamental mechanical properties of the teeth and jawbone. Sound propagation and density measurements will also be presented.

4.1 Background

As covered in section 2.4 there is a large body of evidence to suggest that the lower jawbone is the main reception site of returning echolocation clicks. The actual mechanism by which the sound interacts with the jaw has been debated, including speculation by some researchers that the teeth may have a role in coupling sound to the receiver system [4.1, 4.2, 4.3]. The work presented by Goodson *et al.* draws upon the convenient physiological arrangement of the teeth in the lower jaw of the dolphin with features that are currently implemented in man-made sonar systems. The hypothesis proposed is that the teeth in the lower jaw act as individual hydrophone elements that have a uniform spacing similar to a periodic line arrays that are used in many conventional sonar

arrays. The teeth of the Atlantic Bottlenose Dolphin are arranged with uniform spacing and regular size.

The teeth of the Bottlenose Dolphin are considerably different to those of other mammals. Unlike other mammals dolphins are homodonts i.e. they do not possess different categories of teeth such as incisors, canines, pre-molars and molars; they only posses a single type of conical shaped tooth. From a biological point of view these teeth are ideally shaped for the task of grasping fast moving prey. Dolphins are known to feed upon small fish, which they swallow whole, and generally swallow head first, to prevent choking. Since they do not chew their food they do not need the other varieties of teeth. As fish are still alive when they are caught the conical shaped teeth are ideal for spearing the fish by puncturing their outer layer of skin. While the teeth are used in feeding they are also used during social interaction with other dolphins, in a behaviour termed 'raking.' Raking describes how dolphins scratch one another with their teeth in order to establish dominance within a group.

Dolphins and other odontocetes are born with most of their teeth already formed below the gum line, but unerupted. The teeth at the rear of the mouth typically erupt first shortly after birth, with the front, smaller teeth, arriving last. Once formed, the teeth do not change shape or size, however they do form growth layers on the inside of the teeth which consist of different density dentine. These different layers are deposited approximately annually, in a similar way to rings on a tree and can be used to classify the ages of the animal [4.4]. Figure 4.1 shows a cross section of a tooth under a microscope. In this image some of the layers can be observed along the length of the tooth.

4.2 *Laser Doppler Velocimetry*

LDV is a non-invasive, non-contact method which is capable of accurately quantifying surface velocity due to an acoustic pressure stimulus and as such is an extremely useful technique for determining acoustic wave propagation in solid objects such as a dolphin jaw. A beam of coherent light is projected onto the vibrating surface being measured

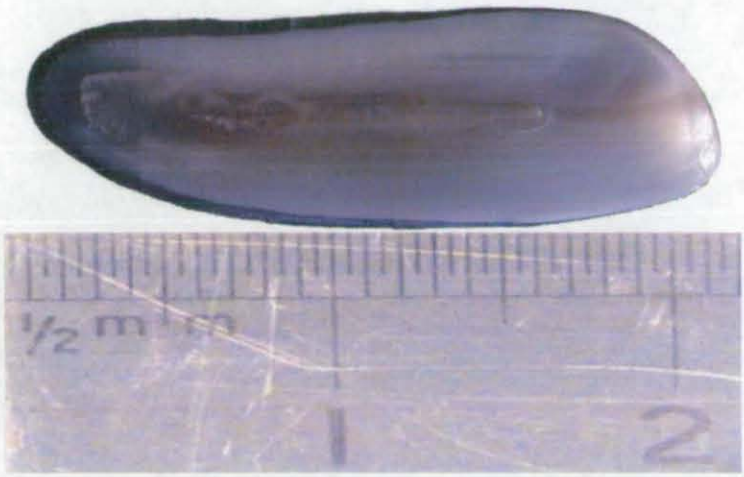

Figure 4.1: Cross-section of a tooth taken from the lower jaw of an Atlantic Bottlenose Dolphin viewed under a microscope.

and undergoes scattering. The back scattered light travelling back along the original optical path is collected by the LDV instrument and the Doppler shift frequency due to the surface movement is extracted by means of a heterodyning technique [4.5]. There is a direct relationship between Doppler frequency shift and the component of the surface velocity which lies parallel to the incident optical beam [4.6]. Once the Doppler frequency is obtained Equation 4.1 can be used to find the surface velocity where f_d is the Doppler shift, λ is the wavelength of light that has undergone a Doppler shift and v is the surface velocity. Once the surface velocity is obtained the acoustic pressure can be calculated for the material undergoing vibration using Equation 4.2. P is the acoustic pressure, ρ is the density of the vibrating material, c is the speed of sound.

$$f_d = \frac{2v}{\lambda} \tag{4.1}$$

$$P = \rho c v \tag{4.2}$$

LDV has another interesting and useful feature when it is used in an aquatic environment which is know as the acousto-optic effect [4.7]. The acousto-optic effect occurs because the propagating sounds causes minute changes in the refractive index of the

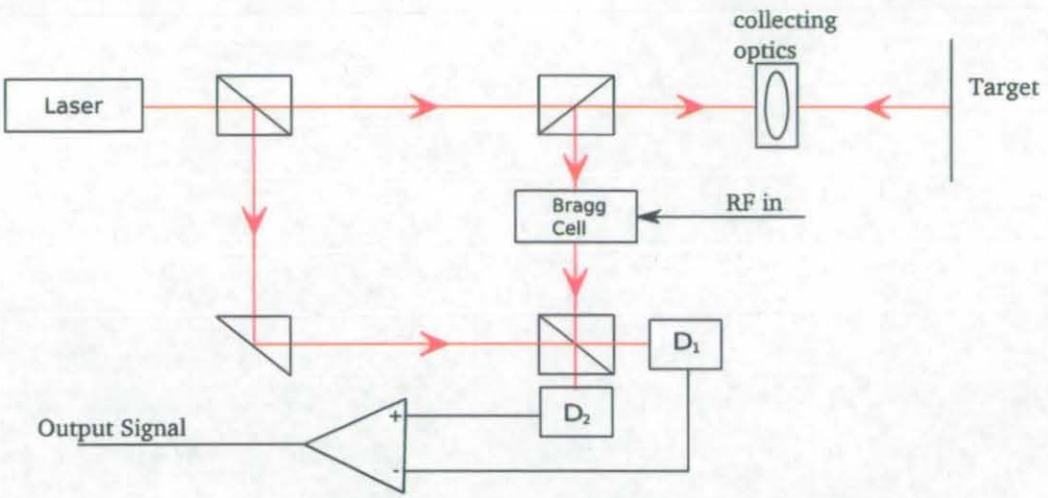

Figure 4.2: Functional Diagram of the internal workings of an LDV Head

material. This has the overall effect of changing the optical path length and consequently local changes in pressure can be resolved. This property has been exploited to measure and visualise complex sound pressure fields propagating around scattering objects in water [4.8].

The LDV technique is widely used for the vibrational analysis of solid materials and has also been applied to high precision underwater sound pressure measurement using an acoustically compliant membrane [4.9] as well as underwater transducer assessment. The results of using a scanning LDV on the teeth and lower jaw of Bottlenose Dolphin will be considered in this thesis. The main reason for utilising this technique is the high accuracy it offers and the benefit of measuring the pressure field without altering it. LDV instruments are also capable of measuring small complex surfaces to which conventional hydrophones could not usually be coupled. The LDV used in this experiment is based upon the design by Pickering *et al.* [4.10].

The commercial LDV used for this work is shown schematically in Figure 4.2. Two beams of light are created from one coherent laser light source by means of a beam splitter, one of these beams is used to illuminate the target and the other is used as a reference beam, which is passed through a homogeneous environment of sufficient length to compensate for coherence length and is then recombined with the beam of light that

has returned from the target under investigation. The returning light is an extremely high frequency, which can not be measured directly by opto-electronics, therefore a reference beam is injected which creates a measurable heterodyne frequency. The signal produced is directionally ambiguous due to the hetrodynde frequency representing the frequency difference in the beams. For this reason the system includes a Bragg cell on the target arm in order to offset the resultant heterodyne technique from zero. The photo detectors (shown as D_1 and D_2 in the diagram) provide an output that is proportional to the intensity of the incident light. This signal is then demodulated with standard electronics in order to provide a voltage output which is proportional to the velocity of the target.

4.3 Bone and Teeth Measurements

Possibly one of the most disputed theories about dolphin hearing is the suggestion of Goodson *et al.* [4.1] that the teeth have a key role in sound reception. If the teeth are acting as sound pressure transceivers it seems reasonable to expect that the acoustic properties of an individual tooth to reveal some useful information in the frequency band of echolocation and have a reasonable impedance match to the surrounding environment.

4.3.1 Tooth Density

To measure density a standard measuring technique was employed. The experimental setup can be seen in Figure 4.3. The weight of a tooth in air was measured by placing a tooth on a calibrated top pan balance as shown on the left of Figure 4.3 and the result was recorded. Then a beaker of pure water was placed onto a top pan balance and the balance was zeroed. The tooth was hung from a spring balance and then lowered into the beaker until it was fully submerged underwater but not resting on the base of the beaker (right side of Figure 4.3). The change in weight that is observed on the top pan balance is due to the weight of water being displaced by the tooth. Pure water was

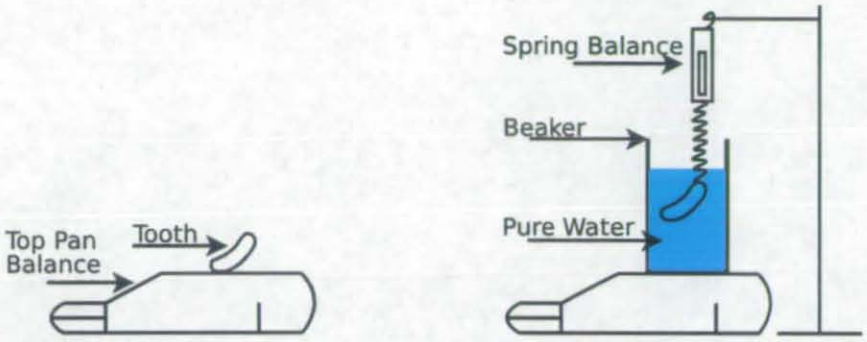

Figure 4.3: Experimental setup for measuring the density of a tooth.

used which has a density of 1000 kgm^{-3}, the weight of the displaced water is used to calculate the volume of displaced water and thus the volume of the tooth. From this the density can be found. This process is expressed in Equation 4.3.

$$Density = \frac{weight\ in\ air}{weight\ in\ air - weight\ inwater} \times Density\ of\ Water \tag{4.3}$$

To improve the overall accuracy three teeth from an adult male dolphin were used in the measurements. These teeth (unlike those of younger specimens) are fully filled with dentine as can be seen in Figure 4.1. The results of the density measurements are shown in Table 4.1.

Tooth Number	**Weight in air /kg**	**Weight in water /kg**	**Density kg·m^{-3}**
Tooth 1	0.00127	0.00063	1983.20
Tooth 2	0.00103	0.00053	2061.99
Tooth 3	0.00138	0.00071	2061.01
		Average	2035.4

Table 4.1: Tooth Density Results

The density for the dolphin tooth compares well to similar densities which can be see in Table 4.2

Material	Density /kg·m^{-3}
Water*	1000
Kidney, Liver, Muscle, Blood*	1050
Human* Fat	920
Polyethylene**	900
Rubber neoprene**	1330
Clay rock**	2200
cartilage***	1100
Human Tooth (dentine)****	2030-2350
Human Tooth (enamel)****	2890-3020

Table 4.2: Tooth Density Results for a selection of other materials *[4.11] **[4.12] ***[4.13] ****[4.14]

4.3.2 *Sound Velocity In A Freely-Suspended Tooth*

The equipment was initially configured as shown in Figure 4.4(a). Two 15 mm long piezoceramic bi-morph vibrational elements shown in Figure 4.5 were attached using a malleable thermosetting glue to one side of the tooth in order to excite the transverse vibrational mode. A 400 μs pulse containing a pure 100 kHz sine wave was transmitted from the top element (T) and received on the second identical element (R). A Tektronix digital oscilloscope with a 10 MHz sample rate was used to record both the outgoing and incoming signals, no other apparatus was used that could cause additional propagation delays. From this data the delay was determined and thus the speed of sound could be calculated. The experiment was repeated using the setup in Figure 4.4(b), this time with a pair of uni-morph elements depicted in Figure 4.6 where attached to the ends of the tooth in order to excite the compressional mode. The same signal processing and measuring techniques were then applied in order to find the transmission delay.

In order to remove unwanted noise and Spectral components from the results, all signals were filtered using a second-order Butterworth band pass filter having corner frequencies at 70 kHz and 130 kHz prior to analysis. The same filter was applied to each signal

Transverse Wave Speed	2200ms^{-1}
Longitudinal Wave Speed	3380ms^{-1}

Table 4.3: Measured sound speeds in the tooth.

so that the phase delays introduced would cancel out. The propagation time delay for the transverse case was determined at 10.45 μs and 7.78 μs for the compressional case. Sound velocity estimates based on these times of arrival are therefore approximately 2200m.s^{-1} and 3380m.s^{-1} respectively. The propagation distance in the transverse measurement was assumed to be slightly shorter (23.11 mm) than the overall tooth length due to the finite contact area of the bi-morph element on the face of the tooth. These results are summarised in Table 4.3 and for comparison the sound speeds of some other materials are listed in Table 4.4.

Material	Longitudinal Wave Speed ms^{-1}
Soft Tissues*	1540
Brain*	1541
Liver*	1549
Kidney*	1561
Blood*	1570
Muscle*	1585
Lens of Eye*	1620
Skull Bone*	4080
Human Tooth (dentine)**	3140-4140
Human Tooth (enamel)**	4500-6250

Table 4.4: Sound speeds for a selection of organic materials. *[4.12] **[4.14]

4.4 Modal Analysis

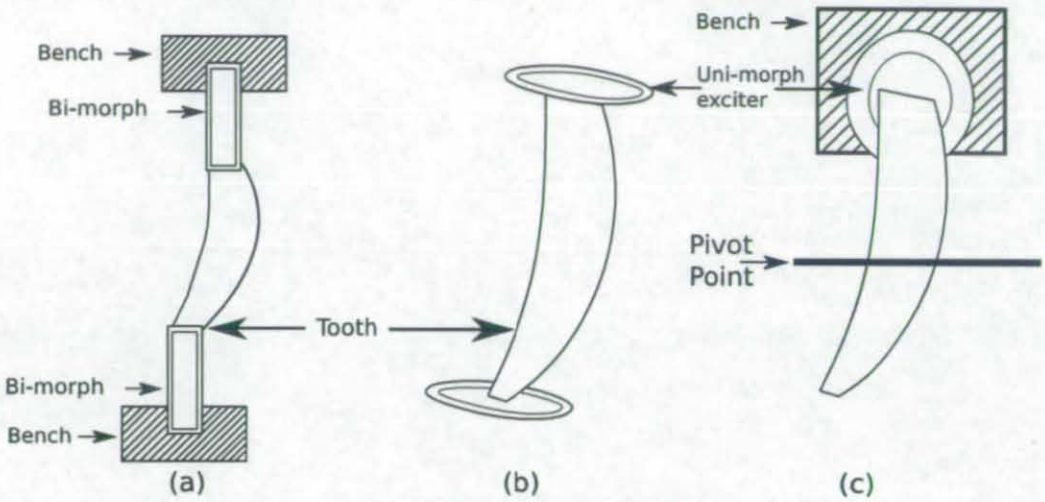

Figure 4.4: Tooth vibration measurement setup

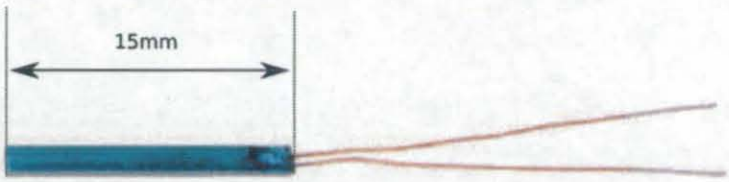

Figure 4.5: Bi-morph Vibrational Element

4.4.1 Measurements Of Tooth Resonance In Air

In this section, the vibrational modes and propagation velocities of individual teeth are examined using both standard and LDV measurement techniques. For the LDV tests the optical unit was placed approximately 2 m away from the tooth with the beam path tangential to the measurement surface. Two different teeth of mid-size were extracted from a lower jaw specimen for analysis. The first tooth had an overall length of 26.30 mm and was used in experiments (a) and (b) while the second tooth, measuring 26.4 mm was used in experiment (c). In order to improve the intensity of the scattered light from the tooth a thin layer of retro-reflective beads were adhered to the surface of the tooth. Retro-reflective beads are small glass spheres that allow light to be scattered back in the direction it originally travelled from, these are commonly used in traffic cones and reflective safety jackets.

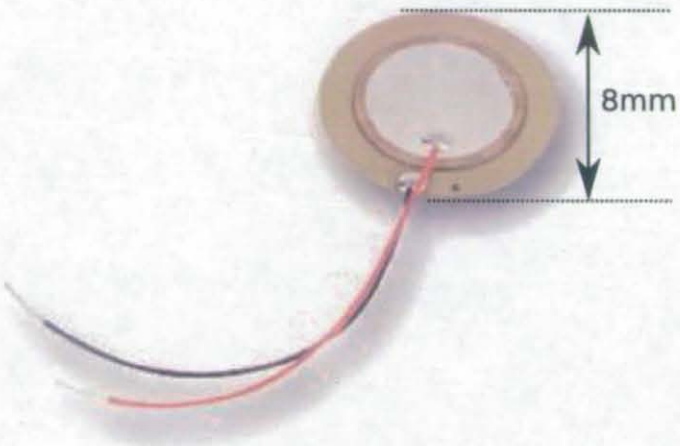

Figure 4.6: Unimorph Vibrational Element

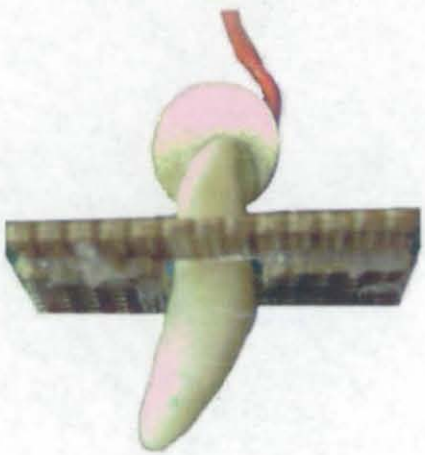

Figure 4.7: Jig Setup for Bending Mode investigation

4.4.2 *Modal Properties Of A Restrained Tooth*

Since the tooth cannot be assumed to be freely suspended when mounted in the jaw-bone, the transverse vibrational mode was studied in more detail by being mounting in a test jig shown in Figure 4.7. The LDV was used to examine the modal structure at several different input frequencies. The rationale behind these frequencies is explained later on. The objective was to examine the phase and amplitude changes as a function of distance along the body of the tooth. To perform this experiment, the tooth was

Figure 4.8: Jig Setup for Breathing Mode investigation

mounted as shown in Figure 4.4(c). The tooth was firmly clamped at approximately 11 mm below the tip using two flat pieces of FR2 strip board, of 2 mm thickness. Other than this clamp, no other physical restraints were applied to the tooth. A single uni-morph disc element was attached to the top of the tooth using the same glue as in the previous experiment. A 500 μs pulsed sine wave at the frequency of interest (80 kHz,100 kHz,123 kHz,134 kHz) was then projected into the tooth, and a number of data points were sampled using a Polytech PSV300 Scanning Vibrometer (PSV).

The results of phase variation along the length of the tooth are depicted in Figure 4.9, which show that for signals which lie within the frequency band of the outgoing echolocation click of the animal, there are between 2 and 2.5 wavelengths along the tooth. There is a clear, and relatively uniform modal structure set up with a reasonably linear

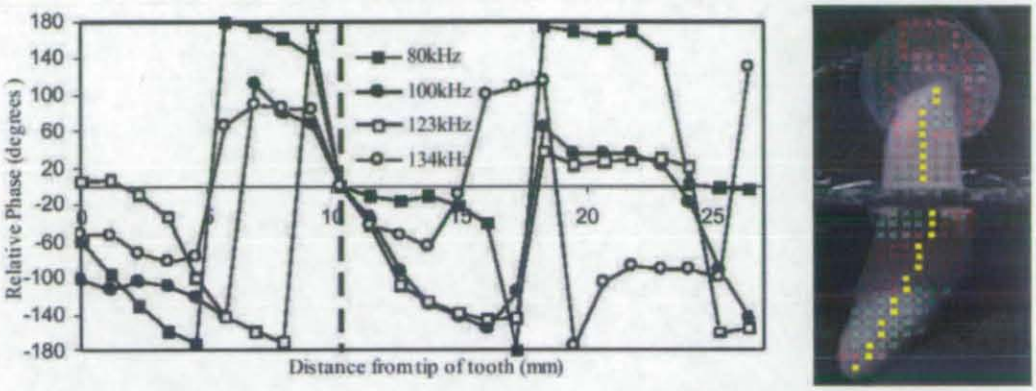

Figure 4.9: (a) Phase variation along the tooth at resonance, (b) Mode structure visualisation at123 kHz. The yellow squares on (b) correspond to the phase measurement positions in (a).

phase variation with distance. The result also confirms the existence of the transverse mode within the tooth at these frequencies. It seems quite possible, therefore, that the transverse mode could be excited by an incoming echo, and that this could be coupled into other tissues for eventual processing at the tympanic bulla, or detection via the neurological system.

A further experiment was carried out with the setup shown in Figure 4.8. This setup was used to examine if the tooth could vibrate with a breathing mode. Such a mode would absorb incoming sounds and cause the structure to grow and shrink, similar to a diaphragm during breathing. In this case the tooth was firmly attached to a uni-morph disc element. The element was driven at a range of frequencies between 50 kHz and 130 kHz, while the LDV measured a point in the centre of the tooth and a point on the transducer. If the tooth were to exhibit a breathing mode then there would be a change in the phase difference between the two points. The results of this experiment were that no phase change was observed and therefore the tooth does not contain a breathing vibrational mode.

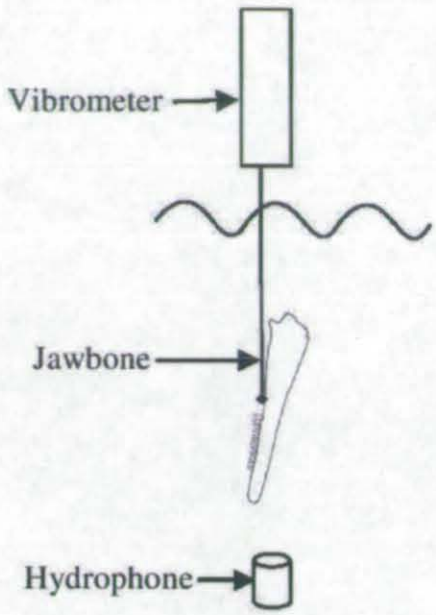

Figure 4.10: Bone velocity measurement setup in water.

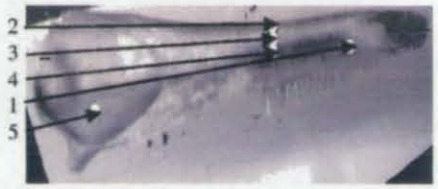

Figure 4.11: Spot measurement locations.

4.4.3 *Bone Propagation*

The work carried out by Brill [4.15] has shown the lower part of the mouth to be the main reception site of returning dolphin echolocation pulses. In order to study sound propagation inside the jawbone, two experiments were devised. Firstly a simple in-air analysis with the PSV, secondly a more sophisticated measurement with the jawbone fully immersed in water and with the PSV laser projecting downwards into the water column.

For the in-air measurements a uni-morph element was affixed to the dense bone material at the front of the jaw. The jaw was freely suspended with tethers. A 400 μs pulsed 100 kHz sine wave was then injected into the uni-morph terminals and the PSV was

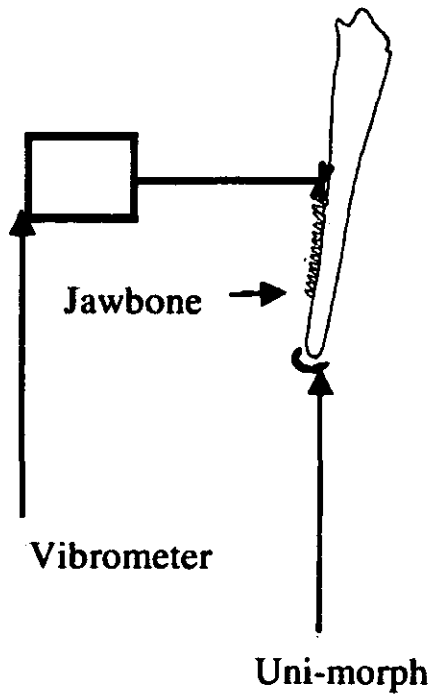

Figure 4.12: Bone velocity measurement setup in air.

used to measure the peak surface displacement as a function of distance from the source. The oscilloscope mentioned earlier was used to obtain time of arrival measurements up to 55 mm from the source. The second measurement was carried out in a large freshwater tank with the experimental setup shown in Figure 4.10. The equipment was configured with the laser directly above the centre of the hydrophone in order to minimise the acousto-optical effect that occurs as the light travels through water [4.6]. For practical reasons the bone had to be tilted relative to the normal of the hydrophone surface plane at an angle of approximately 11°. This was necessary in order to allow the laser to scan the full length of the bone. This tilt angle is close to the 6° offset which forms the natural shape of the dolphin skull. During the LDV measurement a calibrated hydrophone was used to transmit a 1 ms pulsed 100 kHz sine wave. The PSV was used to measure the time of arrival at various positions (see Fig. 3). Due to problems with light scattering and low reflection levels, the bone was treated with retro-reflective beads.

In the directly-coupled measurements of the bone in air, the time of arrival measurements gave a mean sound velocity of 2607 $m.s^{-1}$. Measurements of displacement along the jaw became increasingly difficult on account of the high attenuation rate. Over the first 20 mm from the source an attenuation rate of 1.2 dB mm^{-1} was observed. For the in-water measurements the velocities determined from the times of arrival are shown in Table 4.5. The estimates obtained appear close to the speed of sound in water. On account of the high attenuation rates observed in the direct coupled measurements, and since this estimate of sound velocity is also in conflict with the earlier results we would therefore conclude that the arrival times measured are due to the water-borne sound causing vibration in the bone. Significantly, we do not believe that the largest proportion of the energy arriving at the data points had successfully propagated down the length of the jawbone.

Point	Speed From Point 1 in water
2	1523 m/s
3	1559 m/s
4	1560 m/s
5	1596 m/s
Average	1560 m/s

Table 4.5: Bone velocity measurements in water.

4.4.4 *Tooth And Bone Measurements*

If the teeth are operating as an active element as has been suggested [4.1, 4.3] then it seems likely that they would exhibit resonant behaviour. Further measurements were therefore carried out on the in-water setup of Figure 4.10. The PSV was directed towards two separate teeth on the jawbone. One of the teeth was near to the sound source at the front of the jawbone (referred to as Tooth A) and the second was further back in the jaw (referred to as Tooth B). A swept frequency source was then used to pick out any resonant behaviour. The calibration carried out on the transducer prior to the mea-

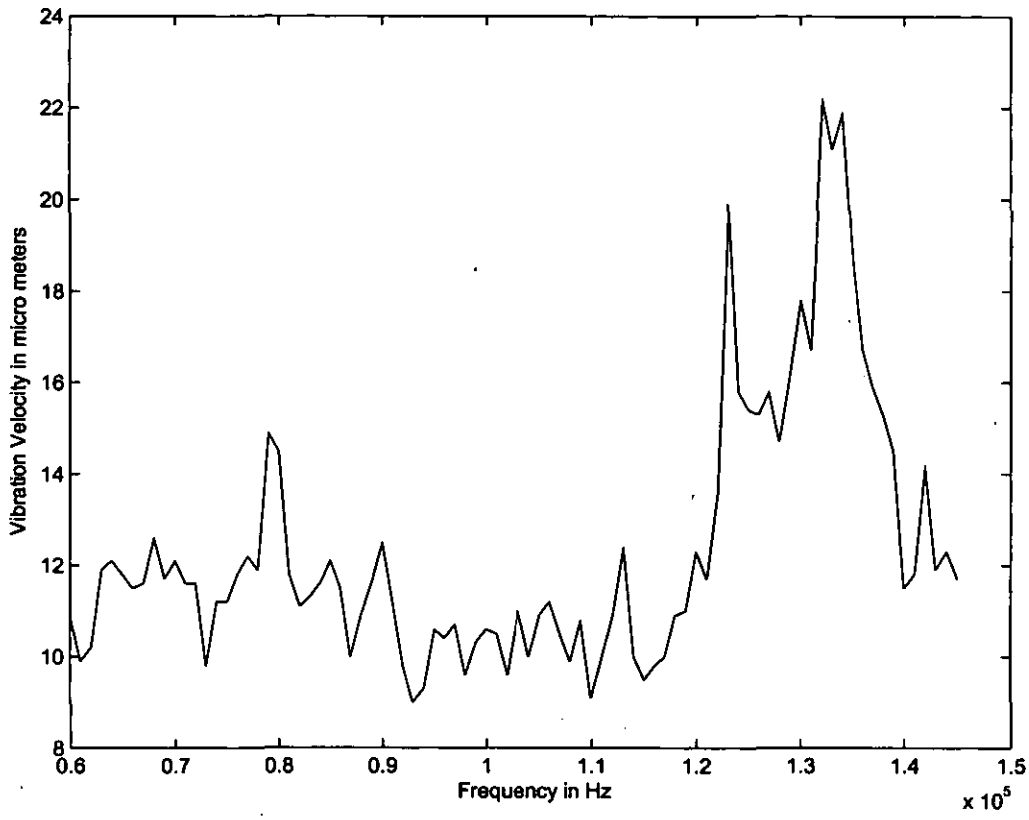

Figure 4.13: Tooth A vibrational resonance

surement ensured that the sound pressure level was equalised over the measurement band. The maximum surface velocity was then determined for each tooth as a function of frequency. From the graphs in Figures 4.13 and 4.14 a clear similarity can be seen, with resonant peaks at approximately 80 kHz to 90 kHz and then a resonant band from 115 kHz to 135 kHz. It is worth noting that these frequencies lie within the commonly accepted band of the Bottlenose Dolphins echolocation signal [4.16].

4.5 Discussion and Further Analysis

4.5.1 Tooth Characteristic Impedance

Characteristic acoustic impedance is the ratio of effective sound pressure at a point to the effective particle velocity at a point in a free progressive wave and is analogous to

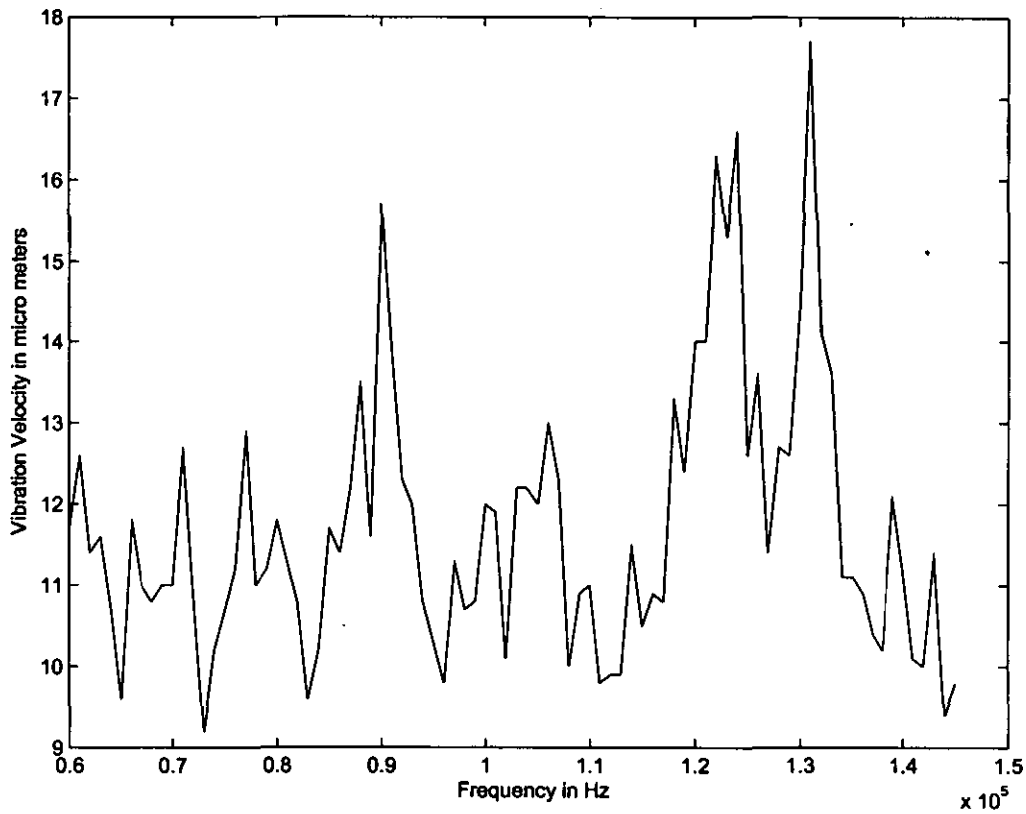

Figure 4.14: Tooth B vibrational resonance

the characteristic electrical impedance of an infinitely long, lossless transmission line. This impedance can be calculated using Equation 4.4. The measurements conducted in the previous section allow an estimate to be made for the tooth impedance. Using the average tooth density from Table 4.1 and taking the transverse mode velocity measured, the impedance is 4.48 MPa·s·m^{-3}, which is approximately three times larger than sea water which is 1.45 MPa·s·m^{-3} [4.17].

At an impedance change boundary, a proportion of the acoustic wave will propagate through the boundary, while the remainder will be reflected back into the original medium.

$$Z = \rho c \tag{4.4}$$

$$\Gamma = \frac{Z_2 - Z_1}{Z_1 + Z_2} \tag{4.5}$$

$$\tau = \frac{2 \cdot Z_2}{Z_2 + Z_1} \tag{4.6}$$

If a plane wave of pressure p_i is incident upon a planar surface and in a medium with impedance Z_1 when the second surface is constructed from a medium with impedance Z_2 the ratio of reflected pressure Γ can be calculated from the impedance relationship using Equation 4.5, while the transmitted energy ratio τ can be calculated using Equation 4.6. Using the assumption that a plane wave is propagating in sea water, the coefficient of pressure that would be coupled into a medium made from the same material as a tooth would be 0.5 while the reflection coefficient would be 0.5. This analogy is not entirely accurate as this does not take account of the translation between longitudinal wave in a liquid medium switching into sheer waves in the solid medium, or the effect of incident angle.

4.5.2 *Experimental Limitations*

It is worth noting that the jawbone of a living animal will normally be filled with fatty lipids [4.18] that are shown to have a varying sound speed close to water. The Acoustic impedance of Caster Oil is 1.54 MPa·s·m^{-3} and seawater at 1.45 MPa·s·m^{-3} [4.17] and the lipids of the lower jaw are assumed to be similar [4.19]. It is also worth noting that the method of clamping the tooth when examining the bending moments is not the same as the mechanism which holds the tooth in the lower jaw, and therefore the bending moments will differ.

4.6 *Conclusions*

The fact that the teeth of the specimen measured exhibited resonant behaviour within the dolphin echolocation frequency range provides further support for the theory that

they are involved in hearing. The LDV technique has produced modal maps showing that the tooth has between 2 and 2.5 wavelengths along its length in this band. The tooth resonance has been confirmed in isolation by several in-air measurements and also when mounted in the jaw in fresh water. The bone measurements suggest that it is possible to couple sound into the jaw, however the attenuation of the wavefront as it propagates from the tip of the jaw seems very high. This would rule out the possibility that the hard material in the bone acts as the primary acoustic pathway from the nose of the animal to the tympanic bulla. A more likely route for sound conduction is via the fatty channel within the jaw cavity. This theory is consistent with the recent work of Ryabov [4.20]. A sound conduction path which is not ruled out by our measurements is therefore from the teeth via the fatty channel and then to the tympanic bulla. It should be emphasised, however that the specimen used in the experiments was devoid of any soft tissue and that the presence of lipid materials, blood etc, which will affect the acoustic properties, especially in the jaw cavity and in the areas surrounding the teeth.

References

[4.1] A. D. Goodson and M. Klinowska, *A proposed receptor for the Bottlenose Dolphin (Tursiops truncatus) modelling the receive directivity from tooth and lower jaw geometry*, vol. NATO ASI Series A of *Sensory Abilities of Cetaceans*, pp. 255–267. Plenum, 1990.

[4.2] J. R. Potter and E. A. Taylor, "On novel reception models for bottlenose dolphin," in *Proceedings of the Institute of Acoustics* (A. D. Goodson and P. F. Dobbins, eds.), vol. 23, pp. 103–110, July 2001.

[4.3] P. F. Dobbins and A. D. Goodson, "Shallow water, very short range biomimetic sonar concepts," in *Proceedings of the Institute of Acoustics*, vol. 26, Apr. 2004.

[4.4] A. Hohn, M. Scott, R. Wells, J. Sweeney, and A. Irvine, "Growth layers in teeth from free-ranging, known-age bottlenose dolphins," *Mar Mamm Sci*, vol. 5, no. 4, pp. 315–342, 1989.

[4.5] S. R. Freeman, M. K. Quick, M. A. Morin, R. C. Anderson, C. S. Desilets, T. E. Linmenbrink, and M. O'Donnell, "Heterodyning technique to improve performance of delta-sigma-based beamformers," *IEEE transactions on ultrasonics, ferroelectrics, and frequency control*, vol. 46, no. 4, pp. 771–790, 1999.

[4.6] C. B. Scruby and L. E. Drain, *Laser ultrasonics : techniques and applications*. Hilger, Bristol, 1990.

[4.7] R. I. Crickmore, S. H. Jack, D. B. Hann, and C. A. Greated, "Laser doppler anemometry and the acousto-optic effect," *Optics and Laser Technology*, vol. 31, no. 1, pp. 85–94, 1999.

[4.8] Y. Wang, P. Theobald, J. Tyrer, and P. A. Lepper, "The application of scanning vibrometer in mapping ultrasound fields," *Journal of Physics Conference Series*, vol. 1, pp. 167–173, 2004.

[4.9] P. D. Theobald, S. P. Robinson, A. D. Thompson, R. C. Preston, and P. A. L. W. Yuebing, "Technique for the calibration of hydrophones in the frequency range 10 to 600 khz using a heterodyne interferometer and an acoustically compliant membrane," *The Journal of the Acoustical Society of America*, vol. 118, no. 5, pp. 3110–3116, 2005.

[4.10] C. J. D. Pickering, N. A. Halliwell, and T. H. Wilmshurst, "The laser vibrometer-a portable instrument," *Journal of Sound and Vibration*, vol. 107, pp. 471–485, 1986.

[4.11] A. Harland, *The application of laser doppler velocimetry to the measurement of underwater acoustic fields*. PhD thesis, Loughborough University, UK, 2002.

[4.12] "Velocity of sound in various media." `http://www.rfcafe.com/references/general/velocity_sound_media.htm` last accessed January 2008.

[4.13] "Physical properties of human tissue." `http://www-ibt.etec.uni-karlsruhe.de/people/mag/frames/papers/EMC99-MD/node3.html` last accessed January 2008.

[4.14] "Medical ultrasonics." `http://www.kayelaby.npl.co.uk/general_physics/2_4/2_4_6.html` last accessed January 2008.

[4.15] R. L. Brill, *The jaw hearing dolphin: Preliminary behavioural and acoustical evidence*, pp. 281–287. Animal Sonar: Processes and performance, NY: Plenum, 1988.

[4.16] W. W. L. Au, *The sonar of dolphins*. New York: Springer-Verlag, 1 ed., 1993.

[4.17] F. W. R. de Haan, "Hearing in whales," *Acta Otolaryngolica*, pp. 1–114, 1957.

[4.18] H. N. Koopman, S. M. Budge, D. R. Ketten, and S. J. Iverson, "Topographical distribution of lipids inside the mandibular fat bodies of odontocetes: remarkable complexity and consistency," *Oceanic Engineering, IEEE Journal of*, vol. 31, no. 1, pp. 95–106, 2006.

[4.19] K. S. Norris, "The evolution of acoustic mechanisms in odontocete cetaceans," *Evolution and Environment, Yale University, Connecticut*, pp. 298–323, 1968.

[4.20] V. A. Ryabov, "Peripheric parts of the dolphin echolocation hearing," in *Proceedings of Marine Mammals of the Holarctic*, vol. 1, pp. 483–489, Oct. 2004.

CHAPTER 5:

BAND GAP HEARING IN THE LOWER JAW AND TEETH

THIS section of the thesis describes the phenomenon of acoustic stop bands or band gaps, and goes on to examine how this phenomenon might play a role in the sound reception thought the lower jaw structure of the dolphin. In order to examine this in detail, numerical modelling techniques have been applied and custom software designed and produced based upon the Transmission Line Modelling technique.

5.1 Introduction

TLM has been used in acoustics for a number of years and has been proved to be an equivalent to finite difference time domain modelling. The main benefit of TLM when compared to other volume element methods are its speed and its ability to model highly complex geometrical features effectively [5.1]. An advantage of choosing a time domain technique is the ability to capture a broad frequency band in a single simulation run. This is a particularly important feature when modelling dolphin sonar excitations which are, by nature, broadband. The use of the TLM technique in this work allowed for rapid design construction and simulation of complex geometries as well as the use of signals that would be difficult to produce and would be time consuming to carry out experimentally.

5.1.1 Numerical Modelling Technique

The Transmission Line Modelling (TLM) method is a time domain, differential numerical modelling technique ideally suited to the study of field problems [5.2]. It has found many applications including those within the field of bioacoustics [5.3, 5.4] and is broadly comparable with the finite difference method in the time domain [5.5]. TLM exploits the analogy between waves propagating in an acoustic field and pulses propagating on an orthogonal mesh of interconnected transmission lines. These transmission lines are governed by differential equations which are isomorphic to those of the transmission medium and thus the network can model the propagating waves. The equivalence of the transmission line model with the linearised Euler equations in acoustics can be proved mathematically and consequently it is possible to conceptually manipulate just the transmission lines. An additional advantage of applying transmission line equivalents is that stability criteria are guaranteed to be met when the model includes only passive electrical components. Typically TLM is applied to a structured arrangement of cubic or parallelepipedic cells (the mesh) which are individually termed nodes.

Discretization

In order to simulate real work problems, the physical geometry must be discretised into meshed mathematical nodes. This process introduces the problem of spherical quantisation which is analogous to the quantisation of voltage in an analogue to digital converter. Figure 5.1 shows a sphere in the real world analogue domain and in the digital form after processing for TLM modelling. It is therefore very important that the correct sampling rate is selected to avoid erroneous results due to the discretisation. The disadvantage to high definition digital models is that more computer memory is needed. However if an insufficient number of nodes are used then dispersion becomes problematic. Typically 10 nodes are required in each spatial direction per wavelength at the maximum frequency of interest. For example, if the model requires simulation at 100 kHz in a pure water medium with a sound speed of 1500 ms^{-1} then the cell size Δl would be calculated as follows,

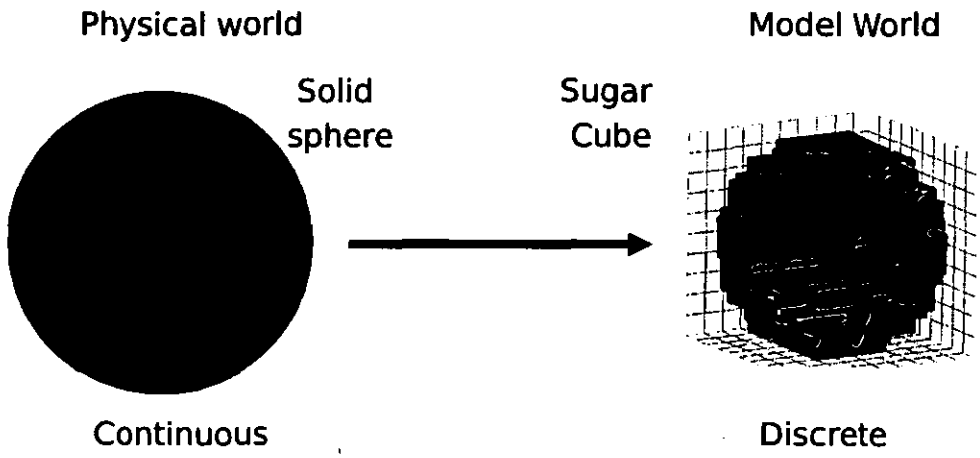

Figure 5.1: Example transformation of real world objects into a TLM mesh

$$\lambda_{100\ kHz,water} = \frac{c}{f} = \frac{1500}{100{,}000} = 0.015\ m$$

$$\Delta l = \frac{0.015}{10} = 0.0015\ m = 1.5\ mm$$

Dispersion

Much more rigorous consideration to the problem of dispersion has been given by De Cogan [5.6] and Neilson [5.7]. Since the focus of this thesis is the application of TLM to the problem of dolphin hearing a detailed theoretical analysis will not be presented. However steps have been taken to establish and confirm experimentally the effect of dispersion. As an example a 2 dimensional shunt-node TLM program was used to study cylindrical wave propagation. In the model a centrally excited single-cycle sinusoid at a frequency of 7.5 kHz was applied. The graphical results are presented in Figure 5.2. The mesh for this model had a node spacing of 0.10 m (2 nodes per wavelength in the chosen medium). As the time domain waveform demonstrates the effect of dispersion vary according to angle with the worst effect of dispersion noticed at 45^o to the meshing axis.

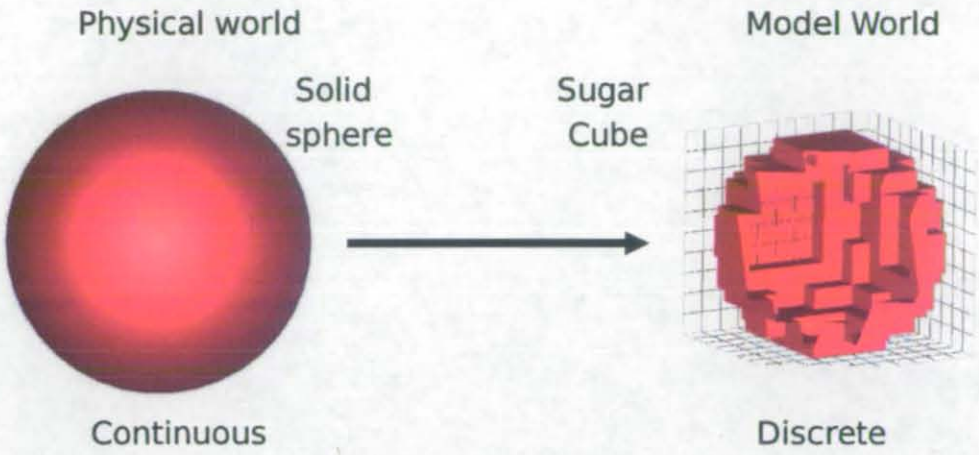

Figure 5.1: Example transformation of real world objects into a TLM mesh

$$\lambda_{100\ kHz,water} = \frac{c}{f} = \frac{1500}{100{,}000} = 0.015\ m$$

$$\Delta l = \frac{0.015}{10} = 0.0015\ m = 1.5\ mm$$

Dispersion

Much more rigorous consideration to the problem of dispersion has been given by De Cogan [5.6] and Neilson [5.7]. Since the focus of this thesis is the application of TLM to the problem of dolphin hearing a detailed theoretical analysis will not be presented. However steps have been taken to establish and confirm experimentally the effect of dispersion. As an example a 2 dimensional shunt-node TLM program was used to study cylindrical wave propagation. In the model a centrally excited single-cycle sinusoid at a frequency of 7.5 kHz was applied. The graphical results are presented in Figure 5.2. The mesh for this model had a node spacing of 0.10 m (2 nodes per wavelength in the chosen medium). As the time domain waveform demonstrates the effect of dispersion vary according to angle with the worst effect of dispersion noticed at 45° to the meshing axis.

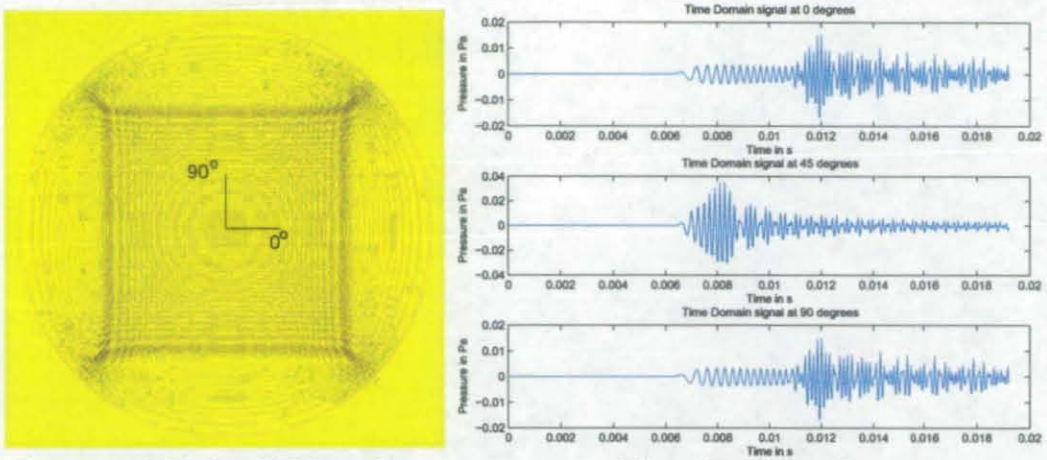

Pressure field after 250 iterations. Time domain results.

Figure 5.2: Example of dispersion in a TLM model

5.2 Acoustic Band Gaps

Wave propagation in 2 and 3 dimensional periodic structures in the field of electromagnetics has received great attention in recent years. This is due to the promise of being able to engineer far field radiation and reception patterns by manipulation of the near field scattering structure. This ability is highly desirable to antenna designers as well as more fundamental uses such as Anderson localisation of light [5.8]. In addition, a number of practical applications have been proposed including 'narrow bandpass filters, enhanced surface mounted microwave antennas, sharp bend radius waveguides, and the zero threshold laser.' As a result of this interest the research community has begun to analyse the similarity of electromagnetic band gaps for acoustic pressure waves. The main motivation for this is the possibility to control the propagation and reception of acoustic signals, as well as producing passive filters for noise and vibration isolation. One example of where this is need in the field of underwater acoustics is for isolating construction noise such as piling in sensitive environments. The symmetry involved in periodic arrays allows a solution to be formed based upon the plane wave expansion techniques. Due to the similarity in the analytical solution method between these problems and the analogous problems in solid state physics much of the terminology has been continued over. The differences between the nature of electron wave functions,

and electromagnetic and acoustic waves are accounted for in adapting these techniques from one regime to another.

For band gaps to be present a periodic arrays of scattering elements must be constructed in a specific structure. When this is done certain frequency bands exhibit dispersive behaviour which prevents the passage of these frequencies [5.9]. It is possible to design such a structure in order that for certain bands, wave propagation is heavy attenuated, and the term band gap is often applied.

In acoustics the experimental observations of Robertson *et al.* [5.8], have demonstrated the existence of acoustic stop bands or band gaps within a periodic scattering array of long cylindrical metallic rods. It was demonstrated that if solid cylindrical rods are placed in a square or triangular lattice with a volumetric filling factor of greater than 0.3 then an acoustic band gap can be sustained. The filling factor F, for a square lattice can be calculated by Equation 5.1, where a is the separation between centres of adjacent elements and d is the diameter of the cylindrical rods.

$$F = \frac{\pi d^2}{4a^2} \tag{5.1}$$

Furthermore it has been established that the centre frequency f_c of the acoustic band gap can be predicted from the periodicity of the lattice geometry by using Equation 5.2, where u is the speed of sound propagation in the medium surrounding the rods.

$$f_c = \frac{u}{2a} \tag{5.2}$$

While it is possible to construct analytical solutions for simple infinite arrays with geometric symmetry, complex geometry and finite arrays typically require a brute force numerical solution method, hence the reason for choosing TLM to examine the propagation in the dolphin jaw.

5.3 TLM Benchmarks

Before applying the TLM software to a complex geometry the code was fully validated against a number of numerical benchmarks with exact analytical solutions.

5.3.1 Spreading

The first benchmark verified the spreading algorithms, which were compared against cylindrical spreading. This has an analytical solution of spreading loss = 10 log r, where r is the distance from the source. A five cycle 100 Hz sine wave was inserted at the centre of a square mesh measuring 1020x1020 nodes, where each node represents 10 cm, which offers 150 nodes per wavelength, which allowed for simulation without any artifacts being produced due to dispersion. The acoustic wave propagation was measured at 1 meter intervals (or every 10 nodes), the numerical mesh was made large enough to avoid any interaction with the external boundaries before the simulation was ended. The comparison between the modelling and the analytical solution can be seen in Figure 5.3. The modelled results were first converted from the raw time domain signal into rms pressure, and then into dB. The dB values were then normalised by subtracting the pressure value at 1 m from all other values. This made the value at 1 m 0 dB to match the analytical theory. From this we can see the cylindrical spreading modelled by the TLM software closely follows the analytical solution. The differences that do occur are at a range greater than the 1 m range, the simulations that follow all operate below 1 m.

5.3.2 Boundary Conditions

As this modelling software was intended for use in underwater acoustics, some of the common boundary conditions that arise in underwater acoustics were implemented. The boundary conditions implemented are described below along with their proof of operation.

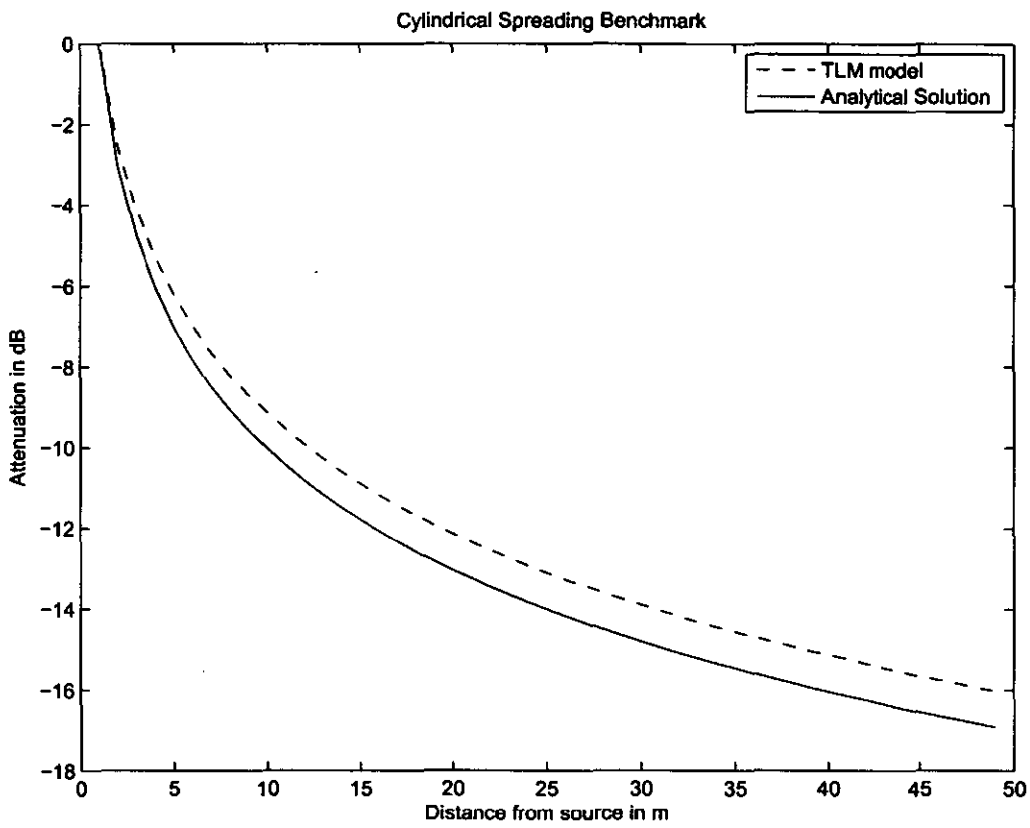

Figure 5.3: Cylindrical Spreading Benchmark of the TLM modelling software

Perfect Reflection Boundary condition Produces an in-phase reflection of the signal, the signal is reflected about the normal axis to the surface so that 'The angle of incidence is equal to the angle of reflection,' in accordance with Snell's law. A simulation was conducted in which a single cycle 1 kHz sinusoid was injected into a 2-d TLM mesh with a node spacing of 0.1 m, the speed of sound in the mesh was assumed to be 1500 ms^{-1}. The time domain signal can be seen in Figure 5.4. The losses in the signal are due to spreading as verified earlier. The distance between the first measurement point and the source is 10m, then the signal travels to the boundary and back which is a distance of 20 m leading to an analytical spreading loss of 4.71 dB. The time delay between the two signals is approximately 0.01333 s, which leads to a distance of 19.995 m. The actual spreading loss seen in the model is 5.73 dB,

Pressure release boundary condition Occurs on the interface between air and water

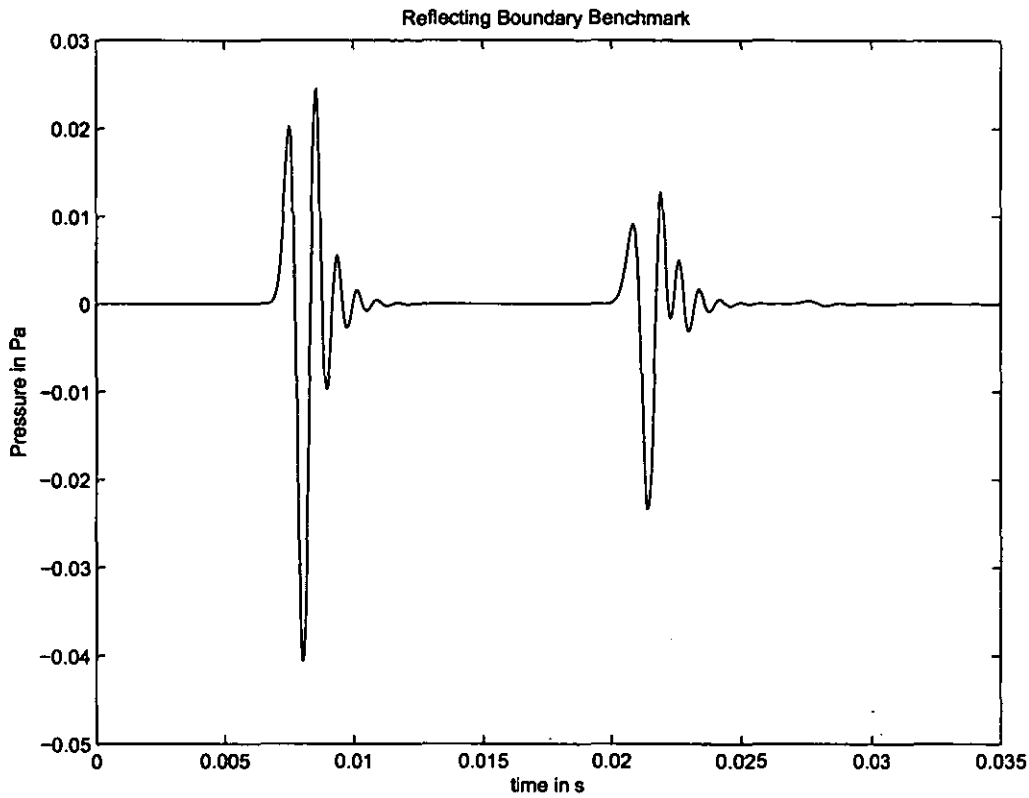

Figure 5.4: Time domain waveform of an incident and reflected sine wave

particularly on the surface of the sea. This boundary inverts the incoming signal and reflects it in the same manor as a conventional reflector i.e the signal is reflected about the normal so that the angle of incidence is equal to the angle of reflection, however the phase of the signal is changed by 180 degrees. The same setup as for the previous boundary condition was used to verify the software and the incident and reflected time domain waveforms can be seen in Figure 5.5. In this graph we can see that the travel time is identical to the previous experiment and that the peak to peak pressure is the same, the only change is that the phase of the signal becomes inverted.

Absorbing boundary condition This boundary is capable of absorbing propagation waves, which can simulate heavily attenuation materials or propagation off into the far field. This boundary condition is not numerically perfect due to the analogy of impulses on a transmission line not being equal to pressure spreading. A single cycle sine wave was transmitted at an absorbing boundary which was placed in the same location as the

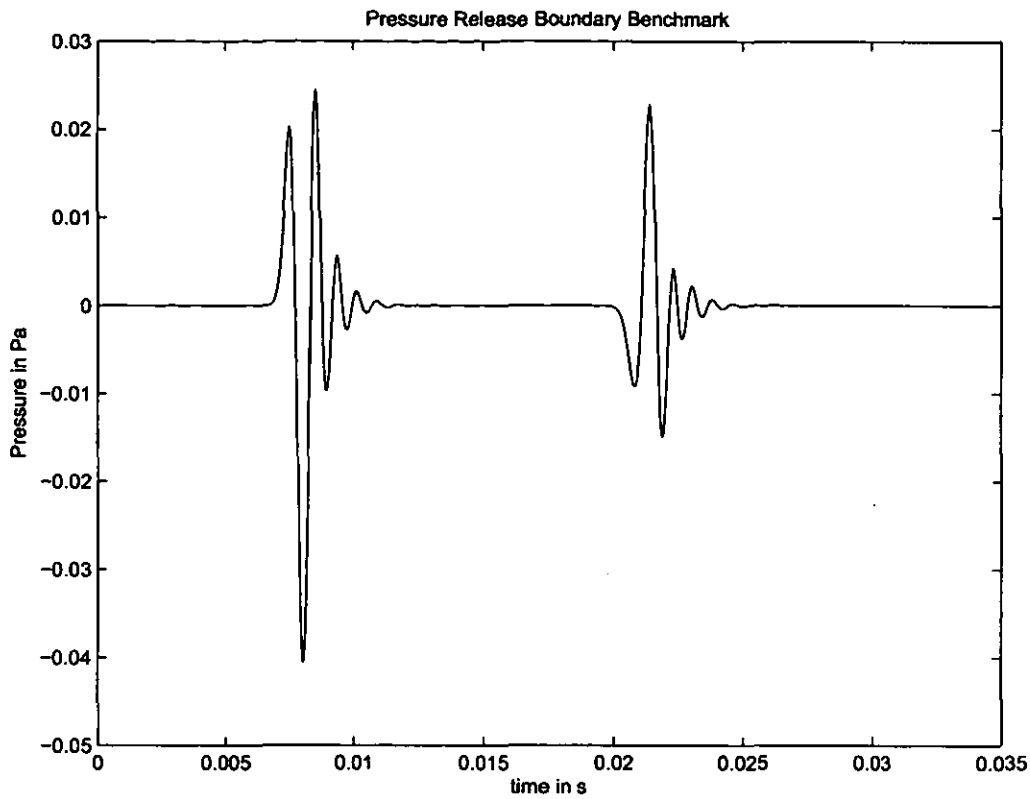

Figure 5.5: Time domain waveform of an incident and reflected sine wave

boundaries in the previous experiments. The signal was measured for the same duration as in the previous boundary conditions to see if a wave was reflected. The time domain wave form for this simulation can be seen in Figure 5.6, note the absence of a reflected pulse when comparing to 5.4 and 5.5. The energy that is returned is -32.5 dB lower when compared to the signals in the other boundary condition tests.

The software was then verified against the experiment performed by Robertson *et al.* [5.8]. A series of rods were spaced to replicate the spacings and diameters used in their experiment, this setup can be seen in Figure 5.7. The results for this bench mark can be seen in Figure 5.8. The source for the benchmark experiment was a Gaussian plane wave which excited frequencies from dc to above 10kHz. The scale of the experimental data has been normalised between 0 and 1 for easier comparison to the TLM results. All TLM results are normalised against a TLM model of exactly the same size, with the source and measurement points kept constant, but with the rods removed. These results

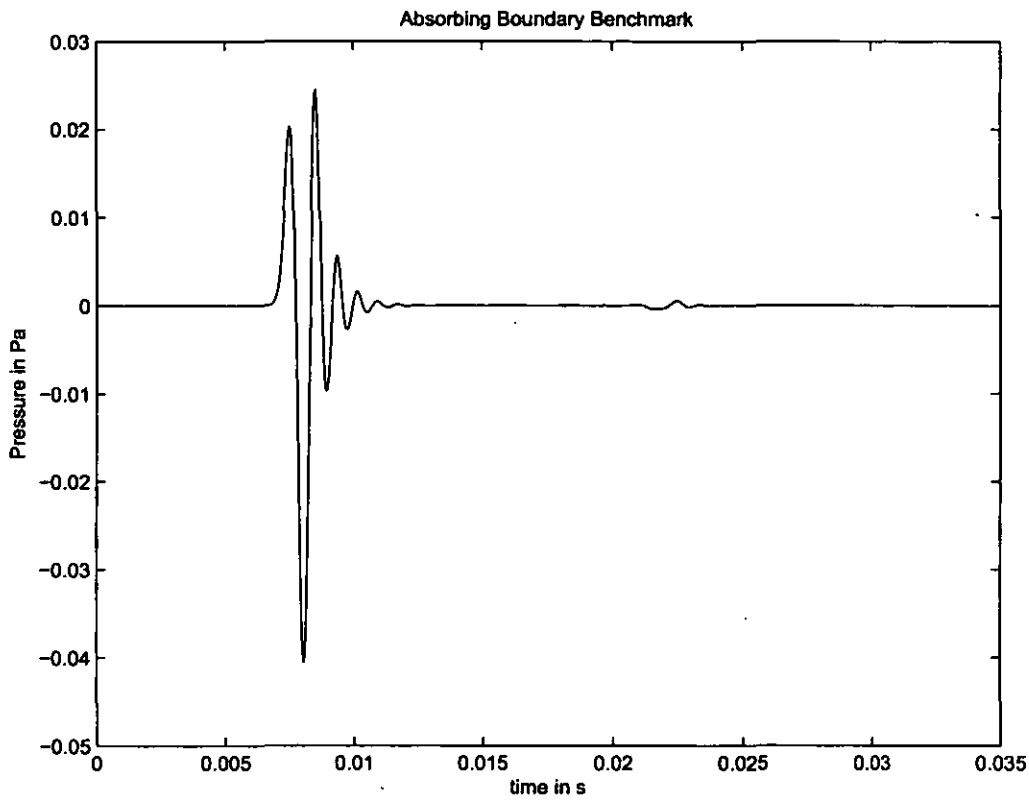

Figure 5.6: Time domain waveform of an incident and reflected sine wave

show very good correlation with the experimental evidence. The low frequency roll off below 2kHz in the experimental results is due to the frequency response of the speaker used. The higher frequency band gaps appear to correlate well and the tail off above 8kHz is very similar. This demonstrates that TLM is a useful modelling technique when looking for acoustic stop gaps.

5.4 Band Gap Hypothesis

The observations of Goodson and Klinoska [5.10] that the teeth in the lower jaw form a periodic structure with an almost uniform separation of 11.4 mm, have lead to the consideration of the existence of acoustic stop bands within the dolphin hearing system. Previous work carried out in Chapter 3 and published in [5.11] has revealed the speed of sound in the lower jawbone of a deceased adult Bottlenose Dolphin with out any flesh

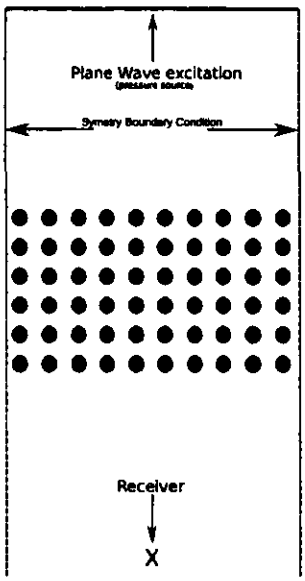

Figure 5.7: Benchmark TLM Geometry

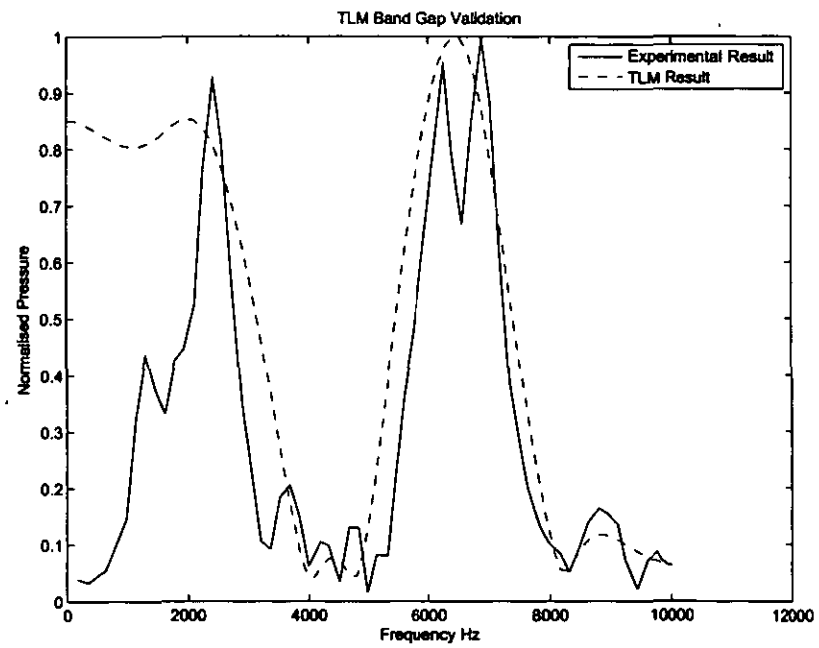

Figure 5.8: TLM Modelling results compared with experimental results performed by Robertson *et al.* [5.8]

Figure 5.9: CT cross section of the lower jaw and tooth of a Bottlenose Dolphin

or fatty materials present, is approximately 2600 m/s which is considerably higher than that of water 1500 m/s. This would result in a hard boundary condition which could act as an acoustic wave guide to any sound trapped inside the hollow bone channel. This work was also able to show that the speed of sound within an individual tooth is between 2200 m/s and 3380 m/s, in the best case this yields an impedance boundary of 4.48 MPa s m^{-3}. This gives a considerable impedance boundary between sound travelling in the hollow bone channel and the tooth. If sound were to enter the top of this channel the sound would have to travel down the hollow channel that is made up of various fatty lipids as has been shown by Koopman *et al.* [5.12]. In this work the authors show that the lower jaw is more complex than first thought, in that the jaw is not just made up from a single fatty material, but is made up from many compounds which are know to have differing sound velocities in much the same way as the melon does [5.13], this might serve to direct the sound around the contours of the jawbone. If this is the case then assuming that the sound is actually travelling in a straight line in a medium of uniform speed would not be far from the actual situation. From this evidence we have hypothesise the sound transmission path to be one where sound enters the hollow cavity of the jawbone near the rostrum of the animal, travels along the fatty sound channel, which is filled with teeth that are periodically spaced, sat within a wave guide and is then projected towards the ear. Using CT data that has been made available to us by the US Navy, which was originally taken by Houser *et al.* [5.14], we have been able to examine how a tooth is sat in the gum and jawbone of a dolphin.

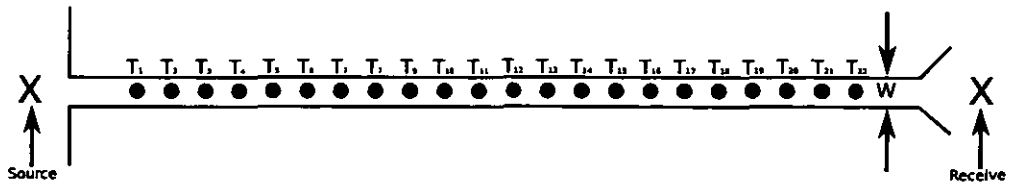

Figure 5.10: TLM Geometry

A small cross-section of the left side of a lower jawbone and the rooted section of a tooth can be seen in Figure 5.9. This picture shows the peg and socket nature of the dolphin tooth. The tooth is held in place by the gum and a soft bone structure that doesn't show up on this image due to its low density. From the header information in the CT images, it is possible to convert the number of voxels into real measurements where each voxel represents 0.6836 mm of space in each coordinate direction. Using this we can estimate the internal width of the channel to be between 8.9 mm near the top of the jaw and 11.6 mm near to the base. Further to this the diameter of the tooth is approximately 4 mm, which is confirmed by measurements with Vernier callipers on a tooth taken from the lower jaw of a deceased Bottlenose Dolphin that were used in chapter 4. With this information it is possible to construct a hypothetical two dimensional model of the tooth structure within the jawbone.

5.4.1 Finite Waveguide Models

Basic Model Set Up

Figure 5.10 shows the geometry used in the first 2-d simulations. A Gaussian signal, (shown in Figure 5.11), was injected as a point source on the left hand side of the simulation mesh aligned with the jawbone. The measurement point was placed at the far right of the mesh. The input signal was chosen in order to allows a wide band of frequencies within the outgoing dolphin click to be simultaneously excited. A horn with a 45^o angle was used at the exit end of the simulated jawbone to increase directivity and to emulate the transition from the jaw to the inner ear. An absorbing boundary condi-

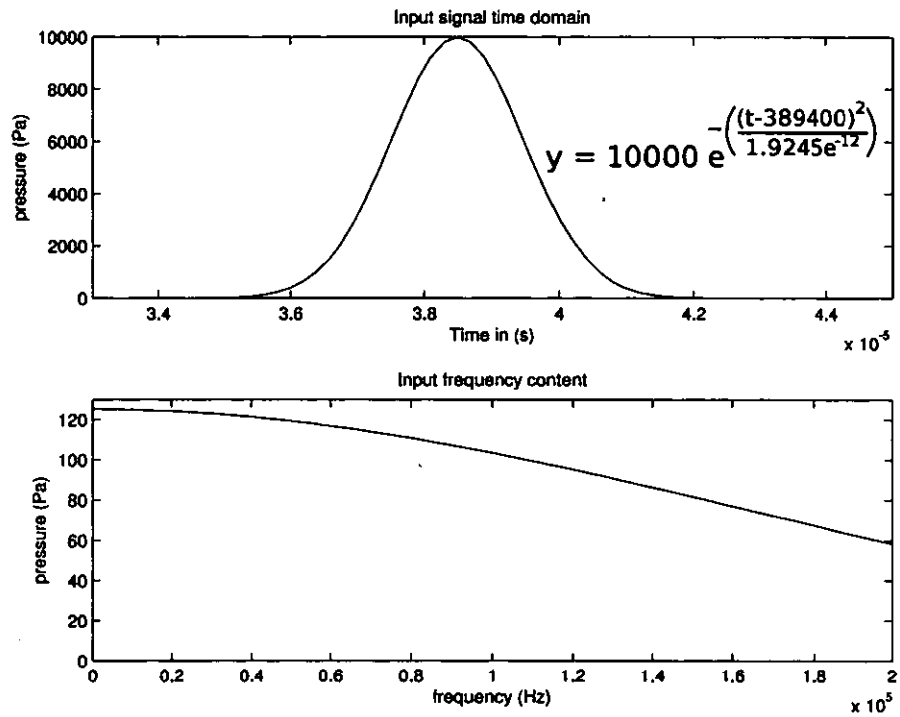

Figure 5.11: Input signal used in TLM simulations to produce a broadband excitation.

tion was applied to the outer surface of the mesh to avoid reflections. The teeth and jawbone shown in Figure 5.10 are modelled by applying a +1 reflection co-efficient at the periphery of each region within the numerical code. The mesh was constructed with a node size of 0.5 mm which given the sound speed of 1500 m/s allowed a maximum modelling frequency of 300 kHz. This scaling factor was chosen in order to minimise the effect of dispersion and the effect of mesh coarseness error (spacial quantisation), which can be an issue when modelling curved surfaces. In order to solely show the effect of the teeth on the model, a calibration simulation was run with all the teeth removed. The output signals were converted to the frequency domain using a 2048 point

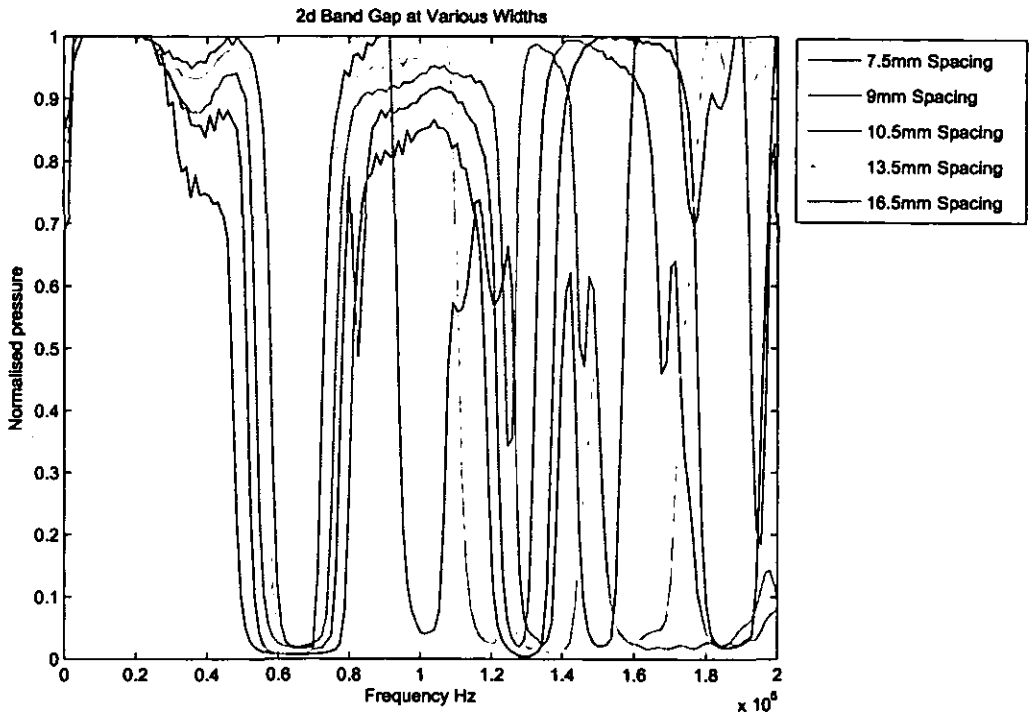

Figure 5.12: 2-D band gap structure for the hypothesised tooth model for a range of widths.

DFT and then the calibration run was used to generate the normalisation factors for the simulations. As the width of the hollow fatty channel is not constant in the dolphin the experiment was repeated for a range of channel widths (7.5 mm 9.0 mm 10.5 mm 13.5 mm 16.5 mm), in order to identify and study the effects on the band gap structure.

Results

Figure 5.12 shows the effect of the teeth upon the transmission of sound through the sound channel with a selection of different widths.

For all widths it can be seen that there is a stable band gap centred upon 65 kHz. This is close to the theoretical value that can be calculated by utilisation of Equation 5.2 which is 68 kHz. However less stability was observed in the secondary band gap that is formed at approximately 120 kHz. This band gap either continues for the rest of the hearing band or allows passage again at 135 kHz. This filter effect could serve to increase signal to noise ratio by filtering out unwanted lower frequencies whilst still

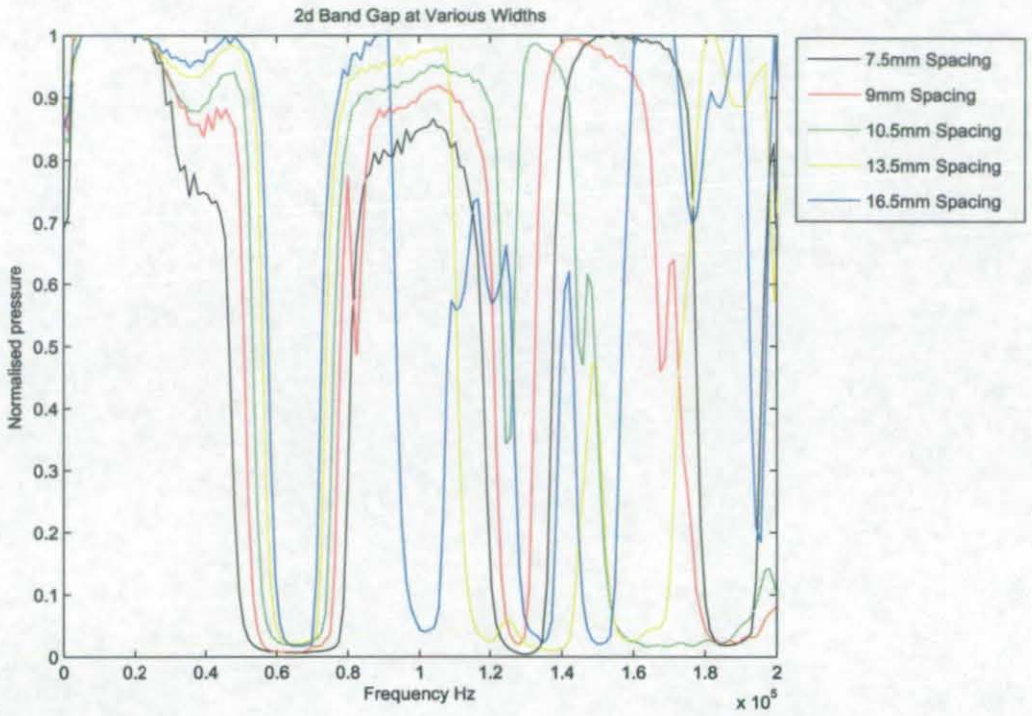

Figure 5.12: 2-D band gap structure for the hypothesised tooth model for a range of widths.

DFT and then the calibration run was used to generate the normalisation factors for the simulations. As the width of the hollow fatty channel is not constant in the dolphin the experiment was repeated for a range of channel widths (7.5 mm 9.0 mm 10.5 mm 13.5 mm 16.5 mm), in order to identify and study the effects on the band gap structure.

Results

Figure 5.12 shows the effect of the teeth upon the transmission of sound through the sound channel with a selection of different widths.

For all widths it can be seen that there is a stable band gap centred upon 65 kHz. This is close to the theoretical value that can be calculated by utilisation of Equation 5.2 which is 68 kHz. However less stability was observed in the secondary band gap that is formed at approximately 120 kHz. This band gap either continues for the rest of the hearing band or allows passage again at 135 kHz. This filter effect could serve to increase signal to noise ratio by filtering out unwanted lower frequencies whilst still

allowing those of interest to propagate to the ear. The slight ringing effect that can be seen in the pass band on the graph is due to the simulation output being substantially in the near field of the scattering array and its proximity to the absorbing boundary.

5.4.2 Finite Model With Teeth Removed

Model Set Up

One further effect that was examined in the 2-d model was the effect of the band gap when some teeth are removed from the jaw. In order to model this, a new simulation was laid out as in Figure 5.10 but this time various combinations of teeth were removed. The same input signal was applied and the same analysis techniques were used as for the previous experiment. A typical result for the model where T_4, T_7, T_{10} T_{11} and T_{19} have been removed is shown in the following section.

Results

The results shown in Figure 5.13 demonstrate that the band gap is sustained and still centred about 65 kHz, however it shows attenuation in what was previously the pass band of the echolocation frequencies. If the theory is correct this could suggest that the dolphin would suffer a decrease in signal to noise ratio as a result of loosening teeth. What is also apparent is that when all the teeth are removed a plane wave can pass directly down the channel without this filtering effect.

The 2-D results look reasonably convincing however it is clear from the CT slice shown in Figure 5.9 that the 2-D simulation is a crude approximation to the real geometry. In fact the tooth is not present for the full depth of the channel, nor is it infinitely long as has been assumed in the 2-D case thus caution should be exercised.

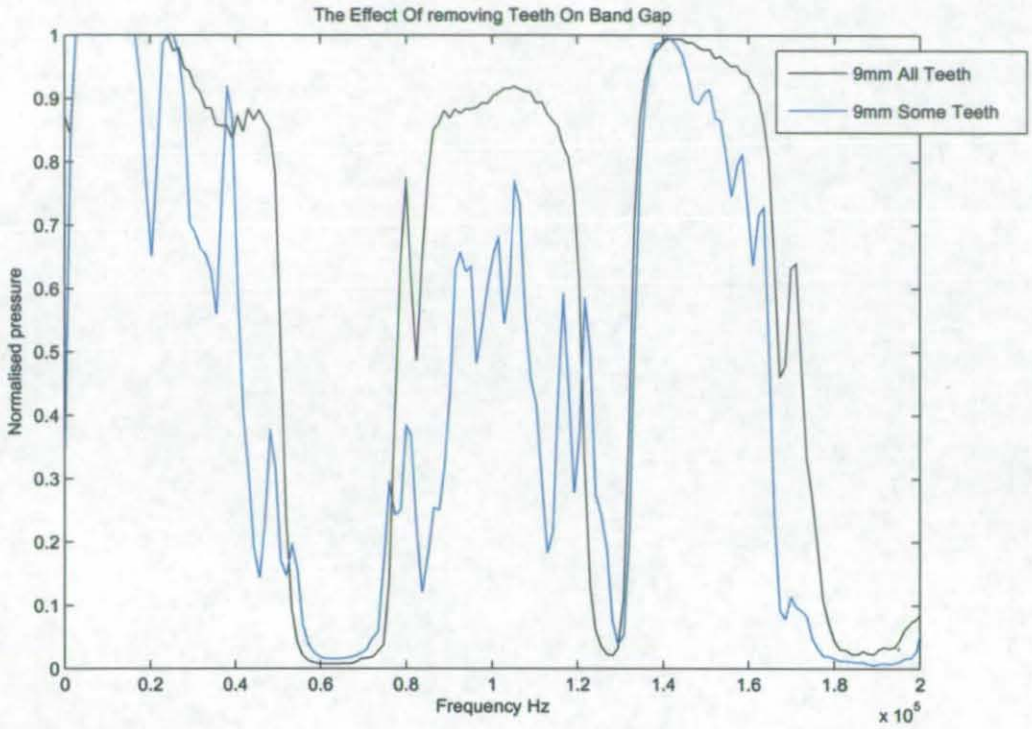

Figure 5.13: A typical result for removing some teeth from the jaw model. W=7.5mm

5.5 Three-Dimensional Models

Further modelling was carried out using a 3-D version of the TLM software used in the previous simulations. The software was again validated against analytical spreading models. The geometry depicted in Figure 5.14 shows the basic setup where rods of similar length to the tooth are contained within the channel. The height of the channel used was 34 mm and the height of the rods(teeth) was 25 mm. These dimensions were measured from the available CT data, however the depth of the channel and the depth of tooth penetration varies along the entire jawbone so this should still be considered to be a simplified model. The channel width was chosen to be 9 mm as this was within the variation and showed the best band gap structure in the 2-D experiment. The rod diameter was 4 mm as in the previous experiments. As before two measurements were taken and a normalised output showing the effect of the teeth was produced. The results can be seen in Figure 5.15.

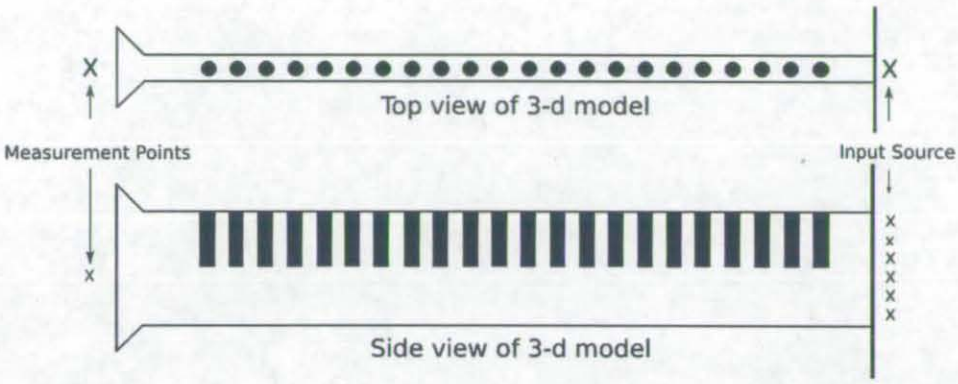

Figure 5.14: 3-D TLM model of a simplified dolphin lower jaw.

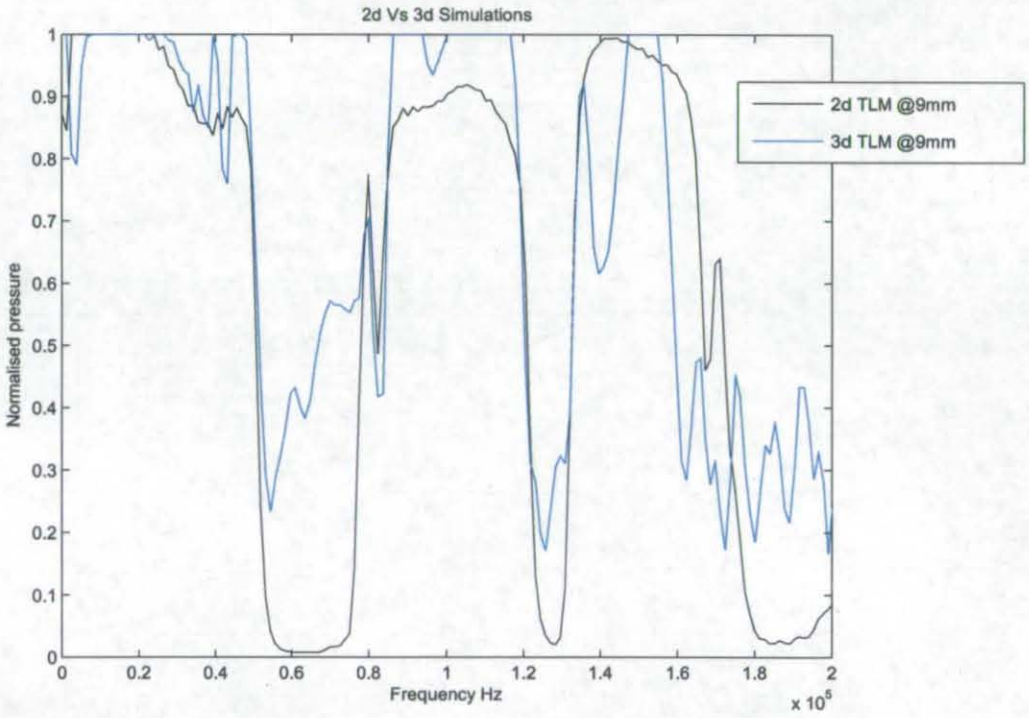

Figure 5.15: 3-D simulation results compared to 2-D results were channel width is 9 mm.

Although the band gap is less defined there is still a clear stop band between 55 kHz and 75 kHz. From this it can be seen that the band structure agrees with the 2-D version well, meaning the properties identified earlier are still applicable. The 3-D model still contains the same artifacts in the pass band that are due to the numerical modelling and the boundary conditions used.

From these models that have been implemented the filter effect has been demonstrated however the effect of this upon the binaural hearing of the dolphin has not been demonstrated. The current model only allows sound to enter at the tip of the rostrum which inhibits directionality data from being obtained. Looking at the CT data shown in Figure 5.16 reveals that for a single 2-D slice sound could propagate through the gum line and into the fatty channel of the lower jaw. As sound travels through the gum line in this manner it would interact with the teeth in a similar way to that previously hypothesised but this time different angles of arrivals could be interpreted.

5.6 2-D TLM Simulation With Real Geometry

Using the previously developed methodology it is possible to take the CT data shown and perform beam pattern measurements upon the real geometry. In order to do this some assumptions need to be made. These are that the walls and teeth of the jaw act as perfect reflectors and that we can model the receivers at each ear as omnidirectional receivers.

The model was constructed based upon the CT slice of Figure 5.16 and can be seen meshed for numerical analysis in Figure 5.17. The same Gaussian input signal show in Figure 5.11 was used as in the previous experiment. The source was positioned at a distance of 31 cm from the central point, and rotated about the central point. The model was scaled to fit a node size of 0.5 mm as was used in the previous models which gave a maximum modelling frequency of 300 kHz. The TLM simulations were run for 4096 iterations and signals were measured at the two receivers. Absorbing boundary conditions were placed behind the receivers in order to prevent the signal for ringing on, as there is no other energy absorption in the model. Once the simulations where run the data from each receiver was passed through a 4096 point DFT using Matlab. The signals where then collated for each angle and the beam patterns plotted. These plots are shown in Figures [5.18 to 5.27]

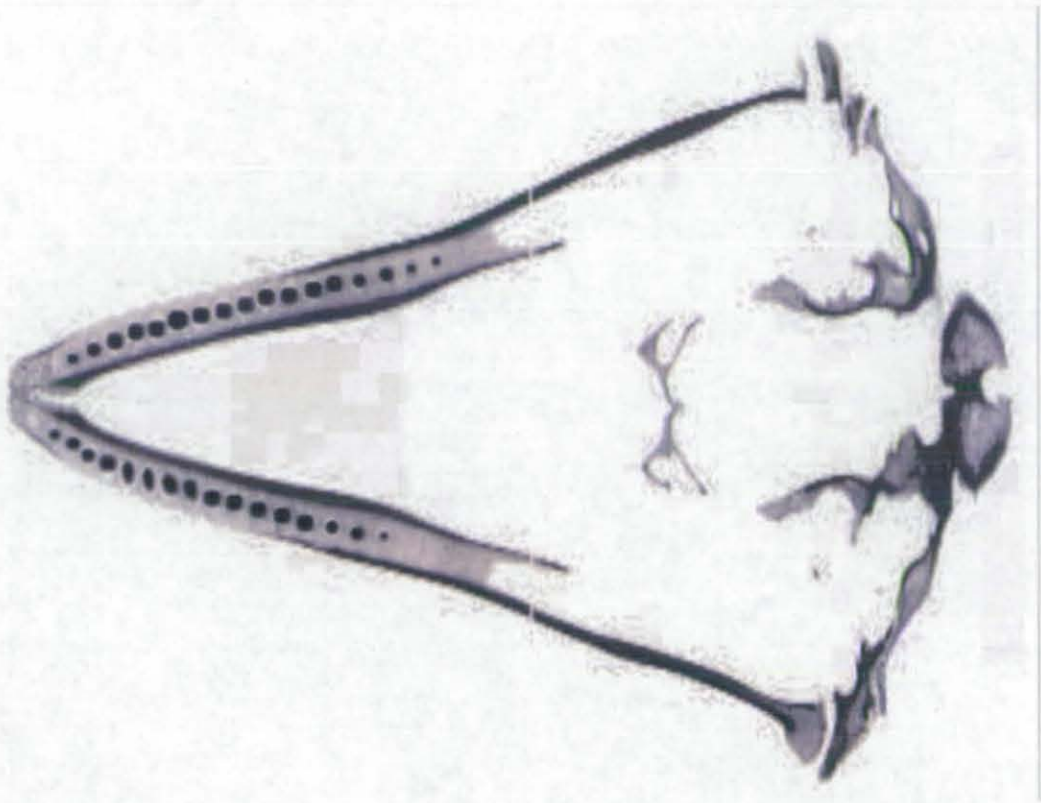

Figure 5.16: A CT slice through the head and mid jaw of the Dolphin

It is possible to compress all of the beam pattern data into 2 plots that reflect the dolphins sensitivity at each frequency with it angle. These can be seen in Figures 5.28 and 5.29.

These graphs show a clear difference between a model with and without teeth in the jawbone. It also shows some possible benefits to the sonar signal patterns.

At 50 kHz the 5 dB beam pattern of both ears is approximately 15^o each and combines to give 30^o. When the teeth are present the patterns have no isolation between patterns but form a single 15^o beam at the 5 dB points. As lower frequencies travel further due to lower attenuation it is likely this frequency is useful in finding the existence of a target at long range.

As we move to 60 kHz we can see that the pattern without teeth has decreased it's isolation between channels and the 5 dB beam width is approximately 30^o, on the graph with the teeth present two nulls have started to for at +/- 5^o-7^o. This is consistent with

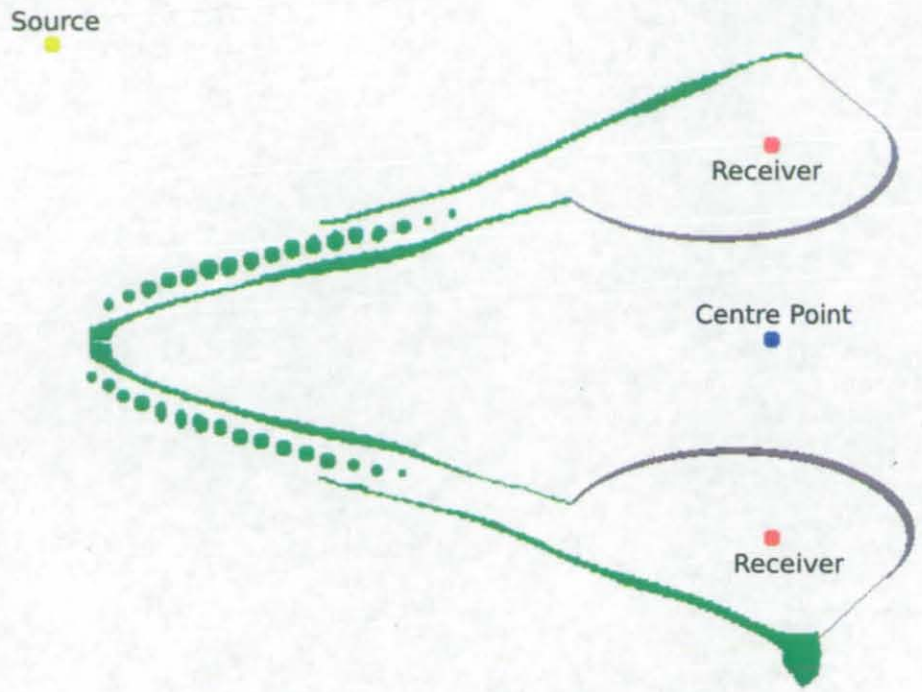

Figure 5.17: TLM Setup using real geometry

the earlier work that showed that a signal travelling directly on to the line of teeth would under go filtering in the region of 60-75 kHz, although the pattern for the ear remains the same width as for 50 kHz the isolation between patterns has increased which makes the combined beam pattern larger.

At 65 kHz, which is near the centre of the band gap predicted in the earlier simulations, the combined pattern without the teeth has increased in size to 40^o due to a decrease in isolation between ears and the spreading of the individual patterns for each ear. The patterns with the teeth present have increased in sensitivity in the null sections, while the isolation has increased. The main lobe of reception is approximately 20^o wide.

At 70 kHz the pattern without the teeth present have broadened, the main angle lobe 5 dB angle is now 55^o. The isolation between the ears has decreased by a small amount. The patterns with the teeth present now have another strong null between $+/-2^o$-5^o. The pattern for the left ear is approximately 15^o wide and the right ear is 30^o. The isolation between ears is greatly increased by the presence of the nulls in each of the patterns,

which could be used to improve target directionality.

At 80 kHz the patterns for the left and right ears without the teeth present have further reduction in isolation between the ears, the total beam pattern for both ears is approximately 70°. When looking at the patterns with the teeth present there is approximately 7° of isolation between the main lobes of the left and right ears. Each of the patterns have a main lobe width of approximately 15°, the nulls between the patterns are on the 0° axis.

At 90 kHz the patterns without the teeth have moved further apart with each pattern approximately 20° wide. The patterns with the teeth present have narrowed but are still separated with an on axis null, each individual pattern is approximately 12° wide.

At 100 kHz the patterns without the teeth present are now isolated with the null at 5° from the main axis. The right ear has a 5 dB beam width of approximately 30° and the left ear has a beam width of 22°. The patterns with the teeth present are considerably narrower at approximately 7° in each ear, with a null between the two patterns being on the 0° axis. This pattern in particular shows a very good improvement caused by the teeth.

At 110 kHz the patterns without the teeth present are isolated by a considerable angle with the null on the main 0° axis. The right ear has a beam width of 25° and the left ear has a beam pattern of 20°. The pattern with the teeth present are less defined than those at 100 kHz, each of the ears now has a 2-prong pattern. The right ear has its first prong at - 2° and is approximately 1° wide. The second prong located at approximately -15° is 10° wide. The left ear has its first prong located at 5° and is approximately 7 °wide. The second prong is again centred about 15° and is 15° wide. While this pattern is less stable than the pattern at 100 kHz the main lobs are still smaller than for two conventional receivers and the patterns are directed more towards the 0° axis which would reduce the need to sweep the head for side to side.

At 120 kHz the patterns without the teeth present have lost their isolation, meaning the loss of directional information at these high frequencies. The left and right ears both have null reception points at +/-5° which makes for a narrower beam pattern. The main

lobes for each pattern are approximately 10°. The patterns with the teeth present are arguably better as they are isolated by a very small but well defined amount on the 0° axis with each 5 dB beam width being 15° wide. The patterns also contain a mid point in each pattern were the signal drops to -3 dB.

At 130 kHz the patterns without the teeth present have narrowed, however there is still no isolation between ears, which would inhibit the gathering of directional information. The beam width for the right ear is 7° and for the left ear it is 18°. The patterns for the teeth show a much more useful beam pattern for precision echolocation. There is a well defined null between the patterns of each ear centred up on the 0° axis Each pattern is 5° in width. There is however a second side lobe that can be seen at -30° -60° and +60° which is less desirable.

Møhl [5.15] observed that sound entering the front of the jaw had an increased delay to what was expected from a simple ray trace of the path. The addition of the teeth to the jaw cavity also has the effect of increasing the propagation time to the assumed ear. For the model used in this simulation the propagation delay induced from adding the teeth to the simulation at zero degrees is 7 μs. Although this does not fully explain the delay this may be one of many features that causes a slow wave propagation.

5.7 Conclusions

Although there is great debate about how sound enters the jaw, either via the pan bone (acoustic window) as identified by Norris [5.16], via the teeth [5.10], via the mental foramens [5.17] or directly through the gums it is clear that once sound is within the bone it will travel along the jawbone and then undergo this filtering. If we make the assumption that the sound enters through the gums as shown in the latter numerical simulations then we can see a vast improvement in the beam width and channel isolation. This type of geometry should be easily reconstructed within a man made system and may serve to enhance system performance and reduce cost and complexity. Whether this is the exact method that takes place in the dolphin is a matter for biologist and

physiologists. This work has examined acoustic band gaps that are a known acoustic principle and seen that they can take place in the dolphin geometry. This effect can certainly be used in a similar way to improve man-made systems

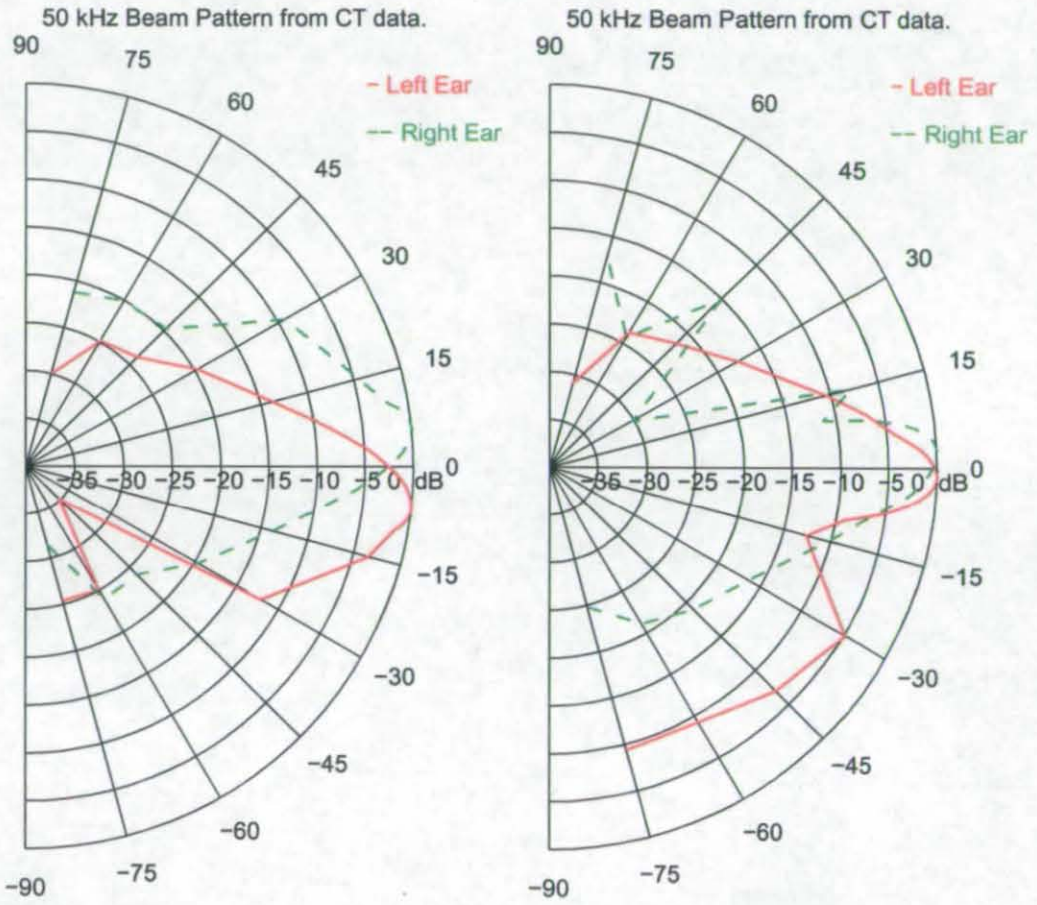

Figure 5.18: The Beam Pattern at 50kHz. Left is with no teeth in the jaw. Right with Teeth in place

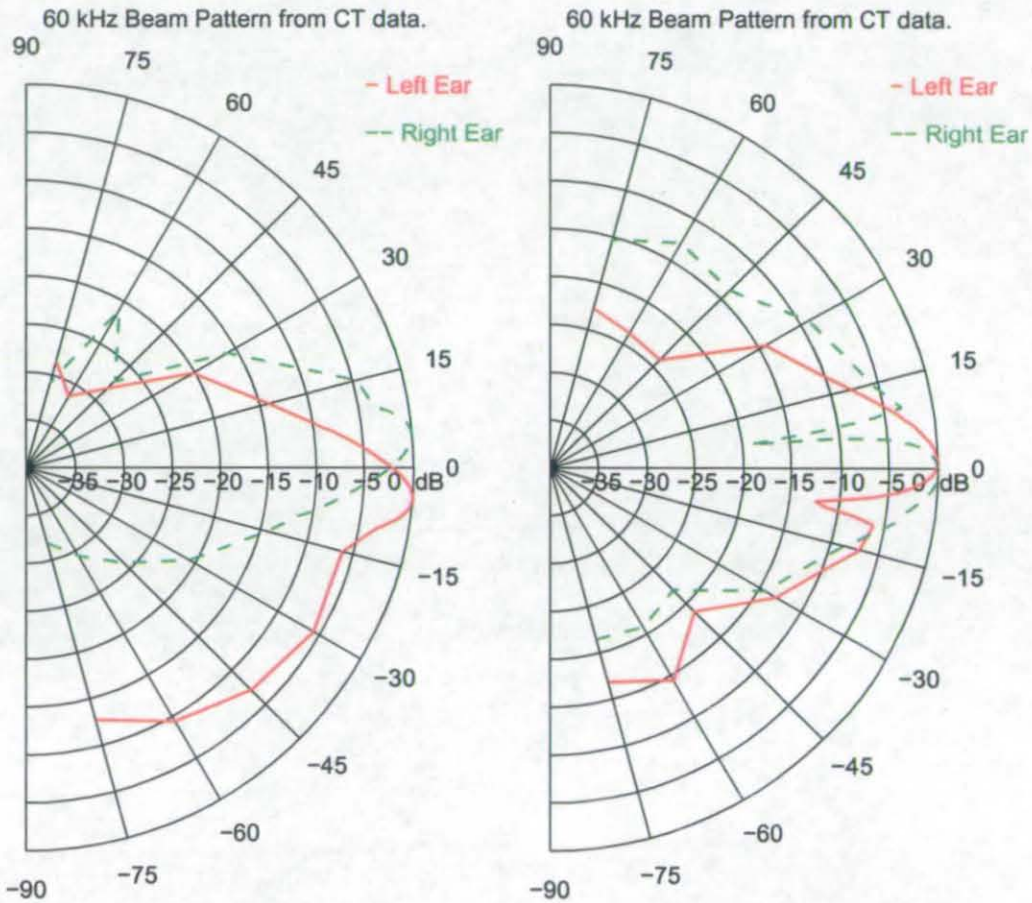

Figure 5.19: The Beam Pattern at 60kHz. Left is with no teeth in the jaw. Right with Teeth in place

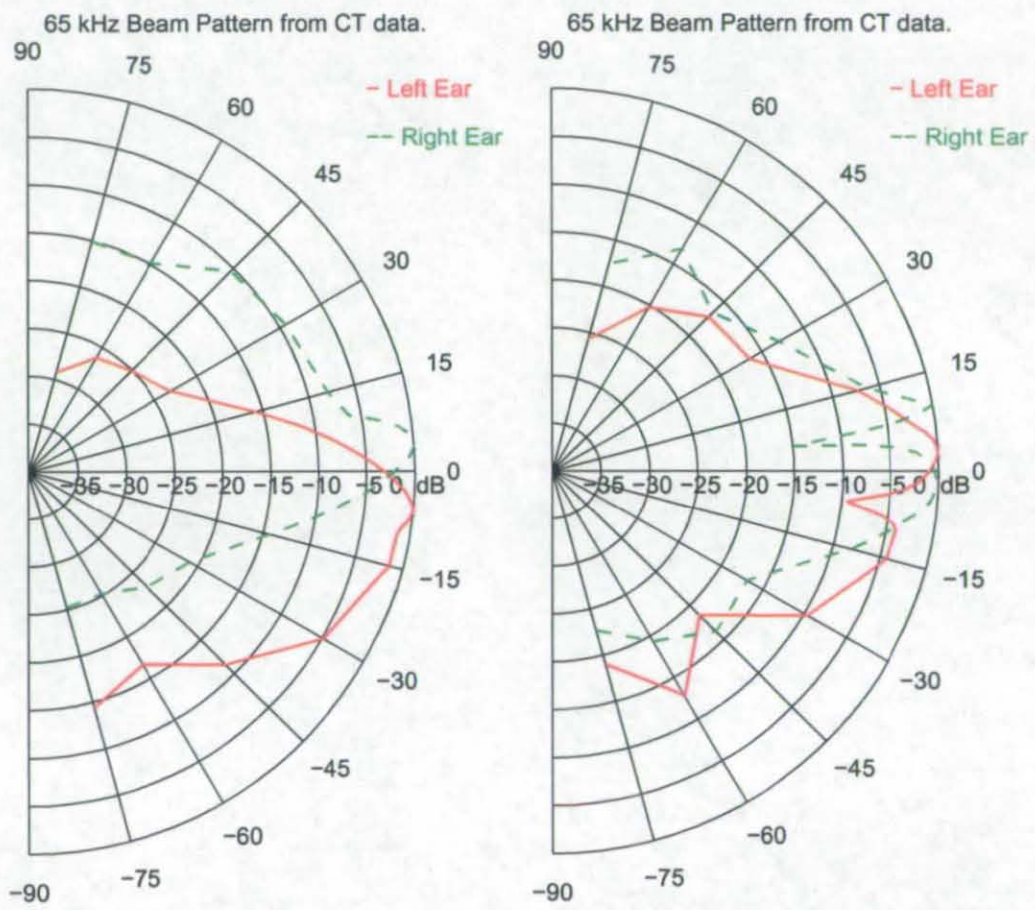

Figure 5.20: The Beam Pattern at 65kHz. Left is with no teeth in the jaw. Right with Teeth in place

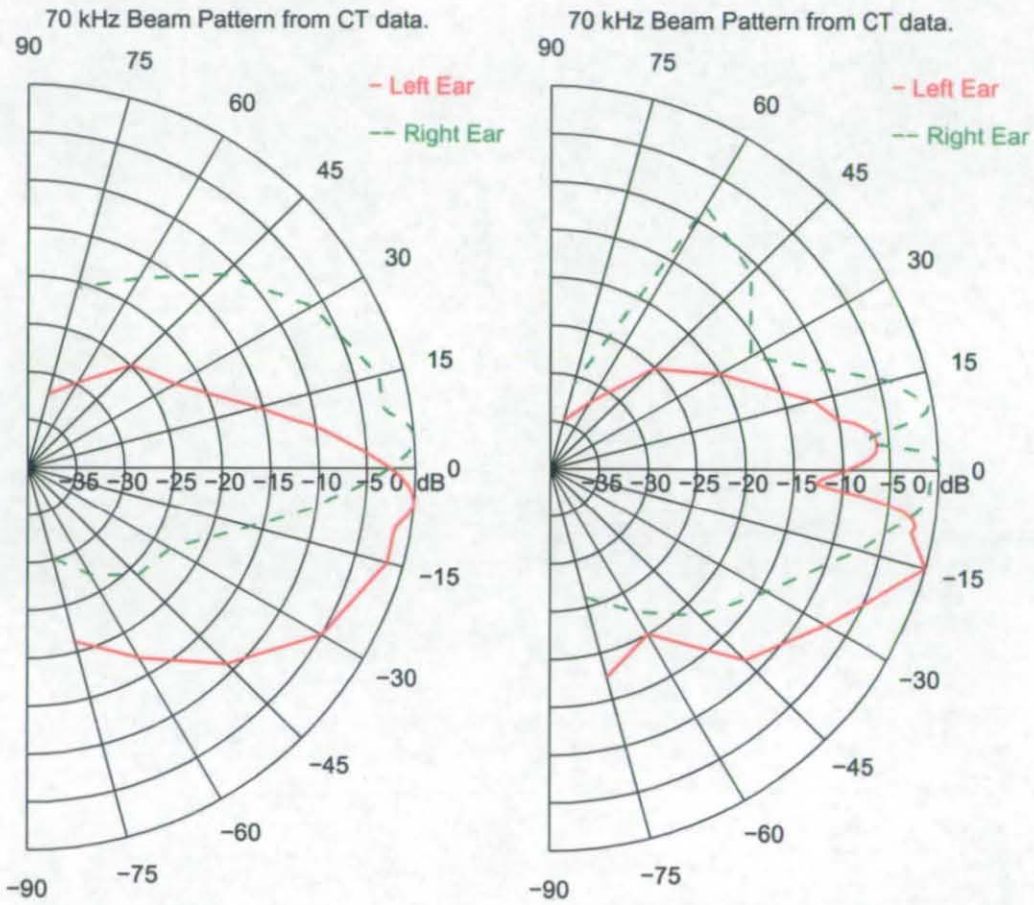

Figure 5.21: The Beam Pattern at 70kHz. Left is with no teeth in the jaw. Right with Teeth in place

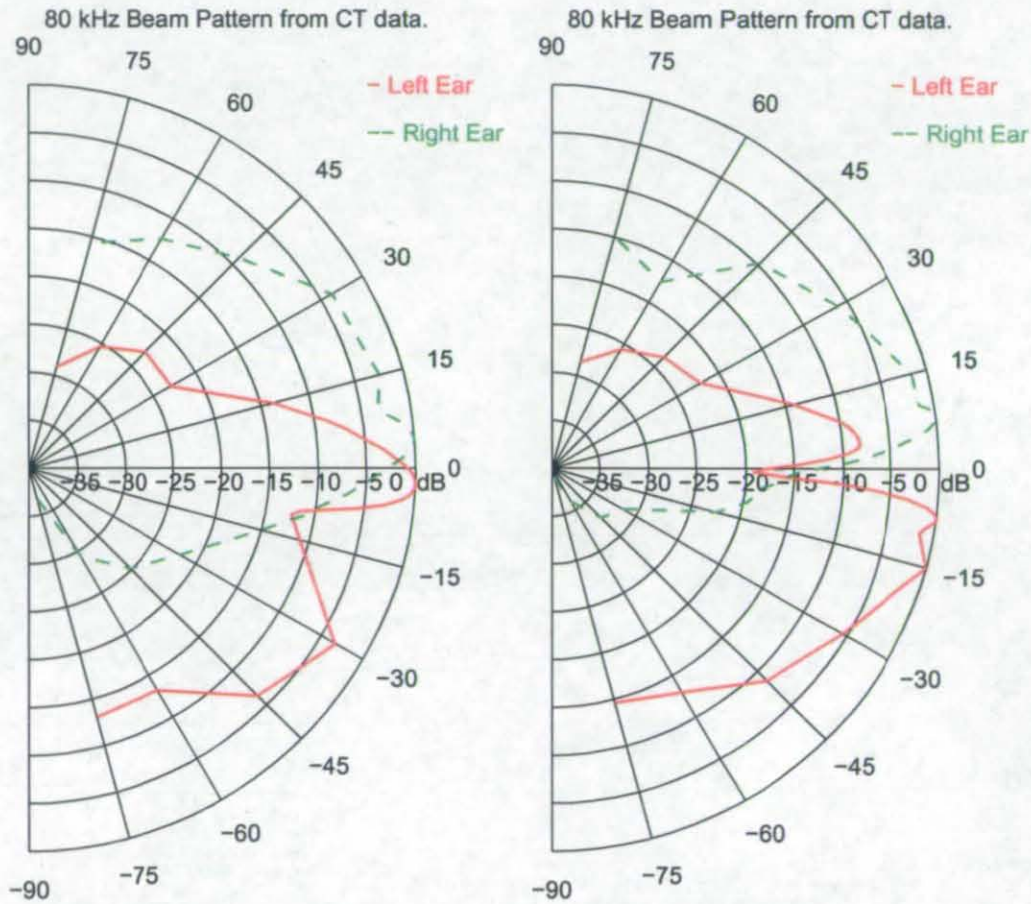

Figure 5.22: The Beam Pattern at 80kHz. Left is with no teeth in the jaw. Right with Teeth in place

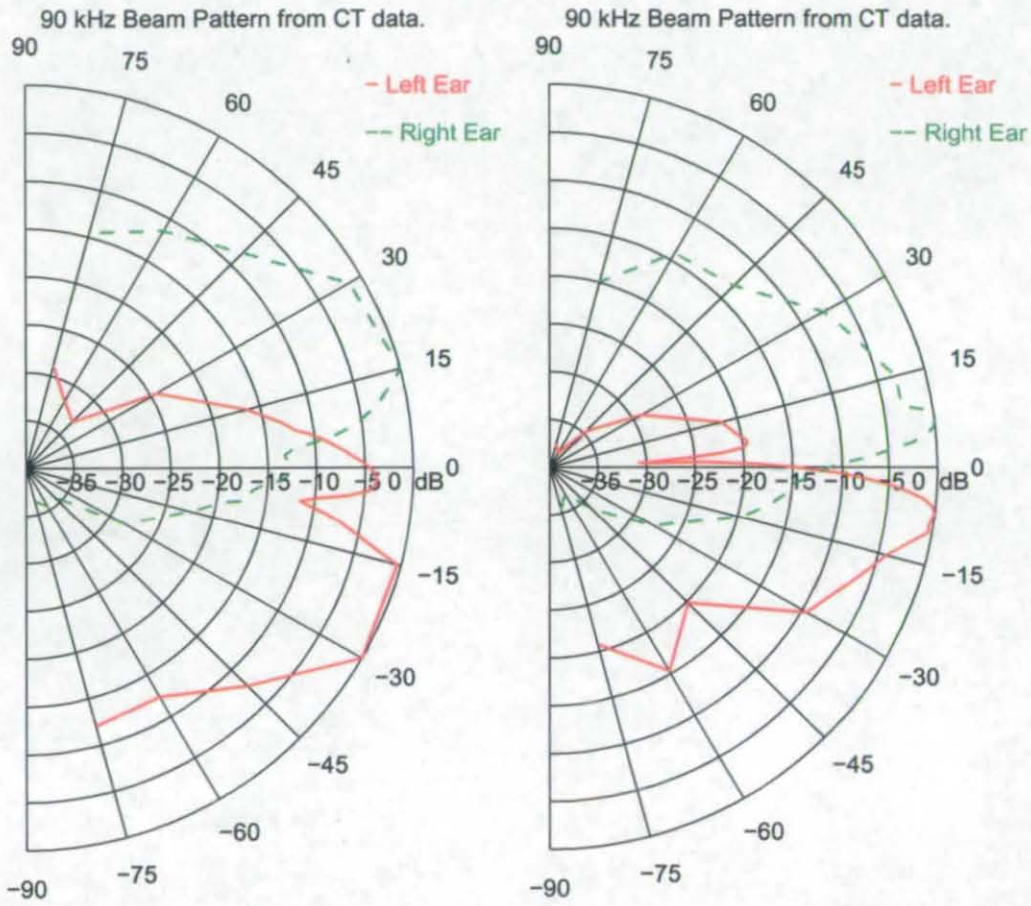

Figure 5.23: The Beam Pattern at 90kHz. Left is with no teeth in the jaw. Right with Teeth in place

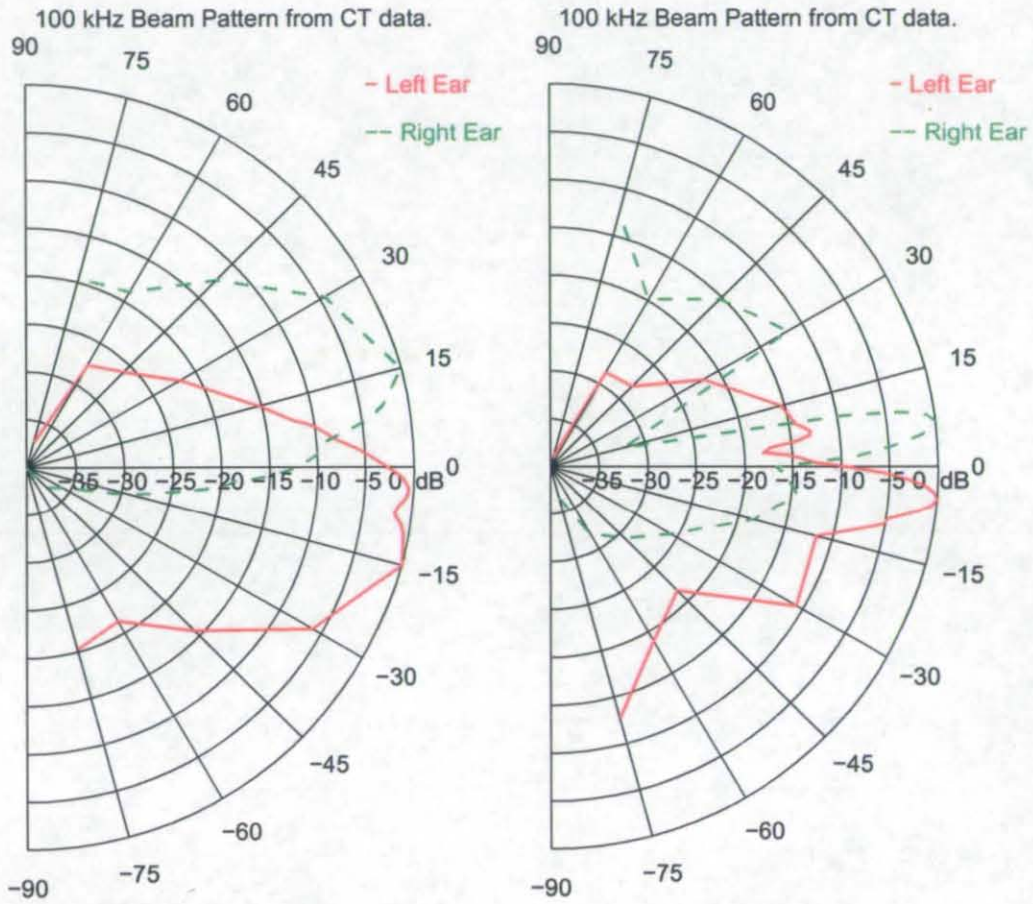

Figure 5.24: The Beam Pattern at 100kHz. Left is with no teeth in the jaw. Right with Teeth in place

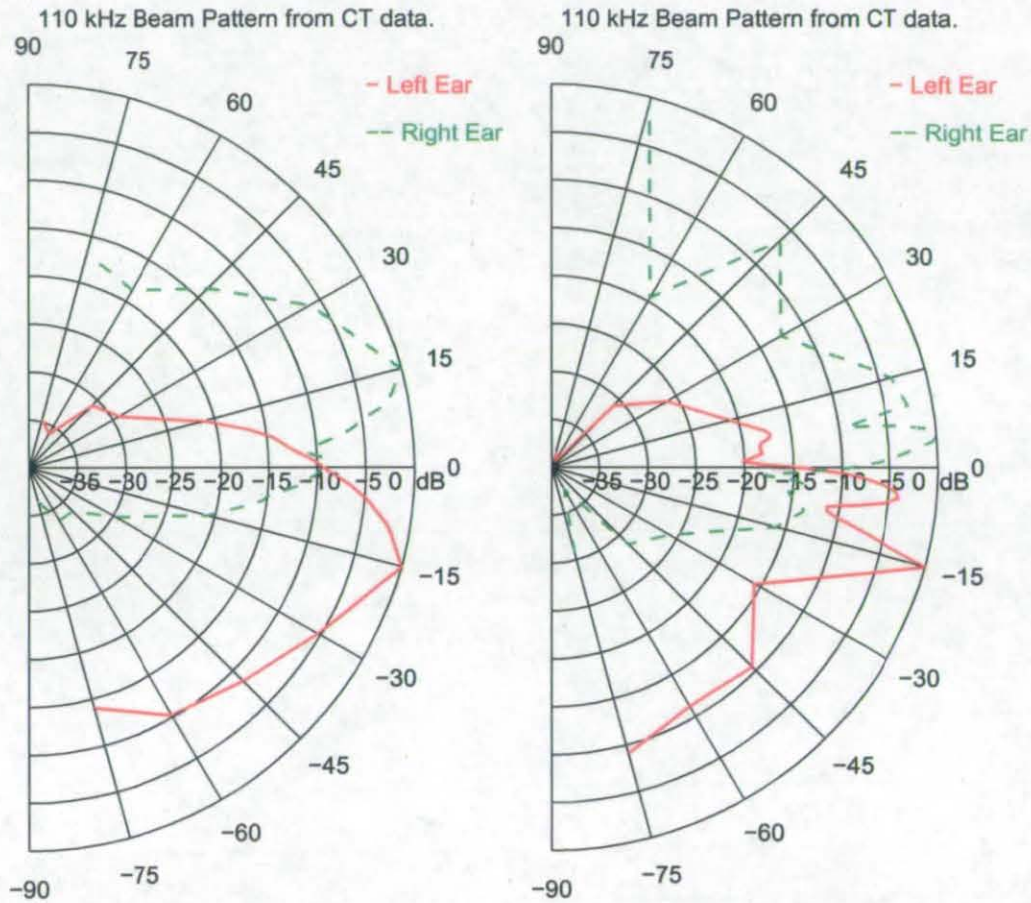

Figure 5.25: The Beam Pattern at 110kHz. Left is with no teeth in the jaw. Right with Teeth in place

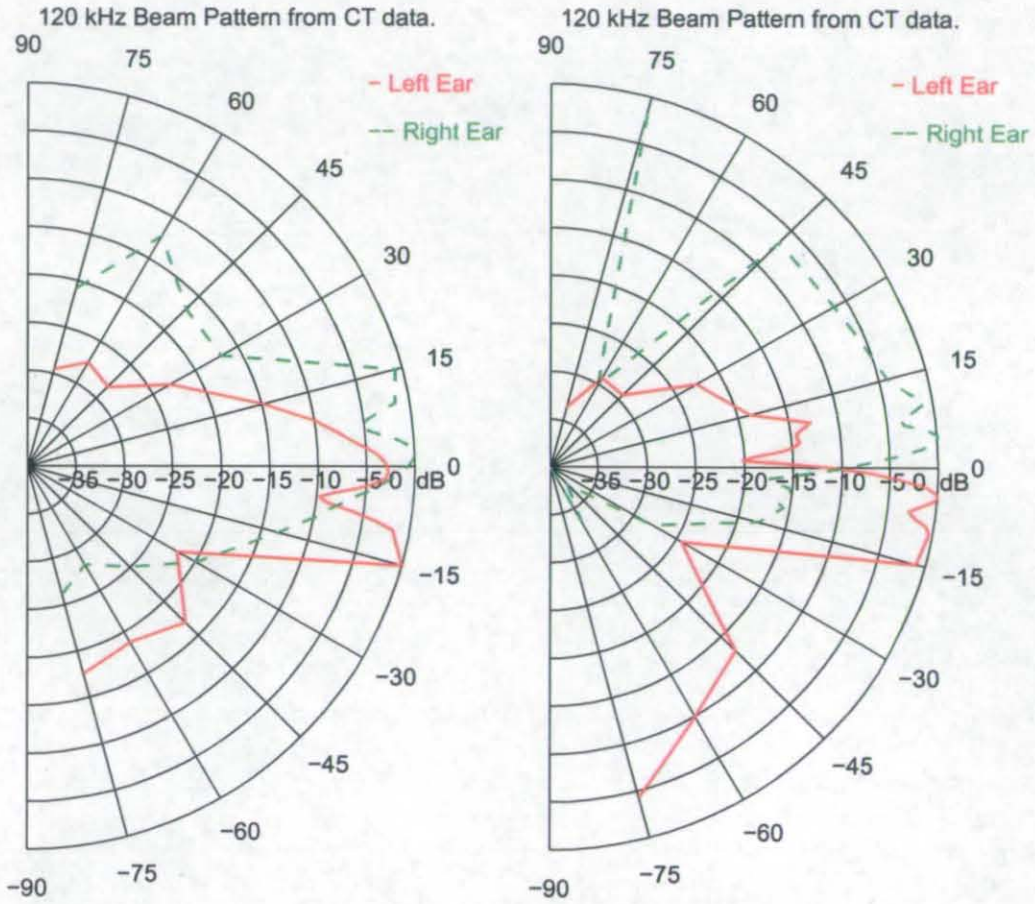

Figure 5.26: The Beam Pattern at 120kHz. Left is with no teeth in the jaw. Right with Teeth in place

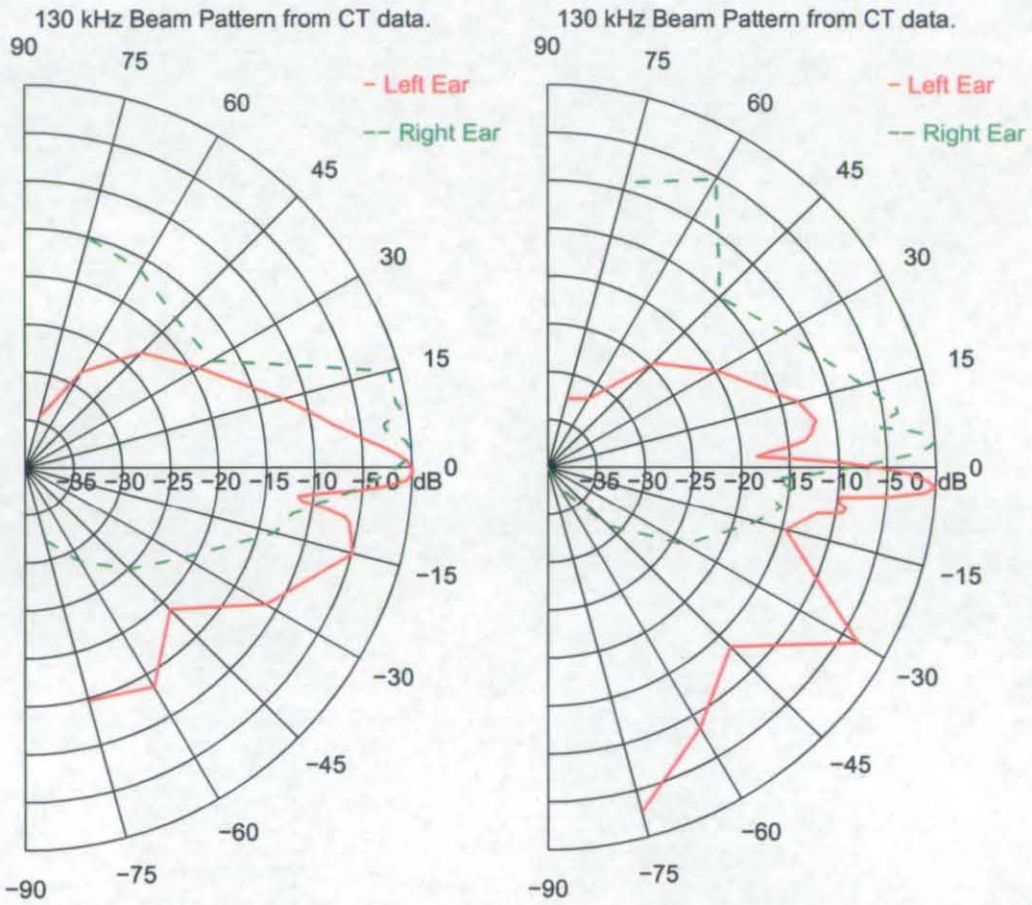

Figure 5.27: The Beam Pattern at 130kHz. Left is with no teeth in the jaw. Right with Teeth in place

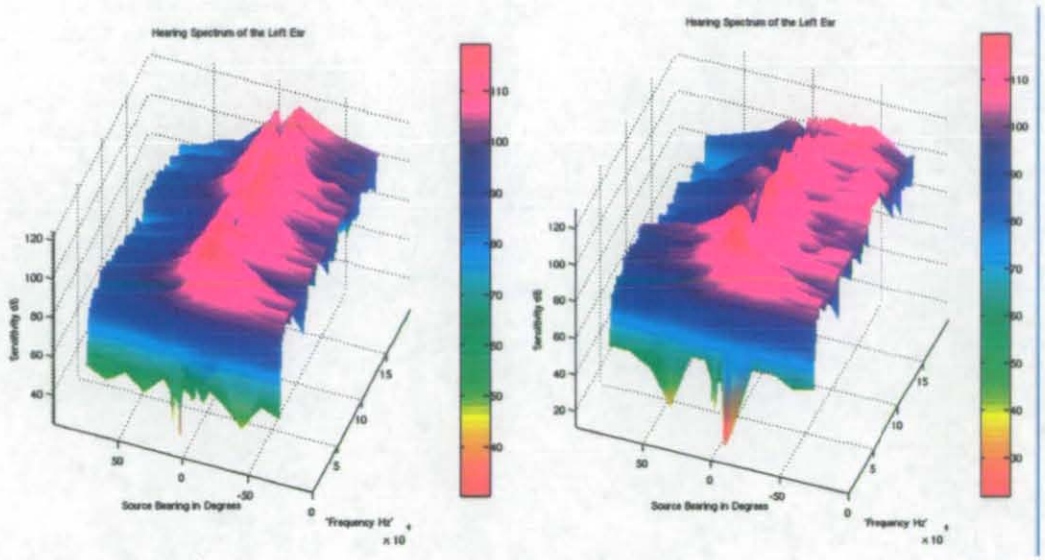

Figure 5.28: Left is the Sensitivity With No teeth. Right is the Sensitivity with the teeth present.

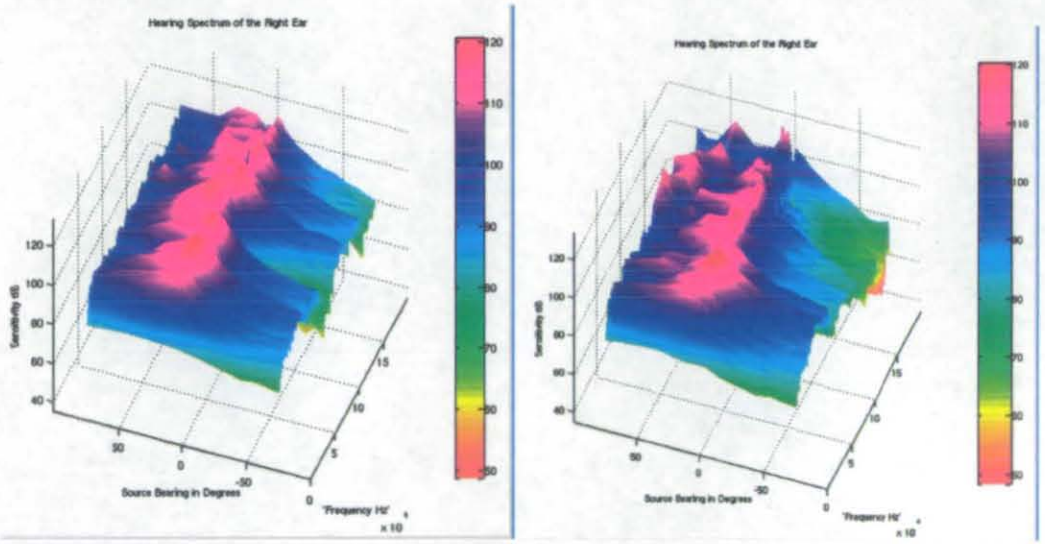

Figure 5.29: Left is the Sensitivity With No teeth. Right is the Sensitivity with the teeth present.

References

[5.1] G. Leonard, *Acoustic modelling of bat pinnae utilising the TLM method.* PhD thesis, Loughborough University, UK, Oct. 2006.

[5.2] P. B. Johns and R. L. Beurle, "Numerical solution of 2-dimensional scattering problems using a transmission-line matrix," *Proc. IEE*, vol. 118, no. 9, pp. 1203–1208, 1971.

[5.3] A. D. Goodson, J. A. Flint, and T. W. Cranford, "The harbor porpoise (phocoena phocoena) modeling the sonar transmission mechanism," *Echolocation in Bats and Dolphins*, pp. 64–71, 2003.

[5.4] S. El-Masri, X. Pelorson, P. Saguet, and P. Badin, "Development of the transmission line matrix method in acoustic applications to higher modes in the vocal tract and other complex ducts," *International Journal of Numerical Modelling: Electronic Networks, Devices and Fields.*, vol. 3, pp. 39–56, 1990.

[5.5] J. L. Aroyan, *Three-dimensional numerical simulation of biosonar signal emission and reception in the common dolphin.* PhD thesis, University of California, Santa Cruz, 1996.

[5.6] D. D. Cogan, *Transmission Line Matrix (TlM) techniques for diffusion applications.* Taylor & Francis, 1998.

[5.7] J. Nielsen and W. Hoefer, "A complete dispersion analysis of the condensed node tlm mesh," *Magnetics, IEEE Transactions on*, vol. 27, no. 5, pp. 3982–3983, 1991.

[5.8] W. M. Robertson and J. F. Rudy, "Measurement of acoustic stop bands in two-dimensional periodic scattering arrays," *The Journal of the Acoustical Society of America*, vol. 104, no. 2, pp. 694–699, 1998.

[5.9] L. Brillouin, *Wave propagation in periodic structures.* Dover Publications Inc., 1953.

[5.10] A. D. Goodson and M. Klinowska, *A proposed receptor for the Bottlenose Dolphin (Tursiops truncatus) modelling the receive directivity from tooth and lower jaw geometry*, vol. NATO ASI Series A of *Sensory Abilities of Cetaceans*, pp. 255–267. Plenum, 1990.

[5.11] S. A. Dible, J. A. Flint, and P. A. Lepper, "Laser doppler vibrometry measurement of the lower jaw and teeth of the atlantic bottlenosed dolphin (tursiops truncatus)," in *8th European Conference On Underwater Acoustics* (S. M. Jesus and O. C. Rodriguez, eds.), June 2006.

[5.12] H. N. Koopman, S. M. Budge, d. R. Ketten, and S. J. Iverson, "Topographical distribution of lipids inside the mandibular fat bodies of odontocetes: Remarkable complexity and consistency," *IEEE Journal Of Oceanic Engineering*, vol. 31, Jan. 2006.

[5.13] J. A. Flint, A. D. Goodson, G. Leonard, and S. C. Pomeroy, "Transmission line modelling of the harbour porpoise (phocoena phocoena) melon," *Journal of Acoustical Society of India*, vol. 30, no. 3-4, pp. 294–297, 2002.

[5.14] D. S. Houser, J. Finneran, D. Carder, W. V. Bonn, C. Smith, C. Hoh, R. Mattrey, and S. Ridgway, "Structural and functional imaging of bottlenose dolphin (tursiops truncatus) cranial anatomy," *J Exp Biol*, vol. 207, no. 21, pp. 3657–3665, 2004.

[5.15] B. Møhl, W. W. L. Au, J. Pawloski, and P. E. Nachtigall, "Dolphin hearing: Relative sensitivity as a function of point of application of a contact sound source in the jaw and head region," *The Journal of the Acoustical Society of America*, vol. 105, no. 6, pp. 3421–3424, 1999.

[5.16] K. S. Norris, "The evolution of acoustic mechanisms in odontocete cetaceans," *Evolution and Environment, Yale University, Connecticut*, pp. 298–323, 1968.

[5.17] V. A. Ryabov, "Peripheric parts of the dolphin echolocation hearing," *Proceedings of Marine Mammals of the Holarctic*, vol. 1, pp. 483–489, Oct. 2004.

CHAPTER 6:
CONCLUSIONS

THE aim of this thesis was to further the understanding of the receiving mechanisms of the Atlantic Bottlenose Dolphin *Tursiops truncatus*. This has been achieved by empirical analysis of current theories, the application of Laser Doppler Vibrometry measuring techniques (to examine previously unquantified properties of the materials that form the lower jaw structure) and numerical modelling of the scattering structure of the skull structure based on CT data that has only recently been made publicly available. Additionally the modelling techniques used within this thesis have been validated and can now be used by others for analysis and simulation of acoustic wave propagation.

6.1 Contribution Of This Thesis

6.1.1 End-Fire Array Hypothesis

Current theories of hearing have been modelled and measured in Chapter 3. It has been shown that an array of hydrophone elements can produce a very useful end-fire beam pattern and, when scaled to the number of teeth that are present in the dolphin, produce a beam pattern that is similar to the beam pattern of the dolphin. The pattern produced by such an array is extremely useful for shallow water applications as it possess low side lobes. The two piston elements can also approximate the acoustic window and produces a pattern that closely matches the patterns measured from the Dolphin. This work does not add support to either theory of hearing, only that they are both plausible.

6.1.2 Acoustical Properties Of Dolphin Teeth

In Chapter 4 of this thesis, detailed measurements were conducted to define the speed of sound in the lower jawbone and the teeth. It was shown that the sound speed in the tooth of a Bottlenose Dolphin is 2200 ms^{-1} for transverse waves and 3380 ms^{-1} for compressional waves. To the best of the authors knowledge these figures were previously unknown. This data can now be used by the wider community and in particular can be used to more accurately map density and sound speed in numerical simulations. The LDV measurements of the modal properties of the teeth have also been presented. It has been shown that the teeth have a resonance response between 80 kHz to 90 kHz and 115 kHz to 135 kHz when mounted in the jawbone without the presence of any tissues. If the teeth are being used as pressure sensors or couplers then this could be used to selectively amplify specific frequencies of sound to enhance performance. The LDV measurements also show that the teeth do not possess a breathing vibrational mode that had been speculated.

6.1.3 Acoustical Properties Of Lower Jawbone

Both LDV and standard acoustic sensors have been used to classify the speed of sound and attenuation levels in a lower jawbone of a deceased Dolphin. After some difficulty the sound speed in the Jawbone has been determined to be 2607 ms^{-1}, this is higher than the sound speed of water and thus would have a higher acoustic impedance. During these experiments it was noted that the attenuation level in the jawbone was extremely high, at 1.8 $dBmm^{-1}$. This property means that it is extremely unlikely for the sound to be coupled from the tip of the jaw to the acoustic window via bone propagation. It is likely that any propagation would occur through the fatty channel within the jaw or through the surrounding water. This would aid in reducing undesired multipath at the receiver.

6.1.4 Acoustic Band Gap Theory

Chapter 5 has discussed acoustic band gap structures and presented numerical modelling evidence for the existence of acoustic band gaps caused by the geometry of the teeth within the lower jawbone. These simulations have been conducted in both two and three dimensions and upon have used both a simplified and real dolphin skull geometry. This work shows that the teeth produce a band gap which serves to shape the reception beam pattern of the animal by increasing inter-aural isolation at higher frequencies and produces a narrower beam than would be available without the teeth. The patterns are again similar to those of Au and Moore. Figure 6.1 Figure 6.2 and Figure 6.3 show the comparisons between the simulation results from Chapter 5 and the measurement work of Au and Moore.

6.1.5 Relation To Current Work

The work presented in this thesis has adapted and developed the existing sound reception ideas of Au and Goodson and introduces the band gap hypothesis. In theoretical terms the band gap idea fills the link between the simple two element receiver suggested by Au [6.1] and the array of periodic receiving elements suggested by Goodson [6.2]. It is also consistent with a large proportion of the work by Ryabov [6.3] in which he assumes that sound travels along the inner channel of the jaw on its way to the middle ear. The band gap theory also correlates well with the recent work of Cranford *et al.* [6.4] who has demonstrated, using FEM modelling, that sound can travel into the lower jawbone channels and then onto the ears in a beaked whale (*Ziphius cavirostris*).

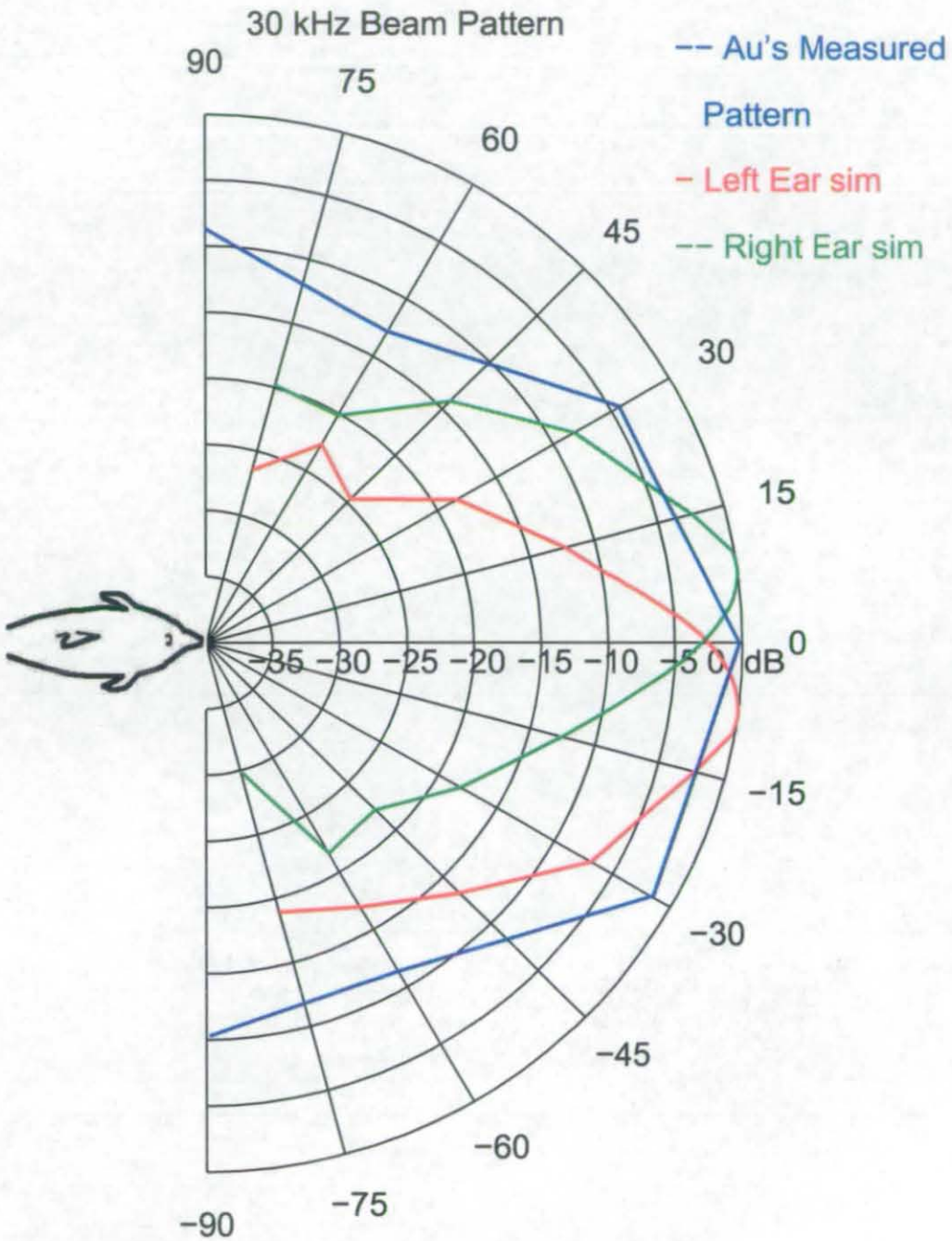

Figure 6.1: A comparison of the TLM simulation results and the measured beam patterns of Au and Moore [6.5] at 30 kHz

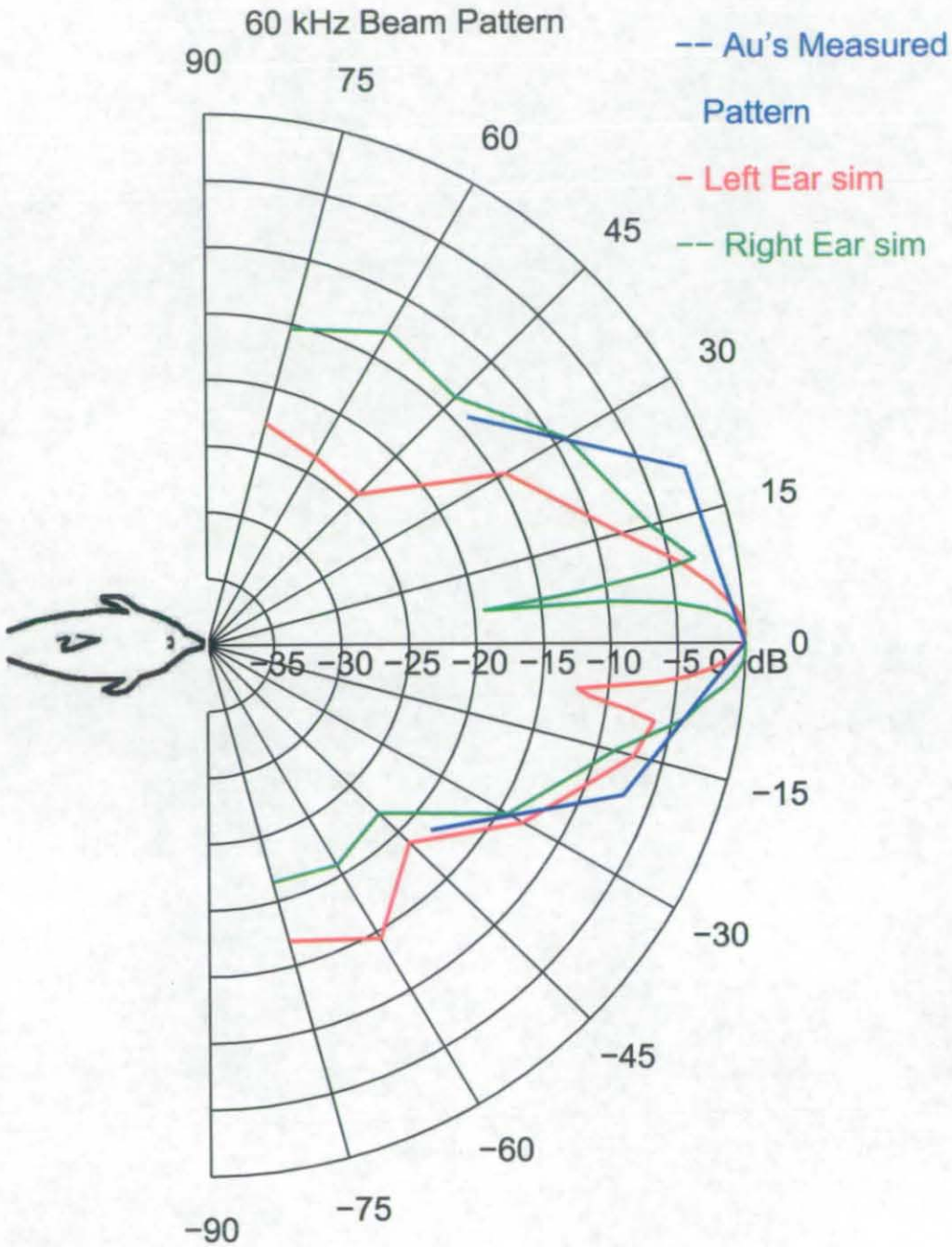

Figure 6.2: A comparison of the TLM simulation results and the measured beam patterns of Au and Moore [6.5] at 60 kHz

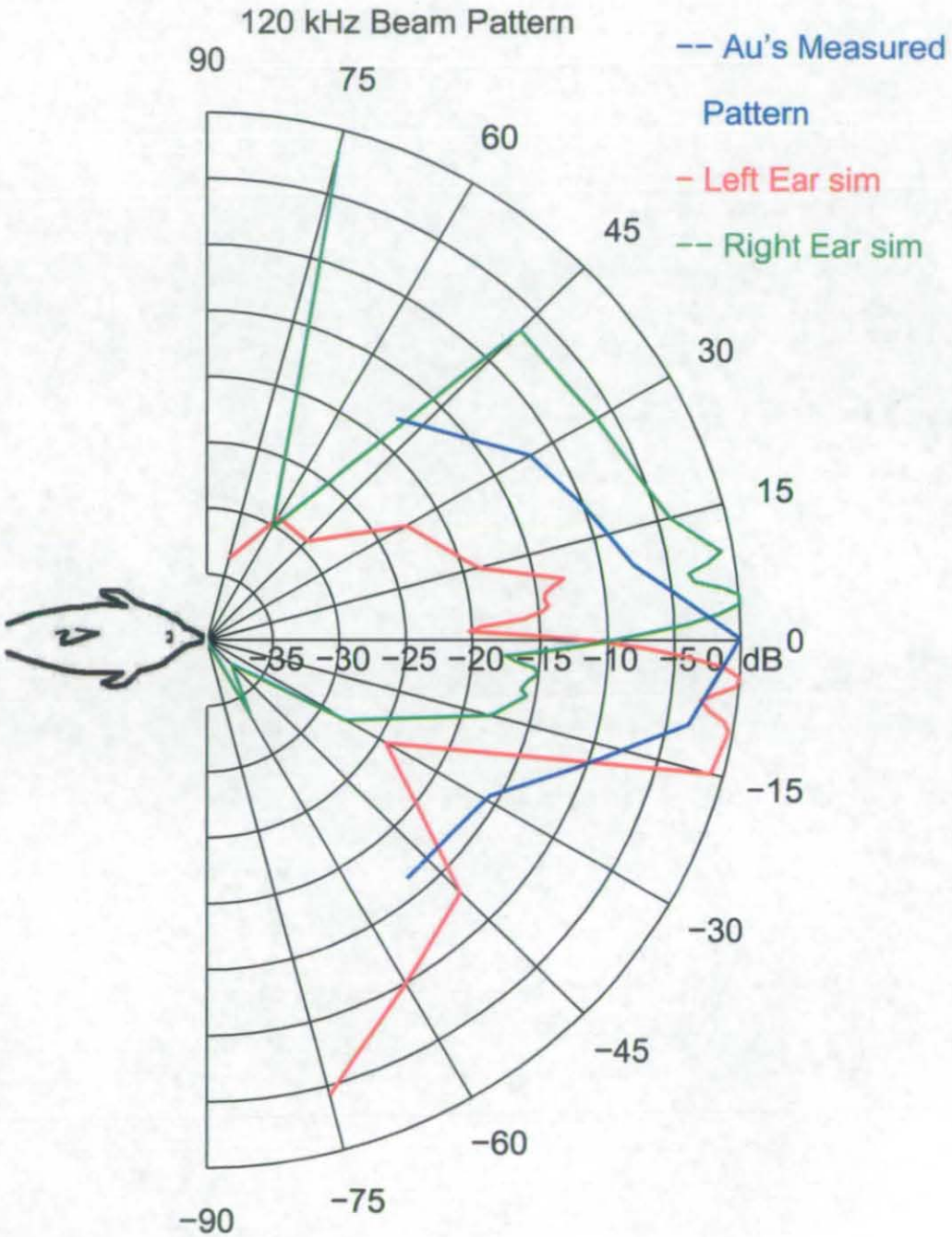

Figure 6.3: A comparison of the TLM simulation results and the measured beam patterns of Au and Moore [6.5] at 120 kHz

6.1.6 Suggestions For Further work

Artificial Jaw Structures

The next stage of this work should be to construct a simple array of periodically spaced scattering objects similar to the layout in Figure 5.17. This could then be used to test if the predicted increased directionality gained from the band gap path is useful. Furthermore this band gap allows for narrower beams to be formed using a smaller number of elements and could therefore be used to reduce system cost.

Field Trials

One theory that is raised by this work is the theory of gum hearing, in which sound is channel along the gums of the animal and then into the normal ear structure. This path contains additional directivity data that could aid localisation. If possible animal trials should be constructed in a similar fashion to Brill's trials to try and prove or disprove this hearing pathway and the effect on localisation.

Material Modelling

In the simulations presented in Chapter 5 the jawbone is modelled as an acoustically hard, perfectly reflecting boundary. The actual bone is constructed from flesh, cartilage, and other tissues which are known not to perfectly reflect incident sound as demonstrated in Chapter 4. In reality the bone and tissue would absorb some of the received sound depending on its frequency content which could alter the directionality patterns and sensitivity response. The modelling results presented in the thesis are still useful as any artificial systems can easily replicate the jawbone based upon the assumptions made in this thesis.

3D Modelling

Currently the CT data available for the head of the Bottlenose Dolphin provided by Houser *et al.* does not contain the full rostrum and therefore prohibits the 3D modelling of the dolphin with all the tissues present. If this data were to become available then a full 3D model should be simulated. 3D modelling of the skeleton provided by digimorph was not performed in this thesis due to computational constraints however future work could concentrate upon this.

Other Species

Currently the CT data available is only for Bottlenose Dolphin. To add further weight to this theory, other animals which are known to echolocate should be examined for a similar band gap structure within the reception frequencies of the animal.

6.2 Closing Remarks

This thesis has shown that the teeth do indeed play a role within the echolocation system of the Dolphin whether it be as an acoustic resonator or as an array of passive scattering elements. The numerical modelling shows that the jaw structure provides excellent isolation of the upper echolocation frequencies, which is important for short range target detection and tracking. This theory of sound reception via the gums works well in parallel with the sound reception via the pan bone. The slow wave nature of the band gap means that signals that arrive as a result of the gum will be received after those of the direct path into the pan bone. This would mean that both sets of data are available to the processing system thereby increasing system efficiency as only one click is needed to produce two return clicks. Such a structure could easily be emulated by man-made systems to improve target resolution via providing additional data. Furthermore the shaping of the acoustic path via passive scattering elements could be used as a mechanism to reduce array construction costs.

References

[6.1] W. W. L. Au, *The sonar of dolphins*. New York: Springer-Verlag, 1 ed., 1993.

[6.2] A. D. Goodson and M. Klinowska, *A proposed receptor for the Bottlenose Dolphin (Tursiops truncatus) modelling the receive directivity from tooth and lower jaw geometry*, pp. 255–267. NATO ASI Series A Sensory Abilities of Cetaceans, Plenum, 1990.

[6.3] V. A. Ryabov, "Peripheric parts of the dolphin echolocation hearing," in *Proceedings of Marine Mammals of the Holarctic*, vol. 1, pp. 483–489, Oct. 2004.

[6.4] T. W. Cranford, P. Krysl, and J. A. Hildebrand, "Ziphius acoustic pathways," *Bioinspiration & Biomimetics*, vol. 3, pp. 01–10, 2008.

[6.5] W. W. L. Au and P. W. B. Moore, "Receiving beam patterns and directivity indices of the atlantic bottlenose dolphin tursiops truncatus," *The Journal of the Acoustical Society of America*, vol. 75, no. 1, pp. 255–262, 1984.

AUTHOR'S PUBLICATIONS

A number of publications have resulted from the work in this thesis. These are as follows:

[1] M. Garg, G. Leonard, S. A. Dible, J. A. Flint, and S. Datta, "TLM modelling of mammal vocal and auditory systems," in *First International Workshop on Generalised Applications of TLM and Related Techniques*, (Pegagocial University, Poland), 2004.

[2] S. A. Dible, J. A. Flint, P. A. Lepper, and S. Datta, "Lower jaw sound propagation of the atlantic bottlenosed dolphin (tursiops truncatus)," in *NSA 2006*, pp. 268–272, Acoustical Society of India, November 2006.

[3] S. A. Dible, G. Farmer, J. A. Flint, and G. Leonard, "Measurement of a biometric antenna in the shape of a bat's ear," in *European Conference on Antennas and Propagation*, Apr. 2006.

[4] S. A. Dible, J. A. Flint, and P. A. Lepper, "Laser doppler vibrometry measurement of the lower jaw and teeth of the atlantic bottlenosed dolphin (tursiops truncatus)," in *8th European Conference On Underwater Acoustics* (S. M. Jesus and O. C. Rodriguez, eds.), pp. 365–370, jun 2006.

[5] S. A. Dible, P. A. Lepper, and J. A. Flint, "On the bandgap theory of hearing in the atlantic bottlenosed dolphin," in *4th International Conference on Bio-Acoustics*, vol. 29, pp. 261–268, apr 2007.

[6] S. A. Dible, P. A. Lepper, and J. A. Flint, "Enhanced hearing directivity via bandgap structures in the lower jaw of the bottlenose dolphins (tursiops truncatus)," in *Biological Approaches for Engineering*, pp. 66–69, Mar. 2008.

[7] S. A. Dible, J. A. Flint, and P. A. Lepper, "Lower jaw sound propagation in the atlantic bottlenose dolphin (tursiops truncatus)," *Journal Of Acoustic Society Of India*, vol. 34, pp. 37–40, Jan. 2007.

APPENDIX A:
PROPERTIES OF THE BAE SYSTEMS ARRAY

This section contains data about the end-fire array shown in Figure 3.14 that was provided by Dr Peter Dobbins and built by BAE Systems. The array performance was not as expected and therefore was not used for the work conducted in Chapter 3 of this thesis. For future reference the wiring design and the beam patterns of the array will have been included.

A.1 End Fire Array Wiring

The array was provided with co-axial connections to each individual element, however the recording equipment available only permitted the simultaneous recording of 4 channels. A digitally controlled analogue multiplexer circuit was designed so that each channel could be selected in turn and then recorded. The multiplexer chosen was the Fairchild 4051, which offered the closest impedance match available with low leakage. The circuit diagram is included as Figure A.1. The input selection signals to the multiplexer are TTL whilst the analogue power rails may be $\pm$ 5 to 15 V and GND

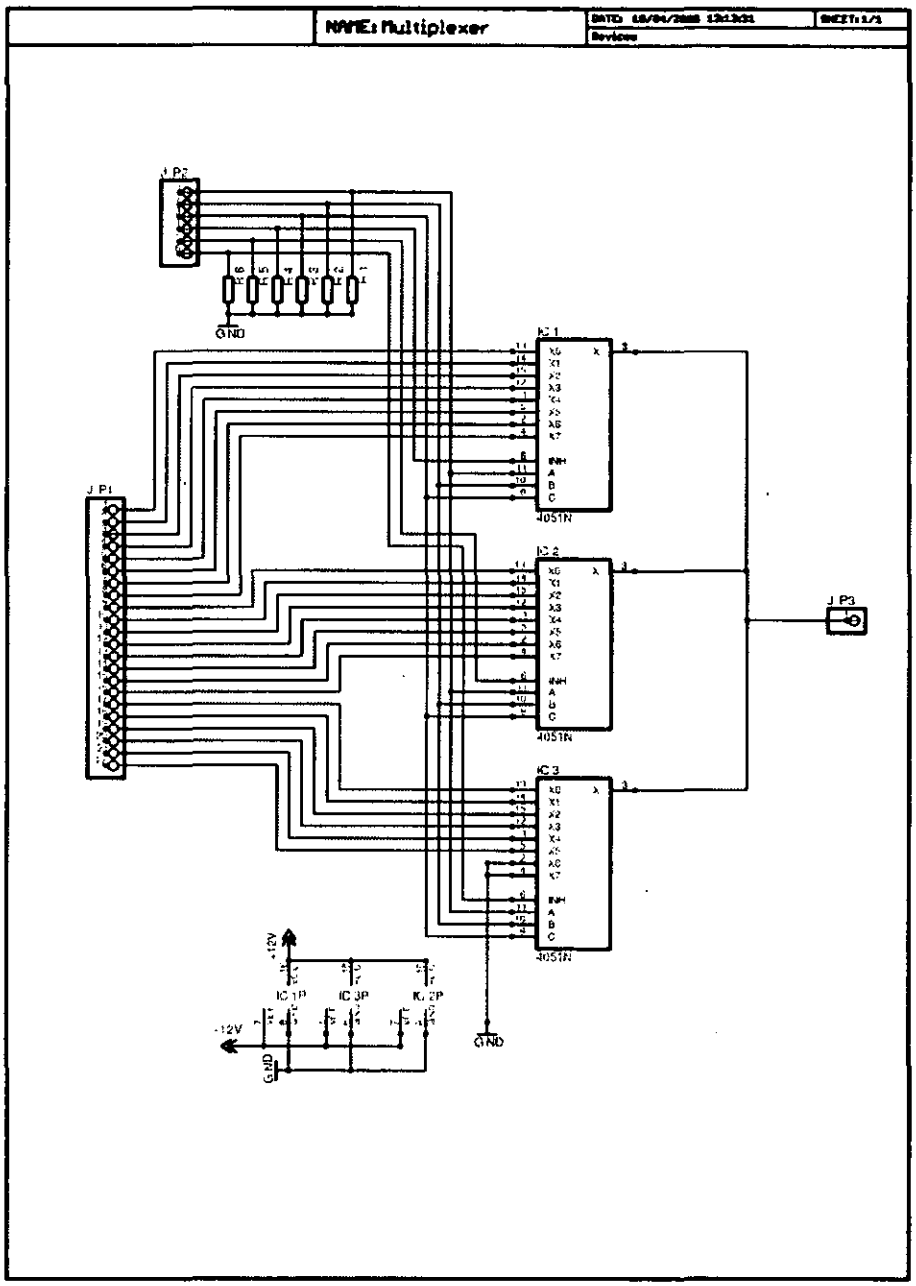

Figure A.1: End-fire array channel multiplexer.

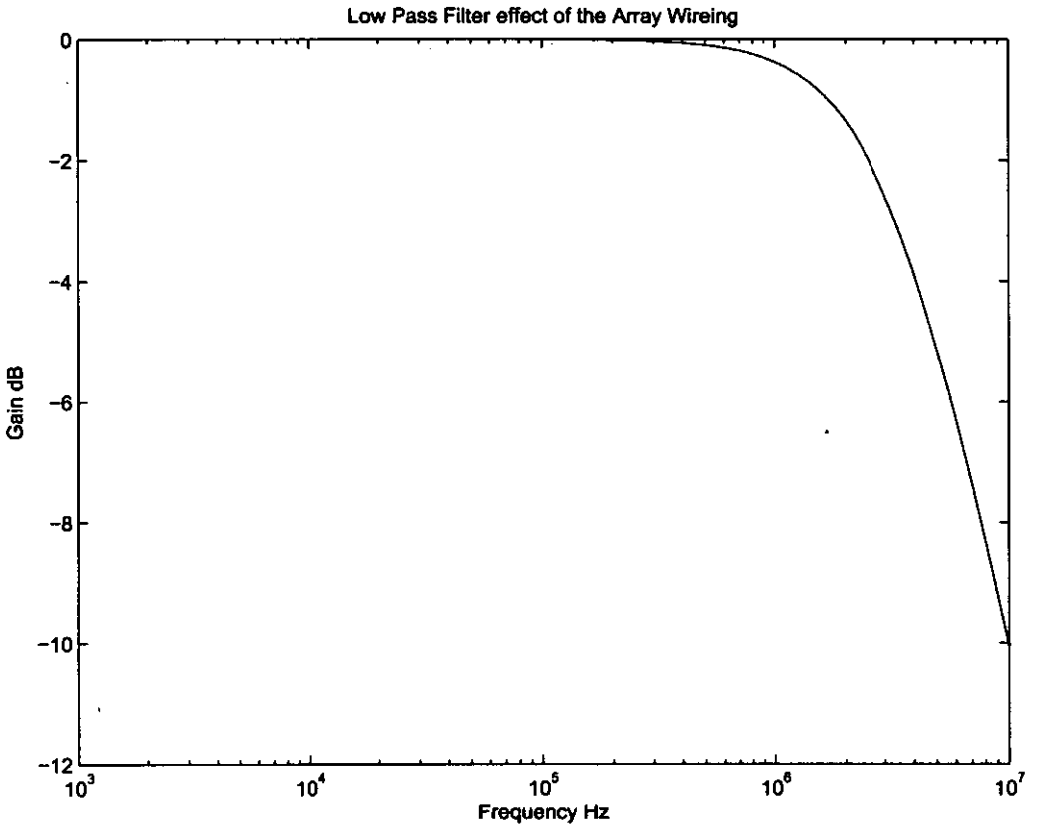

Figure A.2: The filter characteristic of the hydrophone array wiring.

As the ceramic elements of the array are placed in series with the 80Ω multiplexer, a first order low pass filter is formed. The capacitance of the elements in the array was measured using a HP 4193 Network analyser and found to be approximately 600 pF in the range of 50 kHz to 150 kHz. Using the equation for a first order rc filter [A.1] which is shown in Equation A.1 where f is the frequency of interest, c is the hydrophone capacitance and r is the line resistance, the filtering effect that is caused by this design and any impact that it might have upon the sonar reception is evaluated.

$$Gain\ dB = \frac{1}{\sqrt{1 + (2\pi frc)^2}} \tag{A.1}$$

Figure A.2 shows the filter characteristics of the array design, from these results we can see that the frequencies of interest (¡ 100 kHz) are safely within the filter pass band.

To determine the array beam pattern, the replica end-fire array was attached to a pan and tilt system. Careful attention was made to make sure the centre off the array was aligned to the centre of the pan and tilt system. The source transducer used within the experiment was a piston transducer who's resonant frequency is approximately 90 kHz. The acoustic aperture of the hydrophone was 5 cm. Equation 3.5 which calculates the Rayleigh Distance (D) of an acoustic source was used to calculate the minimum separation of the source and the array. Given a transmission frequency of 78.95 kHz and assuming a sound speed of 1500m/s the near field should end at 41cm. The source hydrophone was placed 65 cm from the centre of the array meaning the receiving array should satisfy farfield conditions even when in the end fire direction.

A Hameg HM8130 function generator was used to produce a pulsed 8 cycle sine wave at a frequency of 78.9 kHz. The output signal from the multiplexer was fed into a pre-amplifier with 40 dB of gain between 10 Hz and 100 kHz. As the same pre-amplifier is used with every channel in the array phase effects will be equal on ever signal and should cancel out.

Custom PC software was written to control the position of the pan and tilt system in 1^o steps between $\pm$ 90°, while cycling through each of the channels on the multiplexer and capturing the waveforms on a Tektronics oscilloscope and to store the signal to the PC hard drive at a sample rate of 1 MHz. In order to maintain a fixed time frame for each signal captures on the oscilloscope were triggered from the TTL gating output of the outgoing pule.

The results where then post processed in Matlab and the beam patterns of each element where obtained, which can be seen in Figures A.3-A.24. From these beam patterns it can be clearly seen that the elements are not omnidirectional. This is most probably due to the way in which the elements are fixed close to each other causing interference in the acoustic field, and the presence of the perspex mounting block. The lack of omnidirectionality means that this array could never operate in an end-fire mode. Figure A.25 shows the array working in a broadside configuration.

A.1.1 Beam Patterns

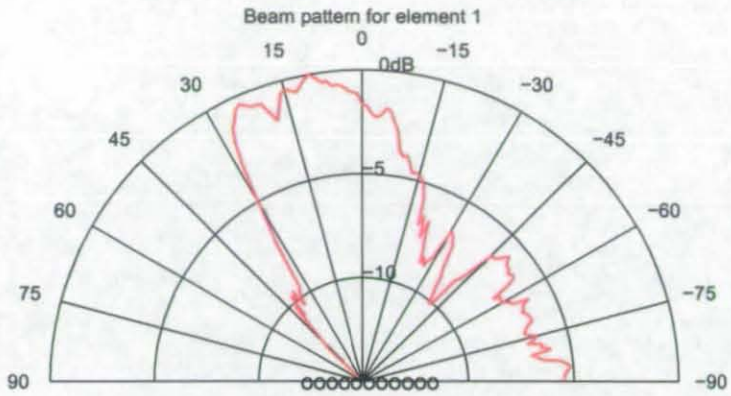

Figure A.3: Element 1 Beam Pattern.

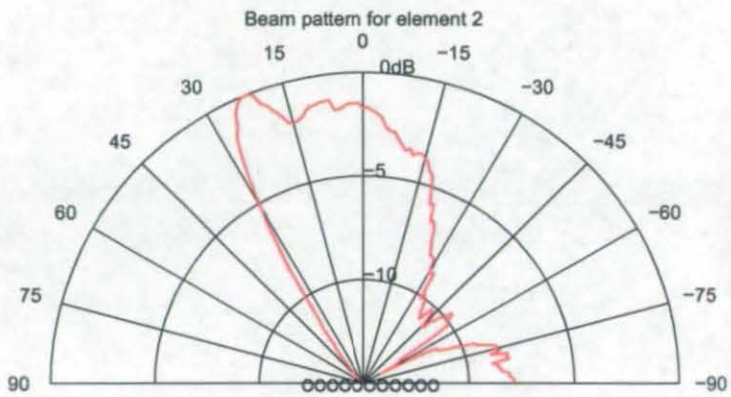

Figure A.4: Element 2 Beam Pattern.

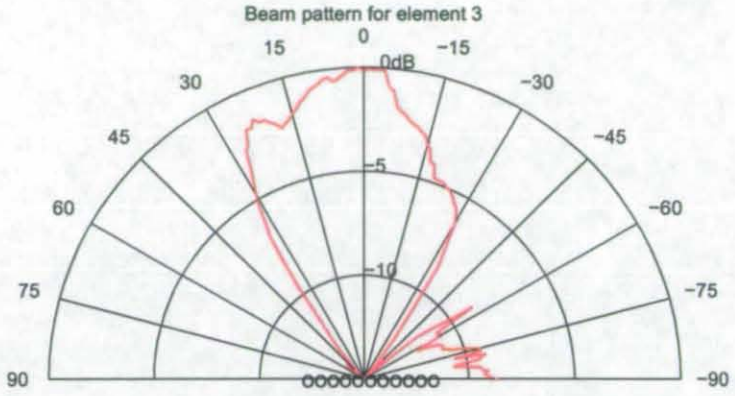

Figure A.5: Element 3 Beam Pattern.

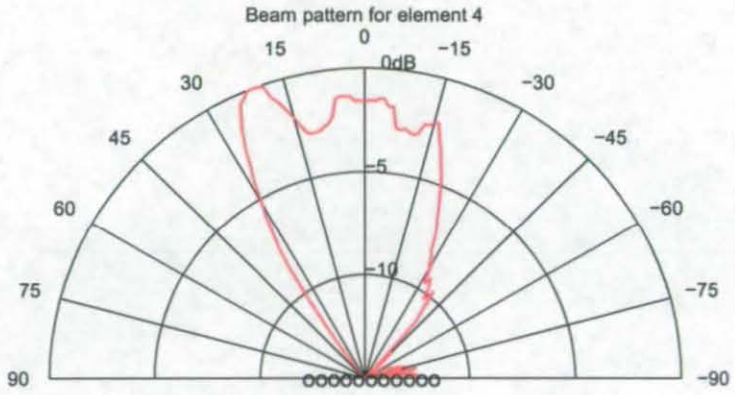

Figure A.6: Element 4 Beam Pattern.

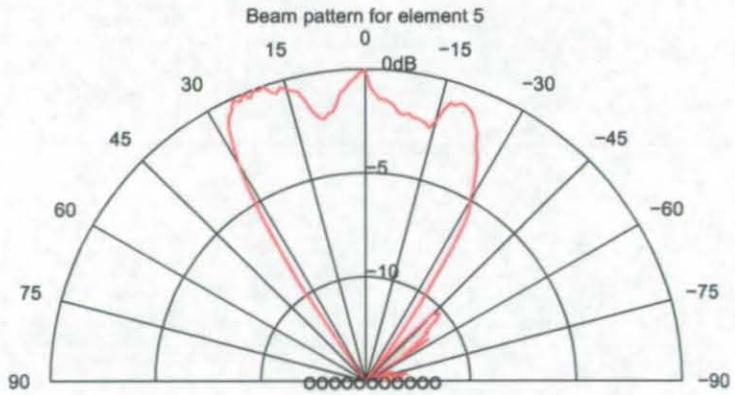

Figure A.7: Element 5 Beam Pattern.

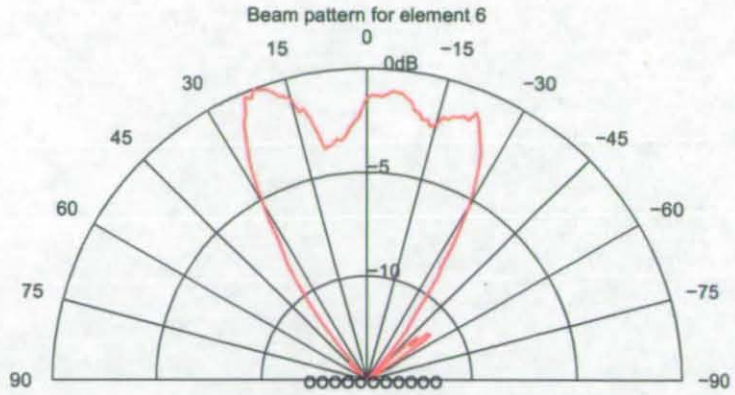

Figure A.8: Element 6 Beam Pattern.

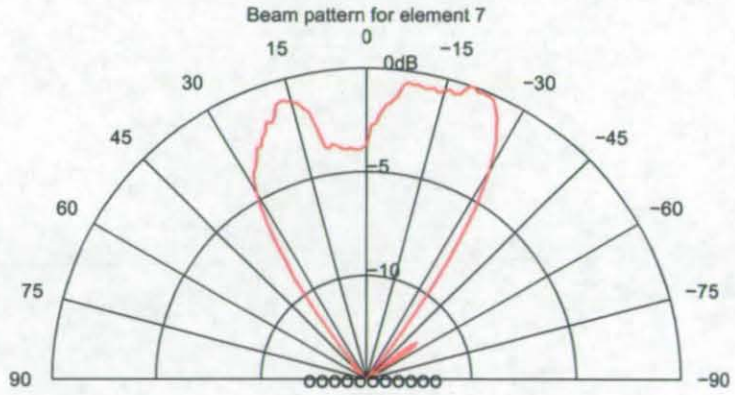

Figure A.9: Element 7 Beam Pattern.

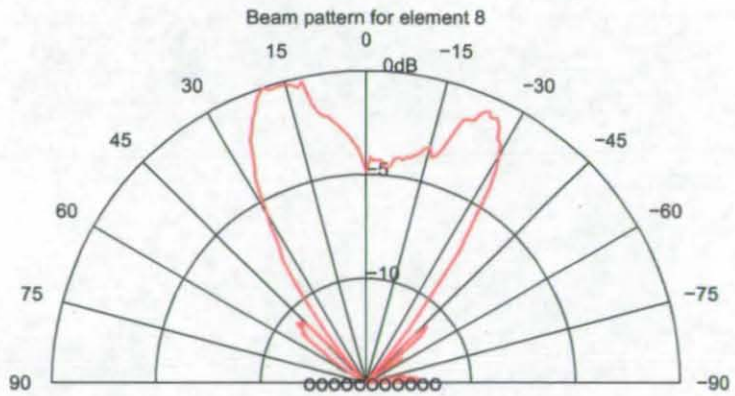

Figure A.10: Element 8 Beam Pattern.

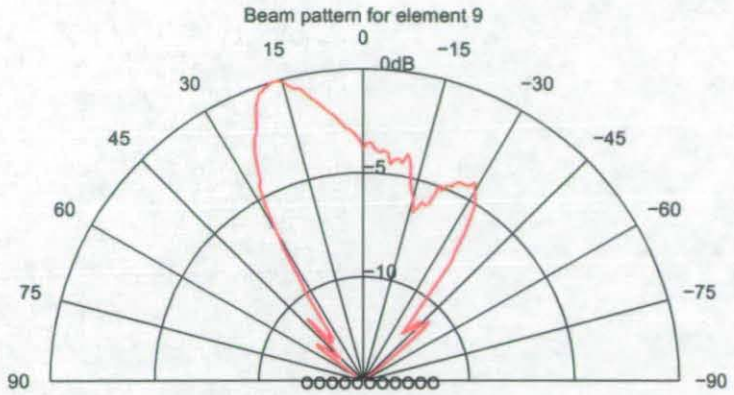

Figure A.11: Element 9 Beam Pattern.

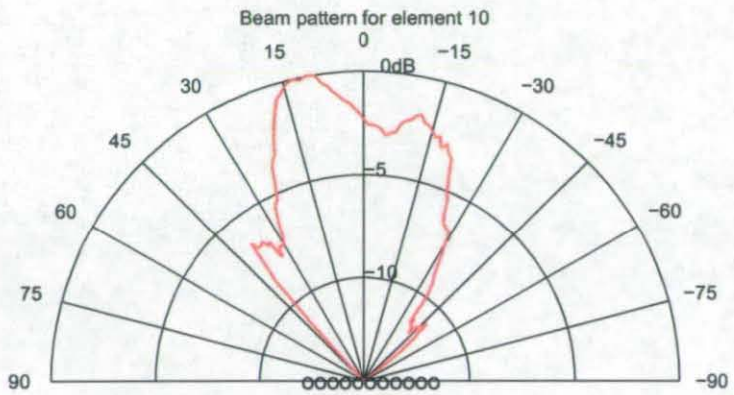

Figure A.12: Element 10 Beam Pattern.

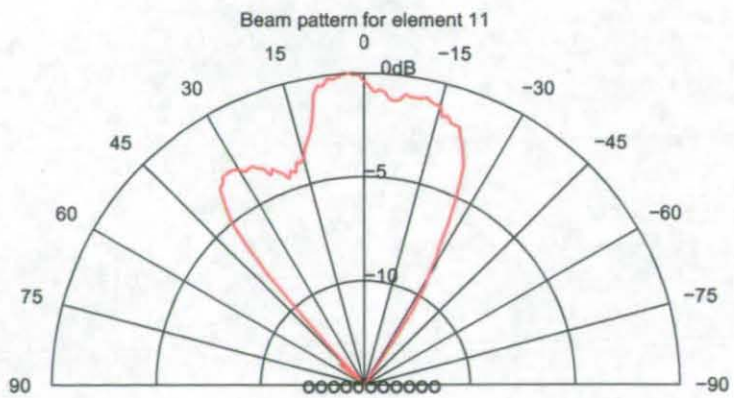

Figure A.13: Element 11 Beam Pattern.

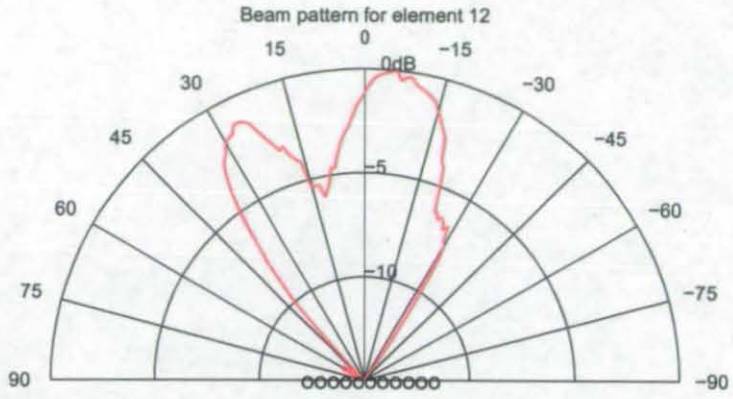

Figure A.14: Element 12 Beam Pattern.

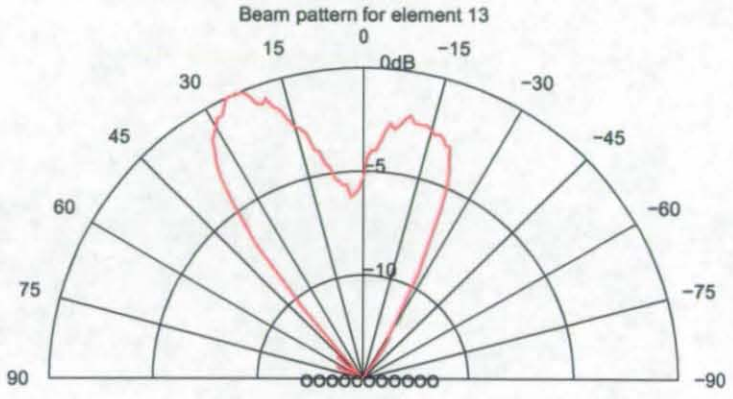

Figure A.15: Element 13 Beam Pattern.

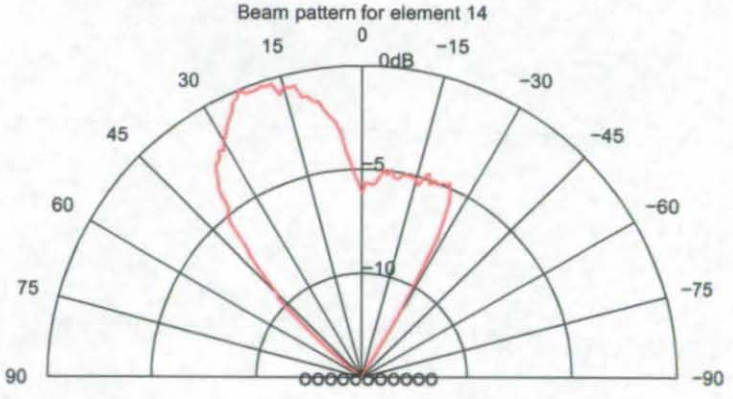

Figure A.16: Element 14 Beam Pattern.

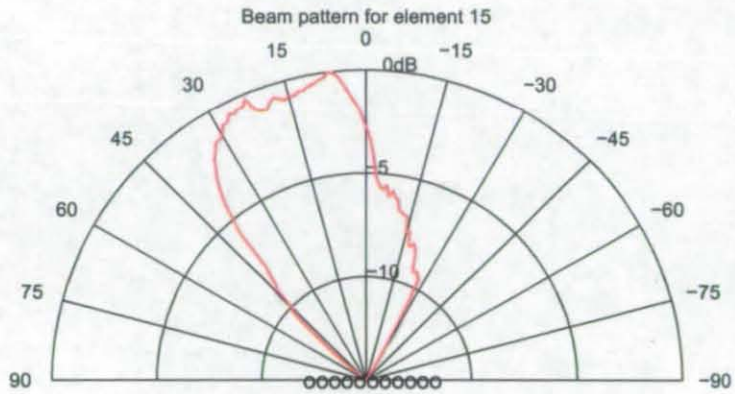

Figure A.17: Element 15 Beam Pattern.

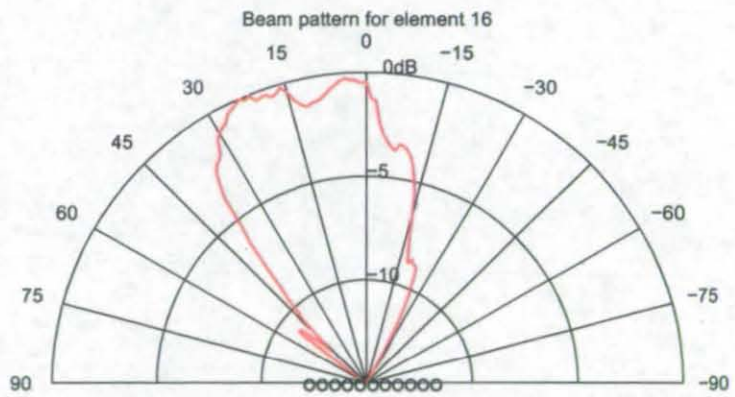

Figure A.18: Element 16 Beam Pattern.

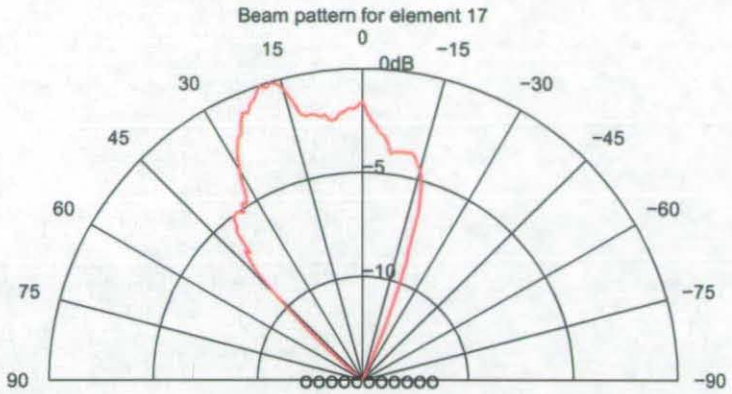

Figure A.19: Element 17 Beam Pattern.

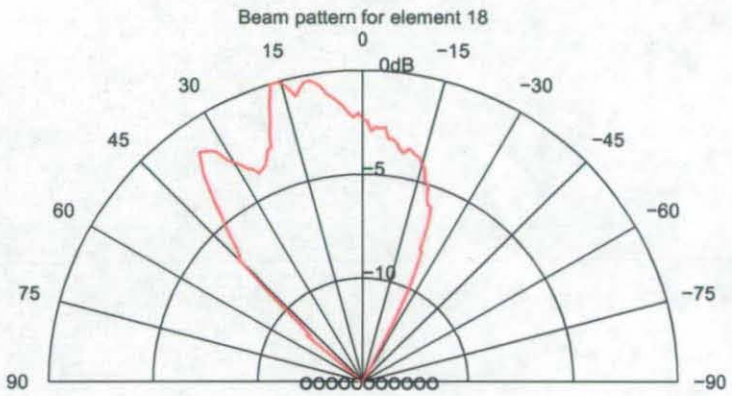

Figure A.20: Element 18 Beam Pattern.

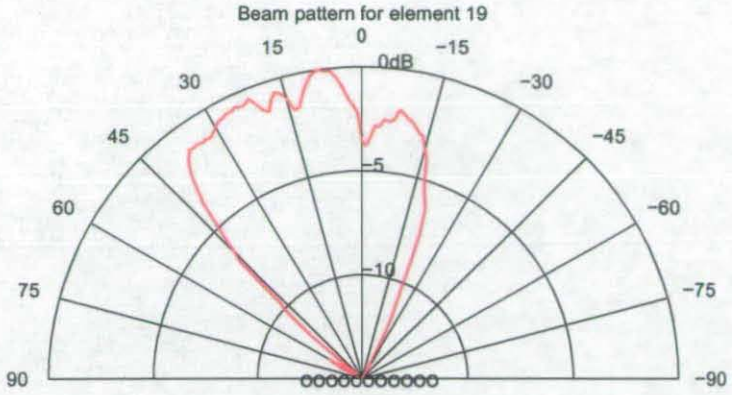

Figure A.21: Element 19 Beam Pattern.

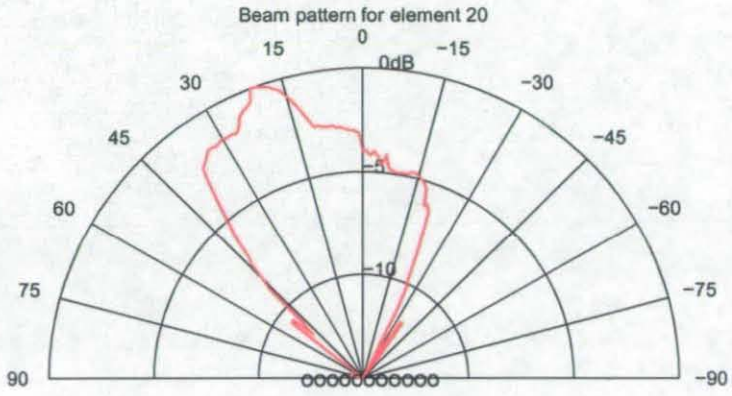

Figure A.22: Element 20 Beam Pattern.

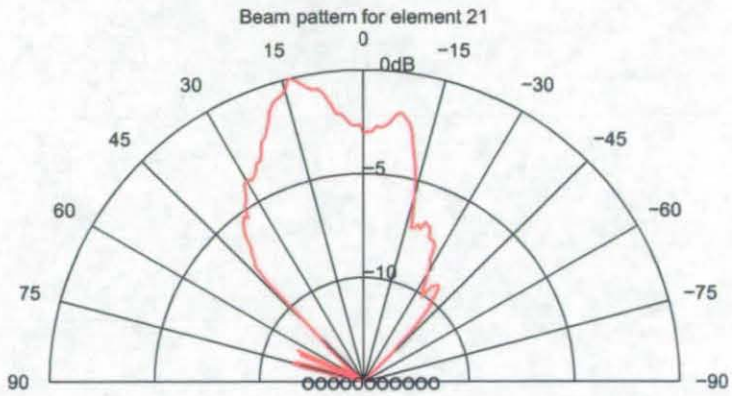

Figure A.23: Element 21 Beam Pattern.

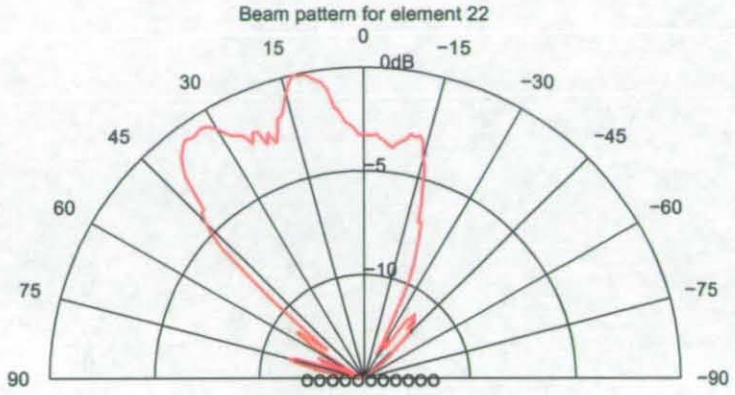

Figure A.24: Element 22 Beam Pattern.

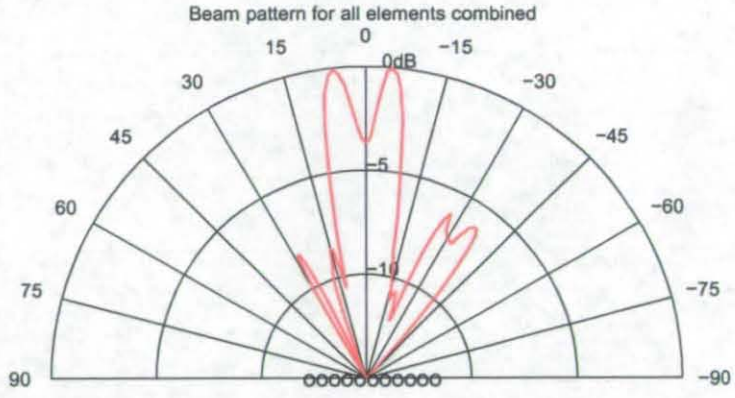

Figure A.25: All elements combined to form a broadside array.

References

[A.1] P. Horowitz and W. Hill, *The Art of Electronics*. Cambridge University Press, 1989.